Synchronization of Coupled Dynamical Systems

DYNAMICS AND SYNCHRONISATION OF TWO COUPLED PARAMETRIC PENDULA

by

Winston Garira

A Thesis Presented to the

CENTRE FOR NONLINEAR DYNAMICS & ITS APPLICATIONS

UNIVERSITY COLLEGE LONDON

In Partial Fulfillment of the

Requirements for the Degree

of

DOCTOR OF PHILOSOPHY

IN

NONLINEAR DYNAMICS

September 2002

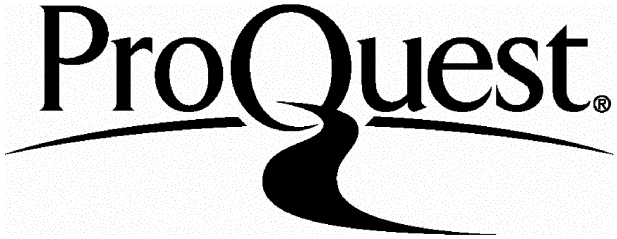

TO MY FAMILY

Abstract

One of the most important discoveries in the study of nonlinear dynamical systems in the last decade is that chaotic systems can be controlled and synchronised. Chaos synchronisation can be viewed as a particular problem of chaos control in the sense that by introducing a coupling term between two independent chaotic systems, we can provide a controlling mechanism in one or both systems (unidirectional or multi-directional coupling) that will eventually cause their trajectories to converge onto each other and then remain synchronised. But in most dynamical systems, chaotic attractors coexist with periodic attractors for a given set of parameters. This guarantees the coexistence of competing synchronous behaviours (chaotic and periodic synchronisation). Therefore in order to fully understand the synchronisation regimes that can occur to a given coupled dynamical system, we need to consider both the chaotic synchronisation component of the dynamics as well as periodic synchronisation and the transition between them. In this thesis we study both periodic and chaotic synchronisation of coupled dynamical systems. We introduce the subject of synchronisation of coupled dynamical systems in chapter 1. In chapters 2, 3 and 4 we study the oscillating, rotating and chaotic solutions of the single parametrically excited pendulum. The study of both periodic and chaotic synchronisation of two coupled parametrically excited pendula (sometimes called pendulums) is considered in chapters 5 and 6 respectively. Then we summarise our main findings in chapter 7 together with some proposals for future research directions.

Acknowledgments

I owe many thanks to several people who helped me in a number of ways during the years 1999 to 2002. At the top of the list of people I wish to thank is Professor Steven Bishop who supervised me during the course of my PhD studies. He was the source of encouragement and many thought provoking discussions during all these years. I am also eternally and profoundly grateful to Professor Bishop for recommending me for a Commonwealth Scholarship without which I would never have been able to undertake this PhD course. I also want to thank Professor Michael Thompson who was my subsidiary supervisor for reading through all my annual reports and making valuable comments. Thanks are also due to Dr. Anna Oliveira, a former research fellow within the centre whom I closely worked with during my first year and jointly published a paper on 'Out-of-phase Vs in-phase synchronisation of two parametrically excited pendula' [Oliveira et al., 2001]. I also wish to express my gratitude to Dr. Gert van der Heijden, a senior research fellow within the centre for reading through chapter 4 and making valuable suggestions. I am grateful to many former PhD students for not only being good officemates but also for their help. These include: Giovanni Santoboni, for many discussions on the subject of synchronisation; Cliburn Chan, Ben Cotton and Rob Sturman for social and academic discussions. I also want to thank Dr. Michael Clifford of the School of Mechanical, Materials, Manufacturing Engineering & Management at Nottingham University for valuable discussions on the overall direction of my research when I visited him. I wish to thank Professor Robin Langley of the Department of Engineering at Cambridge University for some discussions on the experimental work

of two parametrically excited pendula. Above all I wish to thank the Commonwealth Scholarship Commission for supporting me financially during my studies.

Contents

List of Figures

List of Tables

Chapter 1

Introduction

1.1 Dynamical Systems

In this chapter we set the stage and lay the foundations for the subsequent chapters by reviewing concepts on dynamical systems, coupled dynamical systems and synchronisation. Dynamical systems can be modelled by nonlinear differential equations. As an example let us consider a general n-dimensional autonomous continuous-time dynamical system defined by the nonlinear differential equation

$$d\mathbf{x}/dt = f(\mathbf{x}(t), \boldsymbol{\lambda}) \tag{1.1}$$

where $\mathbf{x} \subset \mathbb{R}^n$, is an n-dimensional state space vector, and the vector $\boldsymbol{\lambda} \subset \mathbb{R}^m$ is an independent m-dimensional vector of parameters of the dynamical system. Such nonlinear equations are usually impossible to solve analytically except in a few special cases. Poincaré (1892) was the first to recognise the difficulty of solving such problems and devised geometric methods which give qualitative insight into the problem at hand without the need of getting the actual analytic solution. Poincaré's geometric methods were motivated by the three-body problem, that is, the problem of three celestial bodies experiencing mutual gravitational attraction, for example the moon and two planets. His geometric method involves considering the behaviour of orbits arising from sets of initial conditions, rather than focusing on individual orbits. This allows us to study the properties of solutions without the requirement of obtaining them explicitly. Let me

offer a few rules of thumb about properties of the dynamical response of the systems modelled by the differential equation (1.1):

(a) Suppose $\mathbf{x}(t)$ eventually comes to rest at some point $\mathbf{x}^*$. Then the velocity must be zero, so we call $\mathbf{x}^*$ a fixed point. It corresponds to an equilibrium state of the physical system being modelled by the differential equation (1.1). If all small disturbances away from $\mathbf{x}^*$ damp out (that is, $\mathbf{x}(t) \rightarrow \mathbf{x}^*$ as $t \rightarrow \infty$), then $\mathbf{x}^*$ is called a stable fixed point - it acts as an attractor for states in its vicinity.

(b) Another long term possibility is that $\mathbf{x}(t)$ flows towards a closed loop and eventually circulates around it forever. Such a loop is called a limit cycle. It represents a self-sustained oscillation (no external forcing) of the physical system.

(c) A third possibility is that $\mathbf{x}(t)$ might settle onto a strange chaotic attractor, a set of states on which it wanders forever, never stopping or repeating. Try and imagine what it means for a dynamical system such a sinusoidally driven and damped pendulum, to never stop and never repeat its behaviour yet not run off to infinity, remaining forever confined to a finite region of the phase space. For certain parameters this behaviour can actually be observed. But how can such a simple set of instructions (the differential equation of a forced pendulum) result in infinitely rich dynamics? This question was first confronted in 1963 [Lorenz, 1963], when a Meteorologist E. N. Lorenz found that even a simple set of three coupled differential equations can lead to chaotic behaviour. Lorenz reported one of the first examples of deterministic chaos in a dynamical system.

Since Lorenz's discovery of chaos many researchers have become aware that chaos is a pervasive phenomenon found in many nonlinear dynamical systems as diverse as in chemistry, engineering, ecology, solid state devices, fluid dynamics and even biology. An important class of dynamical systems exhibiting chaotic phenomenon is one which model oscillating physical systems. These dynamical systems are called oscillators. Oscillators can be self-excited, parametrically excited (that is, one of the parameters in the differential equation oscillates), or externally excited. Externally excited oscillators

are also often called forced oscillators. In this thesis we study oscillators which are parametrically excited. But the results are usually generic to all nonlinear systems.

1.2 Coupled Dynamical Systems

Since the discovery of chaos [Lorenz, 1963] there has been many studies of low dimensional systems such as driven oscillators, since these are the simplest systems which can display chaos. These studies have been carried out in pursuit of demonstrating chaos in a wide range of physical situations and studying the properties of chaotic dynamics. But, in recent years there has been a shift from studying these low dimensional systems to studying higher dimensional systems synthesised from these low dimensional systems through coupling since this is a simple way of producing a higher dimensional system. Coupled dynamical systems allow us to explore the behaviour of higher dimensional systems but starting with those with a partitioned form. The emphasis of any study of such systems will be to determine under what conditions the knowledge of the behaviour of a subsystem can help us to understand the response of the full system. Also we are particularly interested in seeing if the full system can exhibit a response not seen in any lower dimensional subsystem. In this spirit let us propose a few generalisations about the collective response of coupled dynamical systems:

(1) If each single dynamical system in the coupled system has stable fixed points and no other attractors, the coupled system tends to lock in a static pattern. Many such patterns may coexist, and in this case, the coupled system may display a wide variety of locally stable equilibria. This type of complex response is seen in many models [Stein, 1989].

(2) Another type of collective behaviour is where each dynamical system has periodic response. This type of response has many applications in biology, ranging from the mutual synchronisation of cardiac pacemaker cells, to rhythmically flashing fireflies and chorusing crickets, to wave propagation in the intestine, the heart,

brain and the nervous system [Winfree, 1980]. Therefore arrays of coupled nonlinear dynamical systems can display different types of periodic synchronisation which depend on the symmetry of the network.

(3) At the opposite extreme, suppose each dynamical system in the network has a chaotic attractor. It is known that chaotic attractors can synchronise. This discovery, first made by [Fujisaka and Yamada, 1983, 1985; Yamada and Fujisaka, 1983, 1984] and publicised through the work of Pecora and Carroll [Pecora and Carroll, 1990] has changed the view of the field of nonlinear dynamical systems, in particular the point of view of chaotic behaviour, leading to new hopes about applications of chaos particularly in the area of encryption and secure telecommunications.

(4) Other common modes of responses of coupled dynamical systems are travelling waves in one spatial dimension, rotating spirals in two dimensions, and scroll waves in three dimensions [Winfree, 1980; Kuramoto, 1984].

1.3 Synchronisation of Coupled Dynamical Systems

The study of coupled dynamical systems has opened up new research problems. One of the most widely investigated phenomenon is the concept that coupled dynamical systems can exhibit synchronisation if their coupling is above some critical level. This problem of synchronisation can be traced back about four centuries ago to Huygens's work on synchronisation of pendulum clocks. Born in the Netherlands in 1629, Huygens is also attributed to a number of scientific discoveries which among other things include: the wave theory of light, the observation of the rings of Saturn and for the effective invention of the pendulum clock. In the area of synchronisation, Huygens studied two pendulum clocks that were suspended side by side, each hanging from a hook embedded in the same wooden beam (see Figure 1.1).

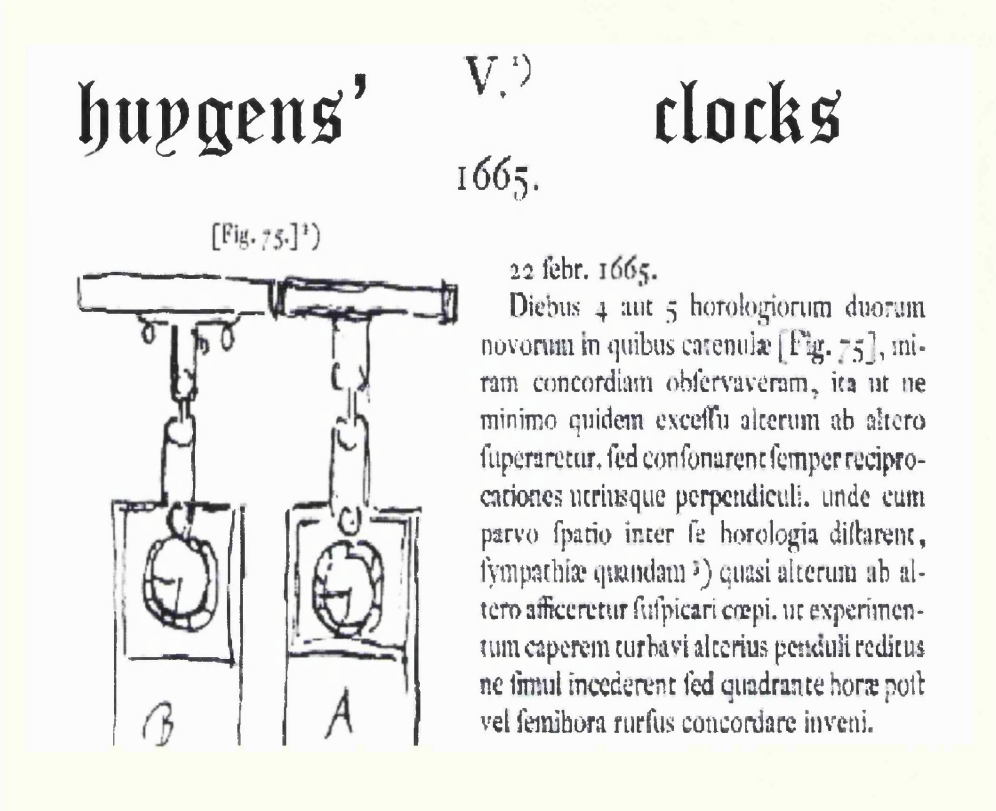

Figure 1.1: Huygens's pendulum clocks. Adapted from [Schatz, 2001].

When Huygens disturbed the pendula, he found the clocks would return to out-of-phase synchronisation as before after about 30minutes. It is now 337 years since Huygens made his observations. Over these years attempts to understand Huygens's observations have been rare. To our knowledge, there are only three studies which were directly motivated by Huygens's observations.

First was Kortewerg's paper [Kortewerg, 1906] in which he analyses a three degree of freedom model consisting of two planar pendula connected to a rigid frame free to oscillate in a plane. He made linear normal mode analysis for small oscillations in the absence of damping and driving effects. Kortewerg concluded that Huygens's observations were entirely captured by the three-degree-of-freedom model, and that the out-of-phase periodic synchronisation, if not the only sustainable motion, enjoyed a distinct advantage over in-phase synchronisation. He attributed the unsustainability of

the in-phase synchronisation to friction.

[Blekhman, 1988] also discusses Huygens's observations. His model is similar to the one studied by Kortewerg, except that Blekhman uses van der Pol oscillators rather than pendula. He concluded that that in-phase and out-of-phase are coexisting attractors. He also reports observing both in-phase and out-of-phase synchronisation in the experimental studies. There is a missing link in Blekhman's work because while his experimental observations agree with his predictions for the coupled van der Pol oscillators, Huygens as far as we know never mentioned stable in-phase synchronisation.

More recently [Bennett et al., 2002], researchers at Georgia Institute of Technology re-examined Huygens's observations both experimentally and analytically. In the experimental results, they reported the coexistence of the out-of-phase attractor with another attractor: the beating oscillation. However, in their theoretical analysis, where they used linear theory to derive a two-dimensional map of the model, they concluded that Huygens's observation of the out-of-phase synchronisation depended on both luck and talent.

Results of our studies in this thesis on periodic synchronisation of two parametrically excited pendula suggest intriguing links to the now 337 year old synchronisation puzzle of Huygens in which he only realised out-of-phase synchronisation in pendulum clocks no matter how they were started. We shall indicate these links in chapter 5.

For some time scientists believed that only periodic systems can be synchronised. It was a stunning revelation when [Fujisaka and Yamada, 1983] and later [Pecora and Carroll, 1990] revealed that even chaotic systems can be synchronised. The bizarre aspect is that despite their sensitivity to initial conditions, chaotic systems were shown to synchronise exactly. Today chaos synchronisation has become a popular subject. Motivated by the need to understand chaos synchronisation, many features of synchronisation have

now been illustrated especially by building a geometric view of this behaviour. In the geometric view, synchronisation is described in terms of the synchronisation manifold. Let us adopt this geometric view and describe some types of synchronisation that have now been studied. First consider a pair of coupled dynamical systems

$$\begin{cases} d\mathbf{x}/dt = f(\mathbf{x}, \mathbf{y}, \boldsymbol{\lambda}) \\ d\mathbf{y}/dt = g(\mathbf{x}, \mathbf{y}, \boldsymbol{\lambda}) \end{cases} \tag{1.2}$$

where $f, g : \mathbb{R}^{2n} \rightarrow \mathbb{R}^{2n}$ are smooth functions. We adopt the following definition of synchronisation:

Definition 1.1 *[Josić, 1998]: The responses* $\mathbf{x}$ *and* $\mathbf{y}$ *of the coupled system (1.2) are synchronised if there exists a compact, diagonal-like, smooth manifold* $\mathbf{M}$ *with boundary which is invariant under the flow, inflowing, and locally attracting.* $\mathbf{M}$ *will be referred to as the synchronisation manifold.*

To motivate this definition, let us consider some examples of synchronisation:

- **Complete synchronisation**: Let $\mathbf{x}(t, \mathbf{x}_0)$ and $\mathbf{y}(t, \mathbf{y}_0)$ be solutions to (1.2). Then $\mathbf{x}(t, \mathbf{x}_0)$ and $\mathbf{y}(t, \mathbf{y}_0)$ are complete synchronised if

$$\lim_{t \rightarrow \infty} \mid \mathbf{x}(t, x_0) - \mathbf{y}(t, \mathbf{y}_0) \mid = 0 \tag{1.3}$$

  This definition is illustrated diagrammatically in Figure 1.2.

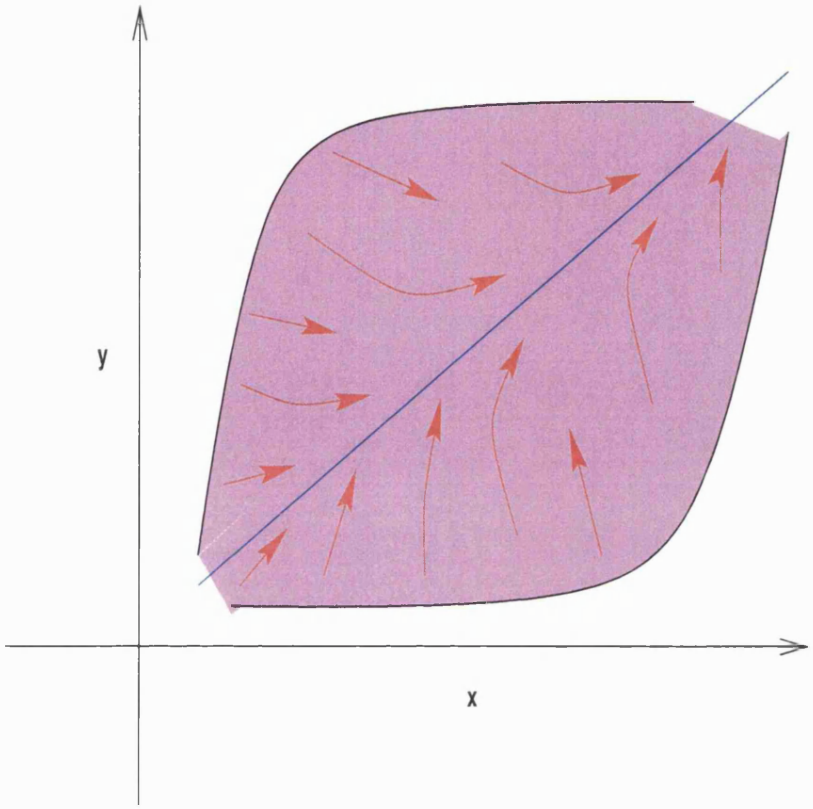

Figure 1.2: Illustration of complete synchronisation.

This occurs after transients have died away. Complete synchronisation, also sometimes called identical synchronisation is the simplest form of synchronisation and describes the interaction of two identical systems, leading to their trajectories remaining exactly in step with each other in the course of time [Fujisaka and Yamada, 1983].

- **Generalised synchronisation**: Suppose that there exists a functional relationship $\mathbf{y} = \mathbf{H}(\mathbf{x}) : \mathbb{R}^n \rightarrow \mathbb{R}^n$, denote by $\mathbf{M_H}$ the manifold $\mathbf{y} = \mathbf{H}(\mathbf{x})$, $\mathbf{x} \in \mathbb{R}^n$. Let $\mathbf{x}(t, \mathbf{x}_0)$ and $\mathbf{y}(t, \mathbf{y}_0)$ be solutions to (1.2). If

$$\lim_{t \rightarrow \infty} \mid \mathbf{y}(t, \mathbf{y}_0) - \mathbf{H}(\mathbf{x}(t, \mathbf{x}_0)) \mid = 0 \tag{1.4}$$

holds for all the initial values $\mathbf{x}_0$ and $\mathbf{y}_0$ in the vicinity of $\mathbf{M_H}$, then it is said that $\mathbf{x}(t, \mathbf{x}_0)$ and $\mathbf{y}(t, \mathbf{y}_0)$ are in generalised synchronisation. This definition is illustrated diagrammatically in Figure 1.3.

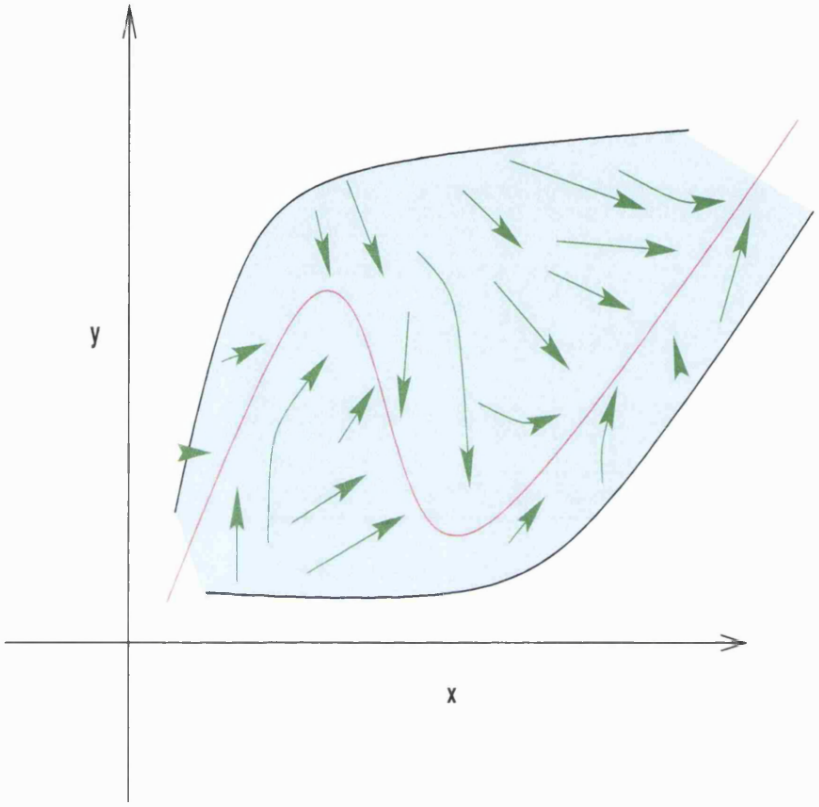

Figure 1.3: Illustration of generalised synchronisation.

This occurs after transients have died away. Generalised synchronisation is the form of synchronisation, which uses completely different systems and associate the output of one system to a given function of the output of the other system [Rulkov et al., 1995; Pyragas, 1996a].

Other forms of synchronisation which have also been studied are:

- **Phase synchronisation**: Phase synchronisation is an intermediate regime characterised by the asymptotic boundedness of the phase difference of the two outputs, whereas the two chaotic amplitudes remain uncorrelated [Yalcinkaya and Lai, 1997].

- **Lag synchronisation**: This is an intermediate state between phase synchronisation and complete synchronisation , implying the asymptotic boundedness of the difference between the output of one system at time t and the output of the other system shifted in time of a lag time τ_{lag} [Rosenblum et al., 1997]

- **Intermittent lag synchronisation**: This type of synchronisation implies that the two coupled systems are lag synchronised most of the time, but intermittent bursts of local nonsynchronous behaviour may occur in concomitance with the passage of the system trajectory into attractor regions with local Lyapunov exponents different in sign from its global value [Boccaletti and VallaDares, 2000].

- **Projective Synchronisation**: This is the dynamical behaviour in which the responses of two coupled identical systems synchronise up to constant scaling factor [Mainieri and Rehacek, 1999].

- **Cluster Synchronisation**: Cluster synchronisation is observed when the coupled dynamical systems synchronise with one another in groups, but there is no synchronisation among the groups [Heagy et al., 1995b; Wu and Chua, 1995; Pecora and Carroll, 1998; Heagy et al., 1998; Belykh et al., 2001].

- **Partial synchronisation**: Partial synchronisation is the phenomenon when, in a dynamical system, only part of the state variables synchronise and the others do not synchronise with them [Pyragas, 1996b; Hasler et al., 1998].

1.4 Motivation for Work in this Thesis

In January 2000, after three months of working on my PhD proposal, I finally decided in consultation with my supervisor Professor Steven Bishop that I was going to do research

on the dynamics of two coupled parametrically excited pendula. My interest in carrying out such research was motivated by direct questions arising in mechanical and structural systems as well as biological systems. In particular, I intended to study periodic as well as chaotic synchronisation and the transition between these two types of synchronisation. While not being an experimentalist my original aim was to study experimentally the synchronisation of this mechanical system. By February 2000 the experiment of this mechanical system was set up. Figure 1.4 shows the original experimental set-up of the system where a thin copper wire was used to couple the two pendula.

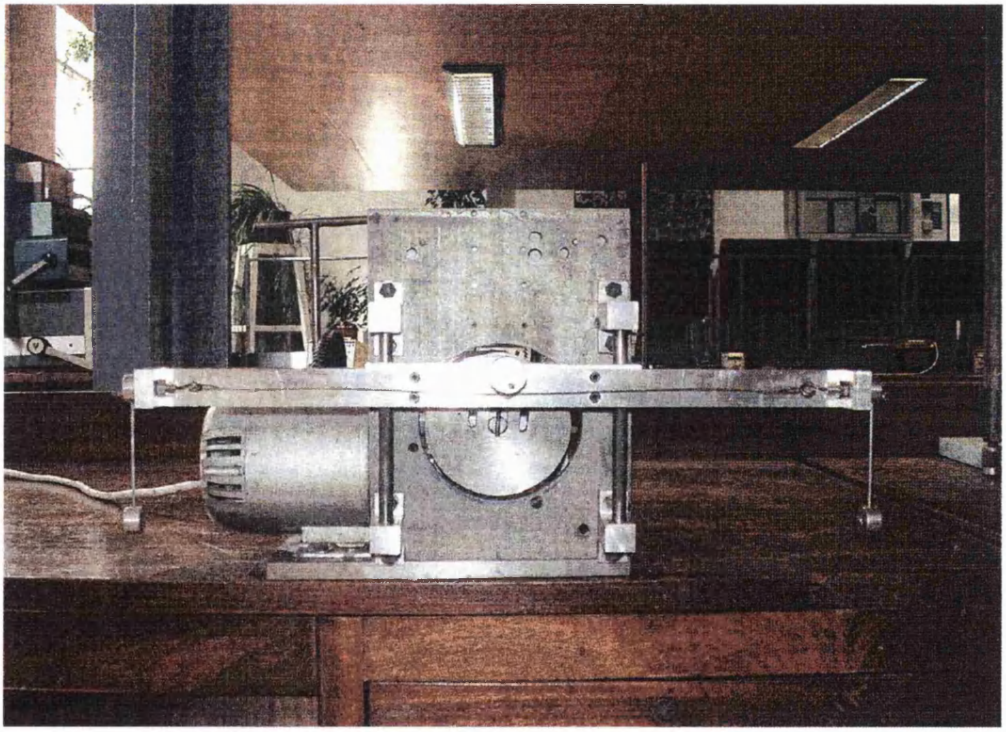

Figure 1.4: An experimental set-up of two parametrically excited pendula coupled by a thin copper wire.

From my point of view studying such a mechanical system that lends itself to both intuitive and physical understanding was useful and rewarding for two reasons: First, experimental studies of synchronised coupled systems are rare and the few that appear typically focus on either laser systems [Tang and Heckenburg, 1997; Roy and Thornburg Jr., 1994; Sugawara et al., 1994] or electronic systems [Carroll and Pecora,

1991; Yu et al., 1995; Newell et al., 1994], rather than mechanical systems. Second, this provides an opportunity to study synchronisation in nonidentical systems. Most numerical and analytical studies assume the coupled systems to be identical. But experimental systems are by their nature never identical. Working on the experiment I could get in-phase periodic synchronisation and out-of-phase periodic synchronisation. But I could not get chaos synchronisation due to limitations in the experimental model. At this stage I realised that in order for me to go beyond just this qualitative assessment of the dynamics the experiment needed more resources. For example, I realised that it required laser monitoring that records the pendulum swings for computer analysis. At that time the department lacked resources for this experiment. But motivated by the experimental observations that I made, I decided to reconsider the whole problem using a combination of numerical simulations and analytical methods.

I also became aware that I need to have a more complete picture of the dynamics of the single parametrically excited pendulum first. Earlier studies of the single parametrically excited pendulum were not adequate enough to give an overall picture of the dynamics of the single parametrically excited pendulum since, for example, they overlooked the behaviour of the system in the lower resonance zones. The contents of this thesis reflects this pattern in my thinking in that in the first chapters of this thesis (chapters 1, 2 and 3) I discuss the dynamics of the single parametrically excited pendulum and then later (chapters 5 and 6) I discuss synchronisation of the two parametrically excited pendula.

1.5 Problem Setting

The aim of this thesis is to examine mechanisms by which synchronous behaviour occurs and persist in a system of two coupled pendula. Parametrically excited pendula are an example of dynamical systems which are modelled by differential equations with periodic coefficients. Closed form analytical solutions of such systems (even for

the linearised case) do not exist and one has to rely on approximate or numerical methods. But a lot of practical applications of such systems can be found in many fields ranging from mechanisms such as gears [Warmiński et al., 2000], robots [Bucklaew and Liu, 2001], current collection systems or pantograph-catenary system [Wu and Brennan, 1999; Ockendon and Taylor, 1971], Vibromachines ([Belovodsky et al., 2002] and references therein), to animal gaits [Banning, 1998]. Legged animals typically employ multiple gaits, that is, phase-locked patterns of limb movements, for terrestrial locomotion. Locomotion in particular has been a subject of much research [Collins and 1993, 1993; Golubitsky et al., 1999, 1998]. Take the example of the horse where motions of its legs depend upon the speed with which it travels. A horse can trot, canter or gallop (see Figure 1.5 reproduced from [Bowling, 1999]).

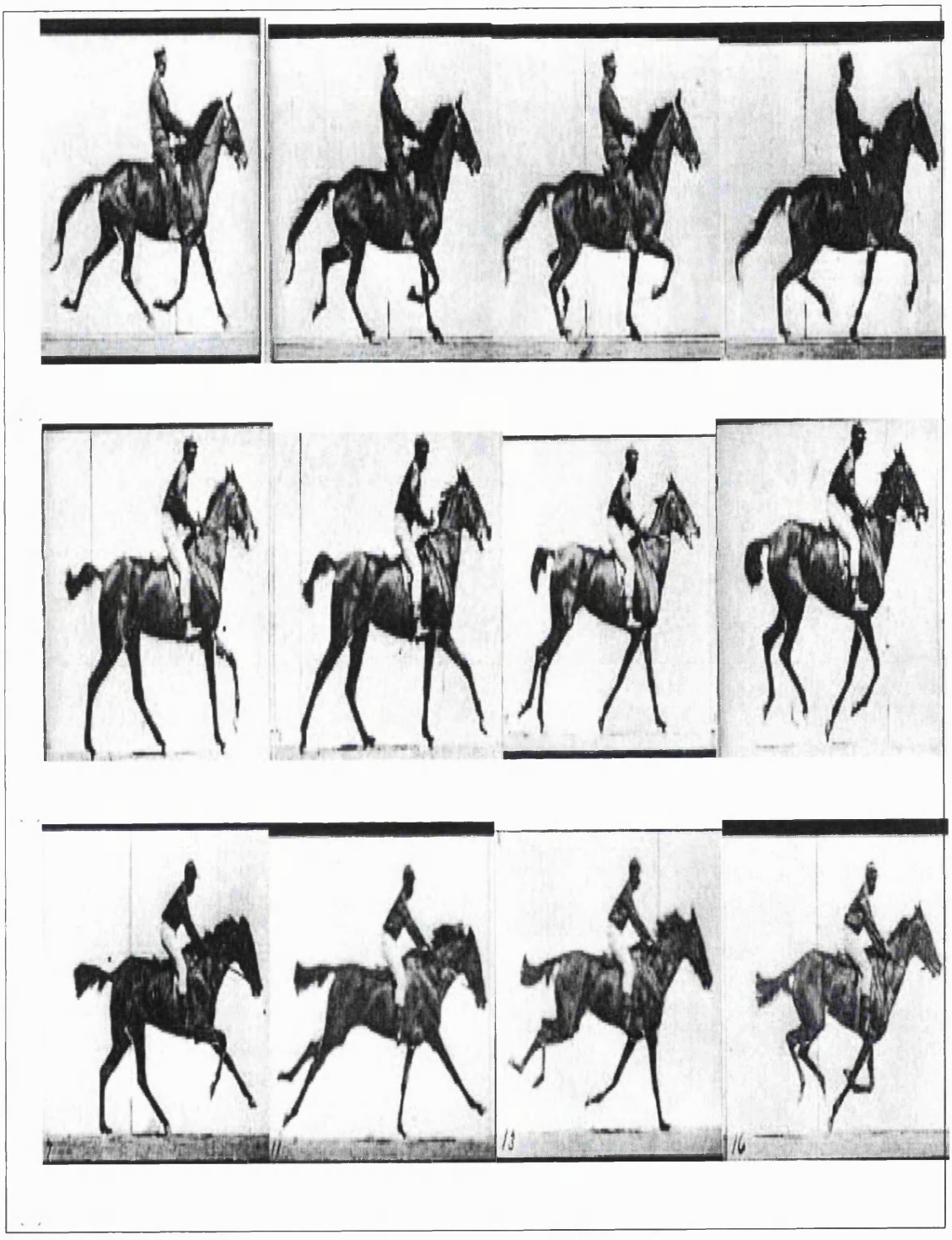

Figure 1.5: Some gaits of horses: Top: trot, Middle: canter and Bottom: gallop of a horse.

These various kinds of motions are known as gaits. Over the past few years, scientists have become increasingly interested in animal gaits [Collins and 1993, 1993; Golubitsky

et al., 1999, 1998]. This interest has been fuelled by the need to design and develop multiple-legged robots [Banning, 1998; Berkemeier, 1995]. Machines capable of legged locomotion are an attractive option, because they can be used to explore rough and uneven terrain, which is often inaccessible to wheeled vehicles. In general oscillating systems are inherent to the mechanics and neural control of legged locomotion and mechanically, animal gaits, can and have been modelled using parametrically excited pendula [Banning, 1998].

1.5.1 The Single Parametrically Excited Pendulum

Let us first consider the single parametrically excited pendulum. The parametrically excited planar pendulum is a nonlinear system with the suspension point driven periodically (see Figure 1.6 for an idealised model) with mass m attached at the end of a light inextensible rod of length l whose suspension point moves up and down according to cosinusoidal time history displacement $z(t) = -a\cos(\Omega t)$. Its equation of motion in terms of the angle θ that defines its configuration is

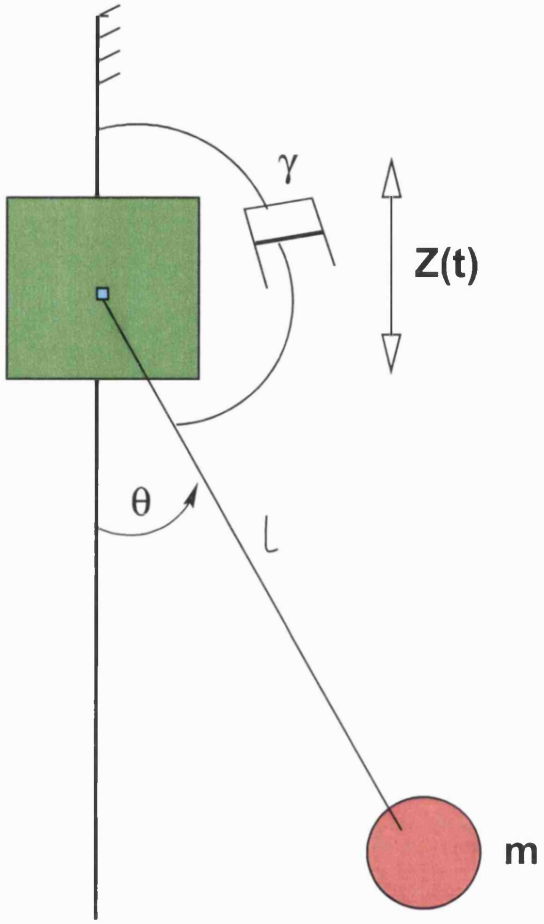

Figure 1.6: An idealised model of the parametrically excited pendulum.

$$ml^2 d^2\theta/dt^2 + \gamma d\theta/dt + ml(g + d^2z/dt^2)\sin(\theta) = 0. \tag{1.5}$$

The most important aspect of equation (1.5) is that the external driving shows up as a periodic modulation of one of the most important parameters of the system, the gravitational acceleration g, hence the name parametrically excited pendulum. Using the prescribed form of the external forcing equation (1.5) becomes

$$ml^2 d^2\theta/dt^2 + \gamma d\theta/dt + ml(g + a\Omega^2\cos(\Omega t))\sin(\theta) = 0. \tag{1.6}$$

If we apply the time transformation $\tau = t\sqrt{g/l}$ equation (1.6) takes the form

$$\theta'' + \beta\theta' + (1 + p\cos(\omega\tau))\sin(\theta) = 0, \tag{1.7}$$

where β, ω and p are the scaled forms of damping coefficient, frequency of parametric forcing and amplitude of parametric forcing respectively while the natural frequency ω_0 is now scaled to 1. The parameters of equation (1.6) and equation (1.7) are related in the following manner

$$\beta = \gamma/ml^2\omega_0, \quad \omega_0 = \sqrt{g/l}, \quad p = a\omega^2/l = a\Omega^2/g, \quad \omega = \Omega/\omega_0.$$

It is evident from equation (1.7) that for $p = 0$, that is, when there is no parametric forcing, we recover the simple pendulum equation

$$\theta'' + \beta\theta' + \sin(\theta) = 0 \tag{1.8}$$

which is frequently encountered in many textbooks and research papers as one of the most familiar examples of a nonlinear mechanical oscillator with many problems in various branches of physics and engineering reducing to this form. Of all the pendulum systems with external forcing, the parametrically excited pendulum is one of those with the same number of stationary points as the undriven pendulum described by equation (1.8), namely, $\theta = 0$ and $\theta = \pi$. In the undriven case described by equation (1.8) these points are always stable and unstable respectively. So the parametric forcing can change the stability/instability and vice versa. This fact seems to have been realised first by [Stephenson, 1908], and has since been demonstrated both experimentally and by numerical simulations by a number of researchers [Kalmus, 1970; Pippard, 1987; Smith and Blackburn, 1992]. [Acheson, 1993] managed to extend this concept to multiple pendulums.

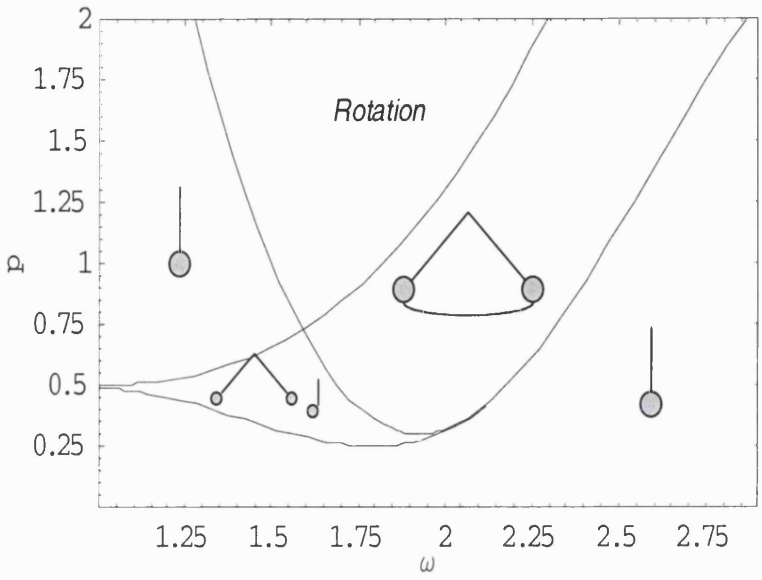

Figure 1.7: Parameter space diagram for the single parametrically excited pendulum.

Different types of behaviour of the single parametric excited pendulum are shown in Figure 1.7 [Oliveira et al., 2001]. For certain values of p and ω the pendulum oscillates, for others it remains in the hanging state, simply moving up and down with the driving force. The region in the above figure defined as "Rotation" also includes chaotic motion which include rotations. The stability diagram shown in Figure 1.7 is only for oscillations about the downward equilibrium.

1.5.2 Two Coupled Parametrically Excited Pendula

When two parametric excited pendula, as described in the previous section, are coupled, the dynamics of the system becomes richer and more complex. There are different ways of coupling two pendula. [Zhang et al., 1999], for example, described two parametrically excited pendula coupled unidirectionally and connected through a periodical feedback. In this work we will concentrate on continuous bidirectional or mutual coupling. In bidirectional or mutual coupling each dynamical system influences the behaviour of the other dynamical system. This type of coupling was described in detail by Banning [Banning and Weele, 1995; Banning et al., 1997], where both the

Hamiltonian and dissipative cases are considered. In the study by Banning the coupling strength is maintained constant throughout. Here we are mainly interested in studying the effect of different coupling strengths on the dynamics of the system.

If the common suspension point of the two pendula is harmonically driven according to $z(t) = -a\cos(\Omega t)$ and configurations of the pendula are defined by angles θ_1 and θ_2, then the equations of motion can be shown to be

$$\begin{cases} ml^2 d^2\theta_1/dt^2 + \gamma d\theta_1/dt + ml(g + a\Omega^2\cos(\Omega t))\sin(\theta_1) + K(\theta_1 - \theta_2) = 0 \\ ml^2 d^2\theta_2/dt^2 + \gamma d\theta_2/dt + ml(g + a\Omega^2\cos(\Omega t))\sin(\theta_2) - K(\theta_1 - \theta_2) = 0. \end{cases} \tag{1.9}$$

It is evident from equations (1.9) that for $a = 0$ and with no coupling $(K = 0)$

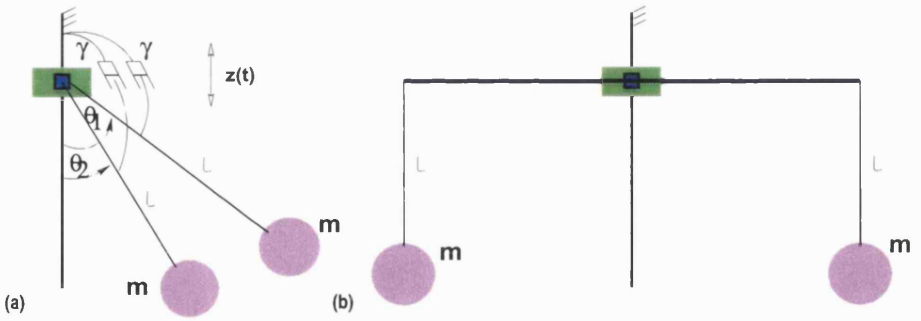

Figure 1.8: An idealised model of two coupled parametrically excited pendula: (a) Side view (b) Top view.

we recover the simple pendulum equation

$$ml^2 d^2\theta/dt^2 + \gamma d\theta/dt + mgl\sin(\theta) = 0. \tag{1.10}$$

In order to reduce the number of parameters in the governing equations (which are now m, γ, l, Ω, a, K) and also in order for us to be able to compare directly the dynamics of systems described by equations (1.9) in any field, for example in lasers and in mechanics, we rescale the time coordinate using the transformation $\tau = t\sqrt{g/l}$. We apply the

relation $d\tau = (\sqrt{g/l})dt$ to equations (1.9) and obtain the scaled equations of motion in the form

$$\begin{cases} \theta_1'' + \beta\theta_1' + (1 + p\cos(\omega\tau))\sin(\theta_1) + k(\theta_1 - \theta_2) = 0 \\ \theta_2'' + \beta\theta_2' + (1 + p\cos(\omega\tau))\sin(\theta_2) - k(\theta_1 - \theta_2) = 0 \end{cases} \tag{1.11}$$

where k is the scaled coupling parameter and β, p, ω are the scaled damping, amplitude of parametric forcing and the frequency of parametric forcing of the pendula respectively with the natural frequency ω_0 now scaled to 1. The parameters of equations [1.9] and equations [1.11] are related in the following manner:

$$\beta = \gamma/ml^2\omega_0, \quad \omega_0 = \sqrt{g/l}, \quad p = a\omega^2/l, \quad \omega = \Omega/\omega_0, \quad k = K/ml^2\omega_0^2.$$

Like the single parametrically excited pendulum the system of two coupled parametrically excited pendula has the same number of stationary points as the undriven single pendulum described by equation (1.10), namely, $\theta_1 = \theta_2 = 0$ and $\theta_1 = \theta_2 = \pi$. In the undriven case described by equation (1.10) these points are always stable and unstable respectively. So the parametric forcing can change the stability/instability and vice versa as first noted by [Stephenson, 1908].

For low values of the amplitude of parametric forcing p equations (1.11) exhibit predominantly two modes of periodic behaviour: in-phase periodic oscillations and out-of-phase periodic oscillations. The occurrence of these two types of periodic oscillations can be illustrated more clearly by using normal coordinates. Using the normal coordinates [see chapter 5 for details] the equations for in-phase oscillations and out-of-phase oscillations can be shown to be

$$\begin{cases} \theta'' + \beta\theta' + (1 + p\cos(\omega\tau))\sin(\theta) = 0 \\ \theta'' + \beta\theta' + (1 + p\cos(\omega\tau))\sin(\theta) + 2k\theta = 0 \end{cases} \tag{1.12}$$

where the first of equations (1.12) describe in-phase oscillations and the second of these equations describe out-of-phase oscillations. In order to numerically establish the stability of the downward equilibrium ($\theta_i, = \theta_i' = 0, \quad i = 1, 2$) around both

zones of in-phase and out-of-phase oscillations in which the pendula simply go up and down with the point of suspension, we consider the characteristic exponents of the full nonlinear equations (1.11). The zones in the (ω, p) space for which the fixed point $(\theta_i, = \theta_i' = 0, \quad i = 1, 2)$ is unstable appear as tongue-shaped regions. In the case of the linearised form of equations (1.11), these resonance zones are called Mathieu zones. Outside the resonance zones the downward equilibrium $(\theta_i, = \theta_i' = 0, \quad i = 1, 2$ solution) is stable.

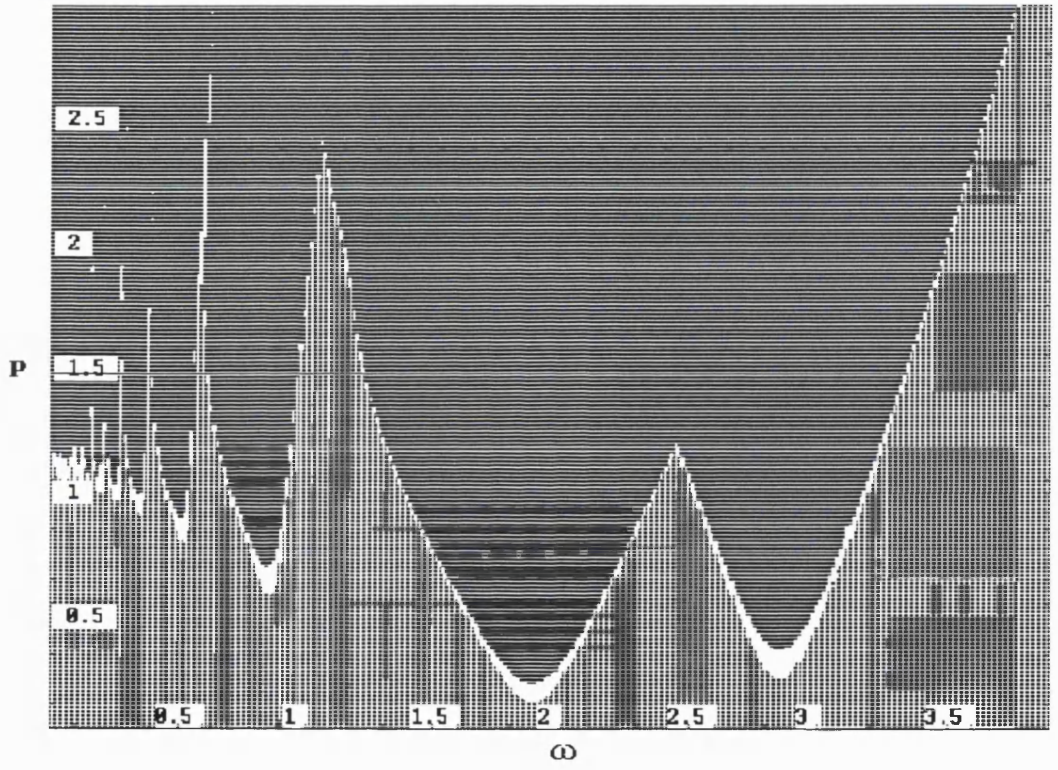

Figure 1.9: The resonance zones of periodic motion in (ω, p)-parameter space for two coupled parametrically excited pendula with $k = 0.6$. The dark grey regions represent the parameter space for which periodic oscillations are realised while the light grey regions represent the regions for which the downward equilibrium is stable for both pendula. This diagram was numerically determined using the software [Nusse and Yorke, 1998].

For in-phase periodic oscillations, the resonance zones occur around $\omega = 2/n$, $n = 1, 2, 3, ...$ in the (ω, p) space while for the out-of-phase oscillations the resonance zones occur around $\omega = 2/n\sqrt{(1 + 2k)}$, $n = 1, 2, 3, ...$ in the (ω, p) space. The position

of the zones of out-of-phase motion change in the parameter space as k changes. Figure 1.9 shows the zones of in-phase and out-of-phase oscillations for $k = 0.6$ which were determined numerically for the full nonlinear equations using the software [Nusse and Yorke, 1998].

The non rotating periodic steady state motions of the pendula can be classified into four categories as shown in Figure 1.10 [Banning, 1998]:

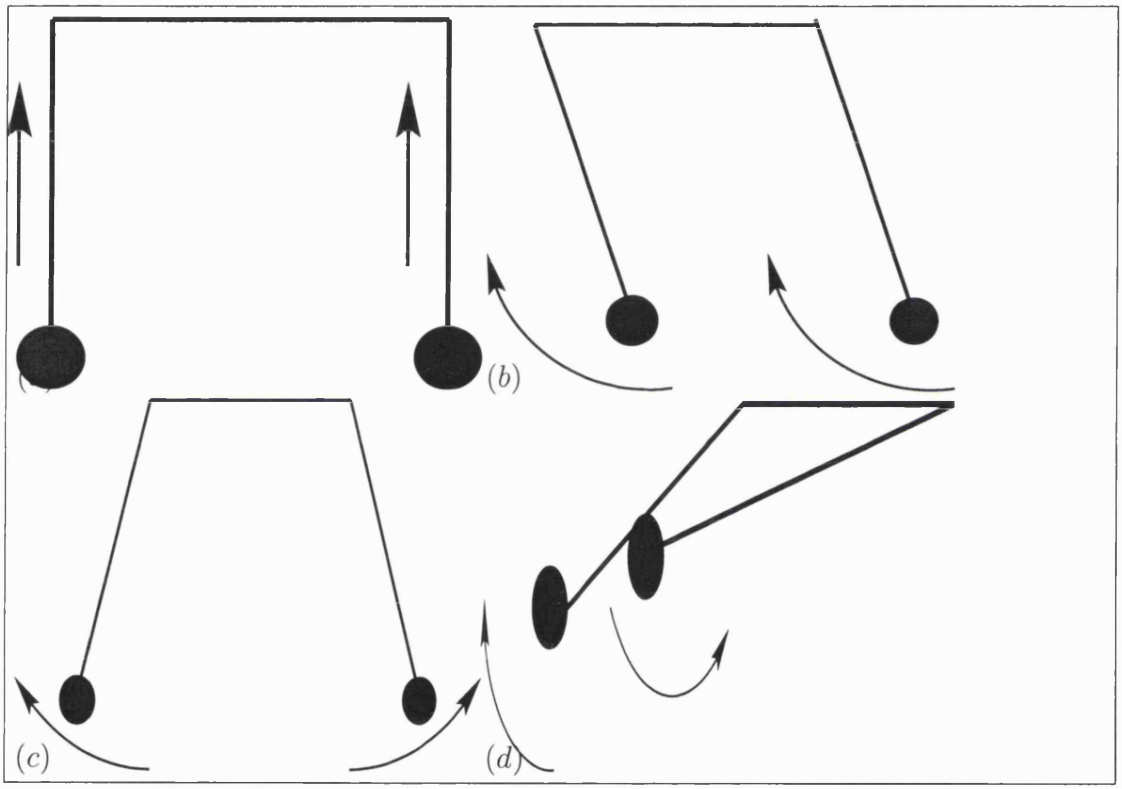

Figure 1.10: (a) 0-motion (b) 1-motion (c) 2-motion (d) M-motion.

0-motion In this case the two pendula move only in the vertical direction for all times (after the transient time) : *Hanging motion*. In this case we have $\theta_1(\tau) = \theta_2(\tau) = 0$.

1-motion In this second motion the two pendula move in phase with each other (again after the transient time): *In-phase synchronisation* in which $\theta_1(\tau) = \theta_2(\tau)$.

2-motion In the third type of motion both pendula move in counterphase with each other: *Out-of-phase synchronisation.* In this case we have $\theta_1(\tau) = -\theta_2(\tau)$.

M-motion This last type of motion are characterised by periodic motions that can not be classified as any of the above: *Mixed motion.*

The two pendula can also rotate in synchrony or exhibit chaotic behaviour, often called *Tumbling chaos* since this motion involves a complicated combination of oscillations and rotations like a tumbling gymnast. Rotating chaos and oscillating chaos [Bishop and Clifford, 1996a] also exists but in a very narrow region of the parameter space and it will not be considered here. We will use the term *chaotic synchronisation* when each of pendula exhibits chaotic behaviour but $\theta_1(\tau) = \theta_2(\tau)$ for all times after the transient motion.

1.6 Structure of the Thesis

In progressing through the work of this thesis, our guiding principle was that in order to understand how coupled nonlinear dynamical systems work together, one must first understand how one dynamical system works by itself. In this spirit the contents of this thesis can be broadly divided into two parts: The first part is composed of chapters 2, 3, and 4. In these three chapters we discuss a wide variety of dynamical responses of the single parametrically excited pendulum. Thus in chapter 2 we discuss oscillatory behaviour of the parametrically excited pendulum. In chapter 3 we study rotating motion of the parametrically excited pendulum. This first part concludes with chapter 4 in which we discuss chaotic dynamics of the parametrically excited pendulum.

In the second part, made up of chapters 5 and 6, we discuss synchronisation of two coupled parametrically excited pendulum. The thesis ends up with chapter 7 which summarises the our main findings in this thesis and point to future research directions.

Chapter 2

Oscillatory Solutions of the Parametrically Excited Pendulum

2.1 Introduction

In this chapter we consider periodic oscillatory solutions or orbits of the parametrically excited pendulum. These oscillatory solutions, sometimes referred to as swinging or non-rotating orbits by different authors are oscillations which do not go beyond the vertical static (but unstable) equilibrium point. In general, a solution $\mathbf{x} = \mathbf{x}(t)$ of a continuous time dynamical system is said to be periodic with least period T if $\mathbf{x}(t+T) = \mathbf{x}(t)$ and $\mathbf{x}(t+\tau) \neq \mathbf{x}(t)$ for $0 < \tau < T$. Usually such solutions correspond to closed orbits in phase space. In the case of continuous time dynamical systems a periodic solution can be treated as a fixed point of an appropriately defined map called a Poincaré map.

There is a lot of theoretical work on oscillatory periodic solutions of dynamical systems (see for example [Thompson and Stewart, 2002] and references therein). In theoretical sudies, the Bendixson's theorem can be used as a tool to exclude the existence of periodic solutions of two-dimensional autonomous dynamical systems [Nayfeh and Balachandran, 1995]. In addition, when a map from $\mathbb{R}^n$ to $\mathbb{R}^n$ which is associated with a continuous time dynamical system (autonomous or nonautonomous) has at least one fixed point, fixed point theorems such as the *c*ontraction mapping theorem and the

*B*rouwer fixed point theorem can be used to prove the existence of a periodic solution of a dynamical system corresponding to the fixed point of the map [Hale, 1969; Arnold, 1973].

The study of oscillatory periodic solutions of the parametrically excited pendulum which resulted in the material presented in this chapter was carried out because we realised that all the theorems mentioned thus far are limited because they do not provide us much information on the location in parameter space and the different types (and their symmetries) of the periodic oscillatory solutions of the system. So the work presented here was carried out to ascertain the existence (and location in parameter space) of oscillatory periodic solutions of the parametrically excited pendulum and their different types using numerical methods. The need to understand more about the different types of oscillatory solutions was motivated by the fact that in some applications of the parametrically excited pendulum, the main interest is in achieving periodic solutions that do not exceed $\theta = \pm\pi$, as this might correspond to failure in some sense. But more importantly, knowledge of oscillatory behaviour of the single parametrically excited pendulum provides the necessary groundwork for subsequent work in this thesis [chapter 5] where we study periodic synchronisation of two coupled parametrically excited pendula when their dynamics is oscillatory.

Earlier studies on the oscillatory solutions of the parametrically excited pendulum include [Bishop and Clifford, 1994; Clifford and Bishop, 1996; Capecchi and Bishop, 1994]. In previous studies, interest was similarly focused on non-rotating solutions of the parametrically excited pendulum but when the parameters are fixed within the main resonance zone. A recent paper by [Szemplińska-Stupnicka et al., 2000] accurately showed a detailed bifurcation structure of these oscillatory solutions in the main resonance zone together with an analysis of the stable invariant manifolds associated with rotating attractors which play a crucial role in separating the oscillating and rotating attractors in the phase plane. We extend this work by also considering oscillatory

solutions in the lower resonance zones. However, the work presented here will not consider oscillatory solutions about the vertical equilibrium which have also recently been a subject of curious interest [Acheson, 1995; Clifford and Bishop, 1998]. The equation of motion in nondimensional form (details of derivation of the equation and the appropriate scalings are given in chapter 1) can be written as

$$\theta'' + \beta\theta' + (1 + p\cos(\omega\tau))\sin(\theta) = 0 \tag{2.1}$$

where β, p and ω are the scaled forms of damping coefficient, amplitude of parametric forcing and frequency of parametric forcing respectively. For sufficiently large values of the amplitude of parametric forcing p, different types of harmonic and subharmonic oscillatory orbits can be realised depending on the frequency and the initial conditions given to the system. These harmonic and subharmonic oscillatory orbits occur in tongue-shaped regions shown in Figure 2.1 in the (ω, p) space. Figure 2.1 is a schematic non-linear version of the well-known stability diagram of the damped Mathieu equation [McLachlan, 1964] to which the equation of the parametrically excited pendulum (2.1) reduces if we set $\sin(\theta) = \theta$ (that is, after linearisation of equation (2.1) about the hanging position). The tongue-shaped regions occur around the values $(\omega, p) = (2/n, 0)$, $n = 1, 2, 3, ...$ in the parameter space. The dotted lines in Figure 2.1 show the approximate position of the resonance tongues in the (ω, p) space when $\beta = 0$. Therefore the damping acts to shift the position of the resonance tongues upwards. Throughout this chapter we shall investigate the properties of oscillatory orbits of the parametrically excited pendulum when the damping is fixed at a representative level of $\beta = 0.1$. It can be seen from Figure 2.1 that with increasing p each resonance tongue is twisted to the right and lies above the other so that for large p the resonance tongues may overlay each other.

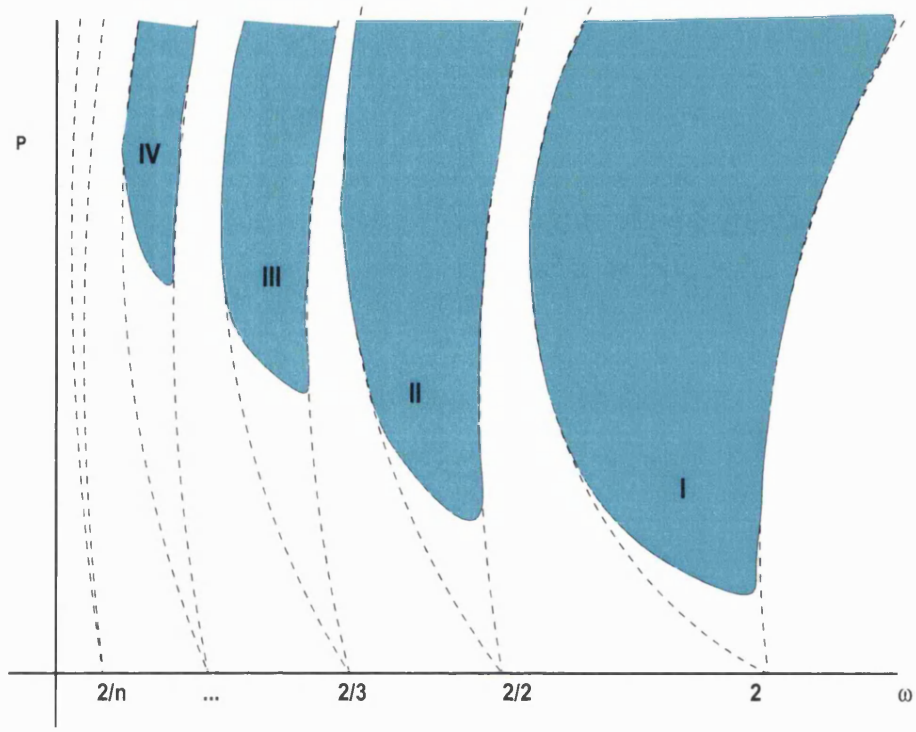

Figure 2.1: Schematic stability diagram showing both the zone of primary instability of the downward equilibrium solution marked **I** and the lower resonance zones marked **II**,**III**, **IV**. The zones are shown here for arbitrary damping. The dashed lines indicate the position of the resonance zones in the absence of damping. Inside the resonance zones the downward equilibrium solution is unstable. Typically stable solutions within these zones are oscillatory, rotating and their combination.

For (ω, p) values inside these tongues the parametrically excited pendulum is said to be in parametric resonance. Inside the resonance zones for the Mathieu equation, solutions are unbounded. However, when the nonlinearity is present, different types of periodic, subharmonic and chaotic behaviours are realised. In this case, the nonlinearity initially stabilises the oscillatory solutions for increasing p. Details of the bifurcations bounding these zones will de discussed in section 2.3.

2.2 Symmetry of the Governing Equations

The second-order differential equation (2.1) for the parametrically excited pendulum can be transformed to a system of first-order differential equations:

$$\frac{d}{d\tau}\begin{bmatrix}\theta\\ \theta'\end{bmatrix} = \begin{bmatrix}\theta'\\ -\beta\theta' - (1 + p\cos(\omega\tau))\sin(\theta)\end{bmatrix} = F(\mathbf{x}, \boldsymbol{\lambda}, \tau) \tag{2.2}$$

where $\mathbf{x} = \{\theta, \theta'\}^T$, $\boldsymbol{\lambda} = \{\beta, p, \omega\}^T$ and $F(\mathbf{x}, \boldsymbol{\lambda}, \tau) = \{\theta', -\beta\theta' - [1 + p\cos(\omega\tau)]\sin(\theta)\}^T$.

Because of the nonlinearity which is odd in θ the equation for the parametrically excited pendulum possesses the inversion symmetry

$$F(\mathbf{x}, \boldsymbol{\lambda}, \tau) = -F(-\mathbf{x}, \boldsymbol{\lambda}, \tau). \tag{2.3}$$

This symmetry property can be written in a more general way as

$$\mathbf{S}F(\mathbf{x}, \boldsymbol{\lambda}, \tau) = F(\mathbf{S}\mathbf{x}, \boldsymbol{\lambda}, \tau) \tag{2.4}$$

where S is defined to be:

$$\mathbf{S} = -\mathbf{I} = \begin{pmatrix} -1 & 0 \\ 0 & -1 \end{pmatrix} \tag{2.5}$$

Thus if an initial condition $\mathbf{x}(0)$ generates a particular solution $\mathbf{x}(\tau)$ of equation (2.2), then $\mathbf{S}\mathbf{x}(\tau)$ is a solution as well generated by the initial condition $\mathbf{S}\mathbf{x}(0)$. Furthermore, since $F(\mathbf{x}, \boldsymbol{\lambda}, \tau)$ is periodic with period $T = 2\pi/\omega$, then

$$F(\mathbf{x}, \boldsymbol{\lambda}, \tau) = F(\mathbf{x}, \boldsymbol{\lambda}, \tau + T). \tag{2.6}$$

Therefore, it follows that

$$F(\mathbf{x}, \boldsymbol{\lambda}, \tau) = -F(-\mathbf{x}, \boldsymbol{\lambda}, \tau + T). \tag{2.7}$$

Equation (2.7) means that for the parametrically excited pendulum, the Poincaré map, denoted here as:

$$P(\mathbf{x}) : \mathbb{R}^2 \rightarrow \mathbb{R}^2; \quad \mathbf{x}(\tau_0) \rightarrow \mathbf{x}(\tau_0 + 2\pi/\omega) = \mathbf{x}(\tau_0 + T) \tag{2.8}$$

has an inversion symmetry such that

$$\mathbf{S}P\mathbf{S}(\mathbf{x}) = P(\mathbf{x}) \quad \forall\ \mathbf{x} \tag{2.9}$$

where $\mathbf{S}(\mathbf{x}) = -\mathbf{x}$. If an orbit of the parametrically excited pendulum is invariant under S as represented by equation (2.9) in which the orbit of the Poincaré map P is invariant under S, then it is defined as symmetric orbit and $\mathbf{x}(\tau) = -\mathbf{x}(\tau + T)$. Otherwise it is unsymmetric in which case there exists a pair of the unsymmetric orbits defined by $\mathbf{x}(\tau)$ and $-\mathbf{x}(\tau + T)$ such that $\mathbf{x}(\tau) \neq -\mathbf{x}(\tau + T)$.

In order to gain more insight into the natural symmetries of the equation of the parametrically excited pendulum, let us briefly contrast its symmetry with that of pendulum with direct forcing. The equation for the pendulum with direct forcing can be written as

$$\frac{d}{d\tau}\begin{bmatrix} \theta \\ \theta' \end{bmatrix} = \begin{bmatrix} \theta' \\ -\beta\theta' - \sin(\theta) + p\cos(\omega\tau) \end{bmatrix} = F_1(\mathbf{x}, \boldsymbol{\lambda}, \tau) \tag{2.10}$$

where $\mathbf{x} = \{\theta, \theta'\}^T$, $\boldsymbol{\lambda} = \{\beta, p, \omega\}^T$ and $F_1(\mathbf{x}, \boldsymbol{\lambda}, \tau) = \{\theta', -\beta\theta' - \sin(\theta) + p\cos(\omega\tau)\}^T$. In the study of the natural symmetries of the pendulum with direct forcing (see [Swift and Wiesenfeld, 1984]) we construct another map:

$$P_1(\mathbf{x}) : \mathbb{R}^2 \rightarrow \mathbb{R}^2; \quad \mathbf{x}(\tau_0) \rightarrow \mathbf{x}(\tau_0 + \pi/\omega) = \mathbf{x}(\tau_0 + T/2) \tag{2.11}$$

which has an inversion symmetry such that

$$\mathbf{S}P_1\mathbf{S}(\mathbf{x}) = P_1(\mathbf{x}) \quad \forall\, \mathbf{x} \tag{2.12}$$

where $\mathbf{S}(\mathbf{x}) = -\mathbf{x}$. Thus if an orbit of the pendulum with direct forcing is invariant under $\mathbf{S}$ as represented by equation (2.12) in which the orbit of the map P_1 is invariant under $\mathbf{S}$, then it is defined as symmetric orbit and $\mathbf{x}(\tau) = -\mathbf{x}(\tau + T/2)$. Otherwise it is also unsymmetric in which case a pair of unsymmetric orbits defined by $\mathbf{x}(\tau)$ and $-\mathbf{x}(\tau + T/2)$ exist such that $\mathbf{x}(\tau) \neq -\mathbf{x}(\tau + T/2)$.

This means that for the equation of the pendulum with direct forcing we have

$$F_1(\mathbf{x}, \boldsymbol{\lambda}, \tau) = -F_1(-\mathbf{x}, \boldsymbol{\lambda}, \tau + T/2). \tag{2.13}$$

This is unlike the equation for the pendulum with parametric forcing where we have

$$F(\mathbf{x}, \boldsymbol{\lambda}, \tau) = -F(-\mathbf{x}, \boldsymbol{\lambda}, \tau + T). \tag{2.14}$$

In the case of the parametrically excited pendulum, we would expect the symmetry with respect to the transformation

$$\mathbf{x}(\tau) \rightarrow -\mathbf{x}(\tau + T/2) \tag{2.15}$$

to be generally broken for arbitrary ω and p because

$$\cos(\omega\tau) \neq \cos[\omega(\tau + T/2)]. \tag{2.16}$$

But on the contrary, we will show that for the parametrically excited pendulum the symmetry defined by the transformation $\mathbf{x}(\tau) \rightarrow -\mathbf{x}(\tau + T/2)$ survives in the resonance zones located around $(\omega, p) = (2/n, 0)$ and is only broken when n is even. For n odd the symmetry defined by the transformation (2.15) survives and is only broken for arbitrarily

large values of p. In much of the rest of this chapter we study the symmetry of the parametrically excited pendulum with respect to the transformation $\mathbf{x}(\tau) \rightarrow -\mathbf{x}(\tau + T/2)$. A symmetric orbit with respect to transformation (2.15) can be harmonic or subharmonic. In this thesis we shall differentiate between the different types of subharmonic oscillatory solutions of the parametrically excited pendulum by specifying their orders using an integer m which denotes the number of oscillations (number of local maxima in the time history) within one period of the solution. Using this proposed notation a subharmonic solution of order $1/m$ is a solution which makes m oscillations within one period of the solution. We shall show that in general $m = n$, where n is an integer which defines the value of the frequency of excitation ω around which the subharmonic solution is realised through the relationship $\omega = 2/n$. Figure (2.2) shows a typical symmetric $1/9$ subharmonic oscillatory orbit (with respect to the transformation (2.15)) of the parametrically excited pendulum of period $2T$. In this case $\mathbf{x}(\tau) = -\mathbf{x}(\tau + T/2)$. This figure was plotted for (ω, p) in the $\mathbf{IX}^{th}$ resonance zone (i.e. $(\omega, p) = (2/n, 0)$, $n = 9$).

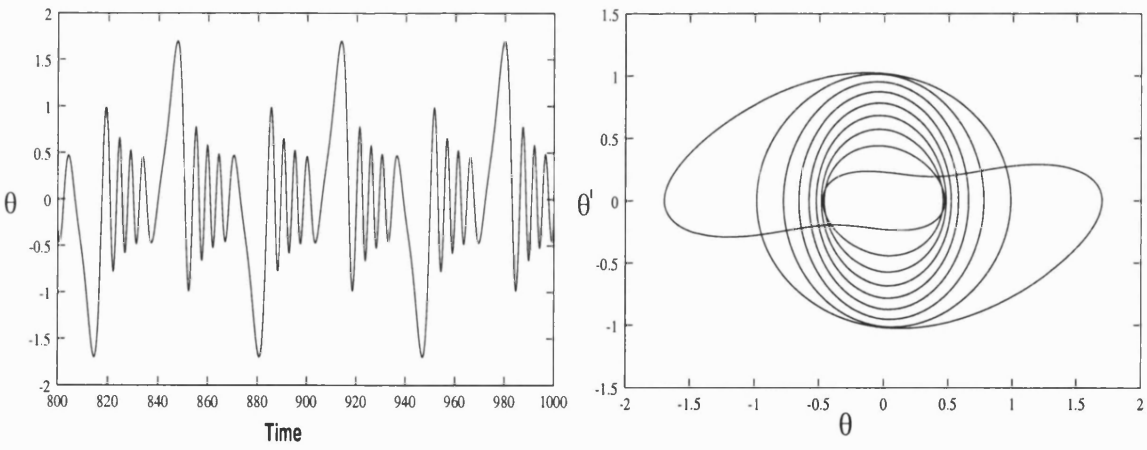

Figure 2.2: Oscillatory orbits of the parametrically excited pendulum: Symmetric $1/9$ subharmonic orbit of period $2T$, for $\omega = 0.19$ and $p = 1.1$. Left: time series of the trajectory. Right: phase space plot of the trajectory.

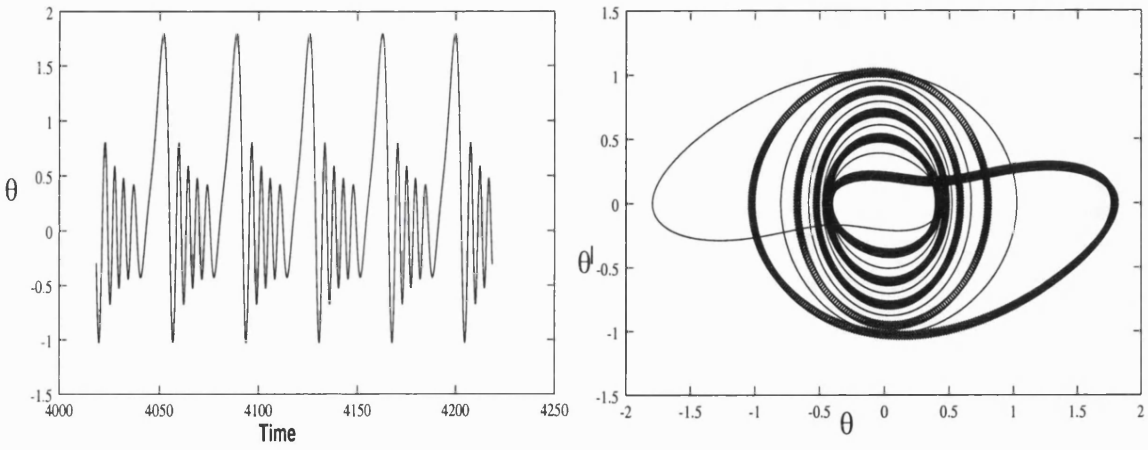

Figure 2.3: Oscillatory orbits of the parametrically excited pendulum: Unsymmetric $1/5$ subharmonic orbit of period T shown by thick line and the conjugate orbit shown thin line (obtained after applying the symmetry transformation (2.15)) for $\omega = 0.17$ and $p = 1.1$. Left: time series of the trajectory. Right: phase space plot of the trajectory.

Figure 2.3 shows an unsymmetric $1/5$ subharmonic oscillatory orbit (with respect to the transformation (2.15)) of the parametrically excited pendulum of period T. This Figure was numerically determined for (ω, p) in the $\mathbf{X}^{th}$ resonance zone (i.e. $(\omega, p) = (2/n, 0)$, $n = 10$). The thin line shows the unsymmetric orbit and the thick line shows the conjugate unsymmetric $1/5$ subharmonic oscillatory orbit obtained after applying the symmetry transformation (2.15). Here the two unsymmetric orbits are defined by $\mathbf{x}(\tau)$ and $-\mathbf{x}(\tau + T/2)$, where $\mathbf{x}(\tau) \neq -\mathbf{x}(\tau + T/2)$. In the rest of this chapter we investigate symmetry with respect to the transformation $\mathbf{x}(\tau) \rightarrow -\mathbf{x}(\tau + T/2)$.

2.3 Symmetry of the Periodic Orbits

In the (ω, p) parameter space the resonance zones in which the pendulum is in parametric resonance occur around $\omega = 2/n$, $n = 1, 2, 3, ...$

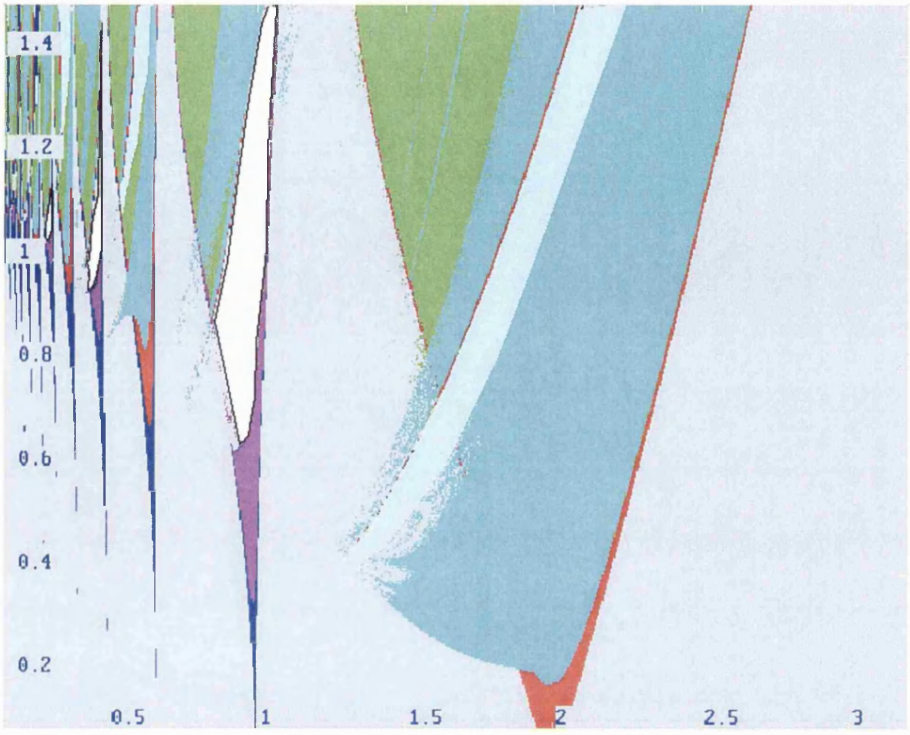

Figure 2.4: Numerically determined stability diagram showing the resonance zones where horizontal axis is $\omega \in [0.14, 3.2]$ and vertical axis is $p \in [0.1, 1.5]$. At these low values of p, nonlinear effects which cause the resonance zones to twist to the right are insignificant. The regions in cyan and white colours represents zones in the parameter space where oscillatory orbits are realised. Green regions represent zones of chaos. Outside the resonance zones dark grey regions represent zones where the downward equilibrium point is stable. Within the resonance zones sky blue strips represent regions of rotating motion.

Figure 2.4 shows some of the resonance zones in (ω, p) space which were determined numerically using the software [Nusse and Yorke, 1998]. Within these resonance zones, regions of the oscillatory motions studied in this chapter are shown by the colours cyan and white, while in the green regions tumbling chaos is realised. Outside the resonance zones the dark grey colour represents regions where the downward equilibrium is stable. The sky blue colour represent regions where rotating motions are realised. From Figure 2.4, it can be seen that we have alternating regions which are bound by red and purple lines. The red lines represent a zone of period doubling bifurcations while

the purple lines represent symmetry breaking bifurcations. The zones located around $\omega = 2/n$, $n = 1, 3, 5, ...$ are bound by the red lines. Therefore these zones are bound by period doubling bifurcations which are subcritical to the left and supercritical to the right. The zones located around $\omega = 2/n$, $n = 2, 4, 6, ...$, which are bound by purple lines are also thus bound by symmetry breaking bifurcations which are subcritical to the left and supercritical to the right.

We now consider in detail the oscillatory motions that occur in the cyan and white coloured regions. A special feature of the first two resonance zones which are located around $\omega = 2/n$, $= 1, 2$ is that stable subharmonic oscillations are rarely located in these zones. Within these two zones the dominant stable solutions are harmonic solutions which are symmetric period $2T$ and unsymmetric period T respectively as shown in Figure 2.5. Figure 2.5(a) was plotted for (ω, p) in the $\mathbf{I}^{st}$ resonance zone (i.e. $(\omega, p) = (2/n, 0)$, $n = 1$) while Figure 2.5(b) was plotted for (ω, p) in the $\mathbf{II}^{nd}$ resonance zone (i.e. $(\omega, p) = (2/n, 0)$, $n = 2$).

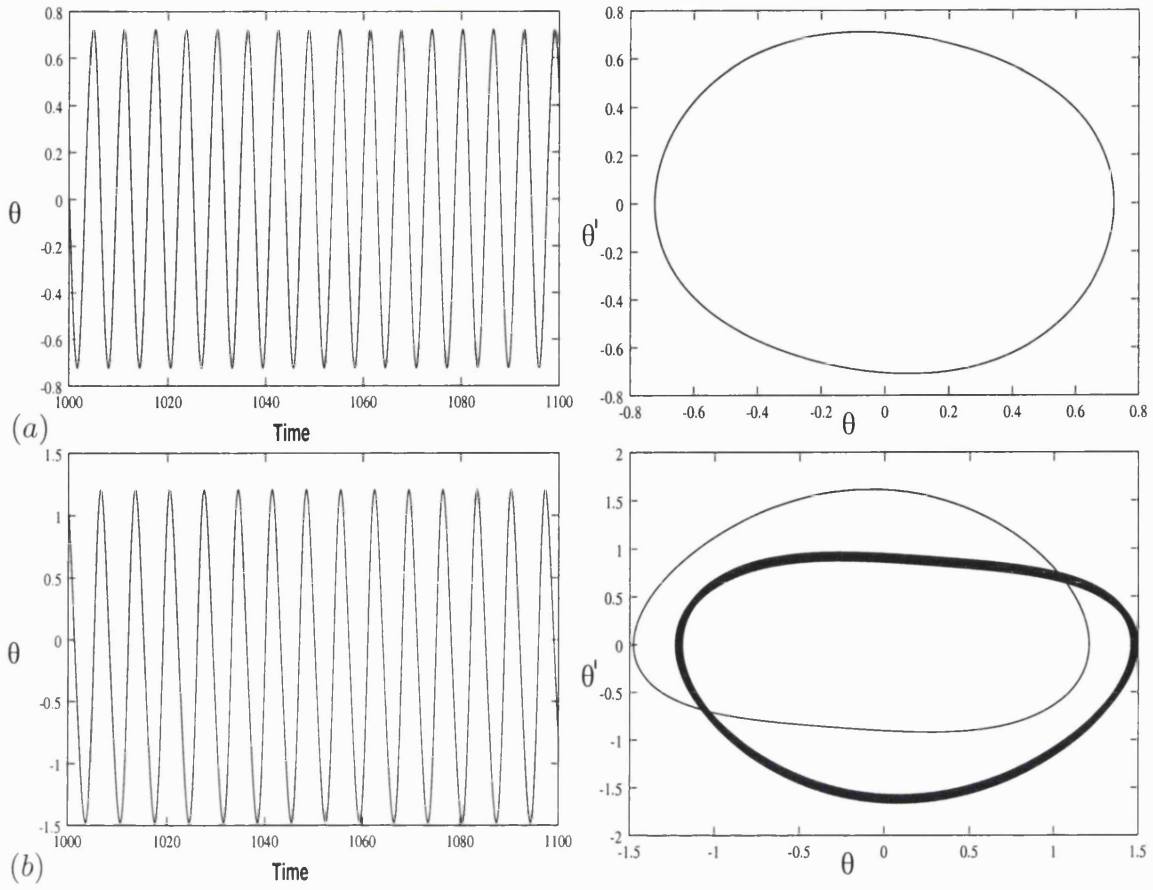

Figure 2.5: Harmonic oscillatory orbits of the parametrically excited pendulum in the first two resonance zones: (a) Symmetric orbit for $\omega = 2.0$, $p = 0.25$ with period $2T$ (parameters fixed in the first resonance zone), (b) Unsymmetric orbit (thin line) with its conjugate orbit (thick line) for $\omega = 0.9$, $p = 0.9$ with period T (parameters fixed in the second resonance zone), for initial conditions $(\theta, \theta') = (0.57, 0)$. Left: time series of the trajectories, Right: phase space plot of the trajectory.

Therefore the first and second resonance zones are regions of harmonic orbits which are symmetric period $2T$ and unsymmetric period T respectively.

Let us now consider the dynamics in the lower resonance zones (i.e. the zones located around $(\omega, p) = (2/n, 0)$, $n > 2$). Numerical simulations reveal that for n odd we have symmetric subharmonics of order $1/n$ with period $2T$. Typical examples of the symmetric orbits for n odd are shown in Figure 2.6. These $1/n$ subharmonic orbits

were numerically calculated for values of (ω, p) in the $\mathbf{VII}^{th}$ (Figure 2.6(a)), $\mathbf{V}^{th}$ (Figure 2.6(b)) and $\mathbf{III}^{rd}$ (Figure 2.6(c)) resonance zones (i.e. inside the zones located around $(\omega, p) = (2/n, 0), n = 7, 5, 3$).

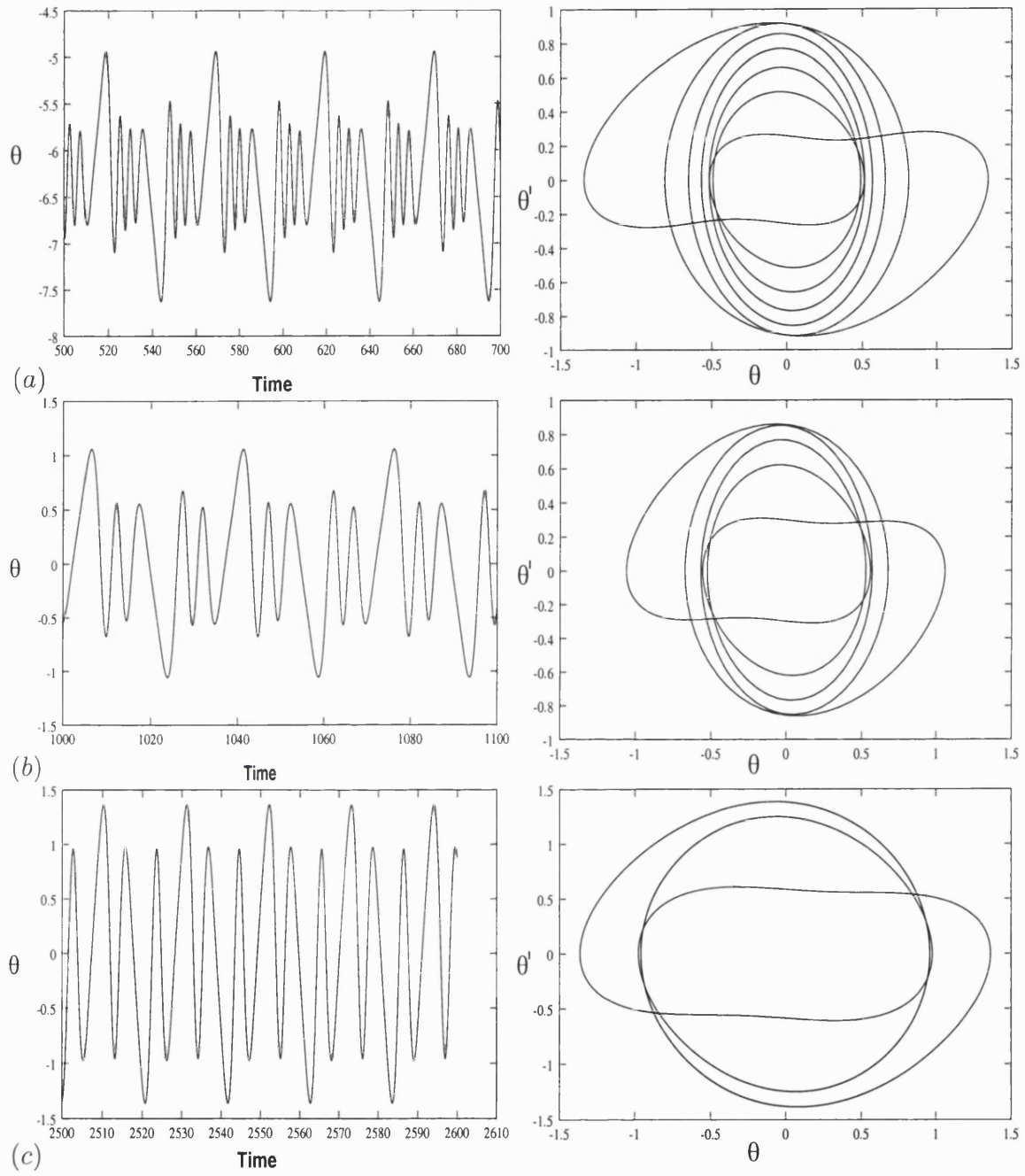

Figure 2.6: Subharmonic oscillatory orbits of the parametrically excited pendulum when n is odd for $p = 1.106$: (a) Symmetric $1/7$ subharmonic for $\omega = 0.25$, period $2T$, (b) Symmetric $1/5$ subharmonic for $\omega = 0.36$, period $2T$, (c) Symmetric $1/3$ subharmonic for $\omega = 0.60$, period $2T$, for initial conditions $(\theta, \theta') = (0.57, 0)$. Left: time series of the trajectories, Right: phase space plot of the trajectory.

Numerical simulations also show that when n is even we generally have unsymmetric subharmonics of order $2/n$ and period T. Examples of these unsymmetric orbits are shown in Figure 2.7. These $2/n$ subharmonic orbits were numerically calculated for values of (ω, p) in the $\mathbf{IV}^{th}$ (Figure 2.7(a)), $\mathbf{VI}^{th}$ (Figure 2.7(b)) and $\mathbf{VIII}^{th}$ (Figure 2.7(c)) resonance zones (i.e. inside the zones located at $(\omega, p) = (2/n, 0)$, $n = 4, 6, 8$).

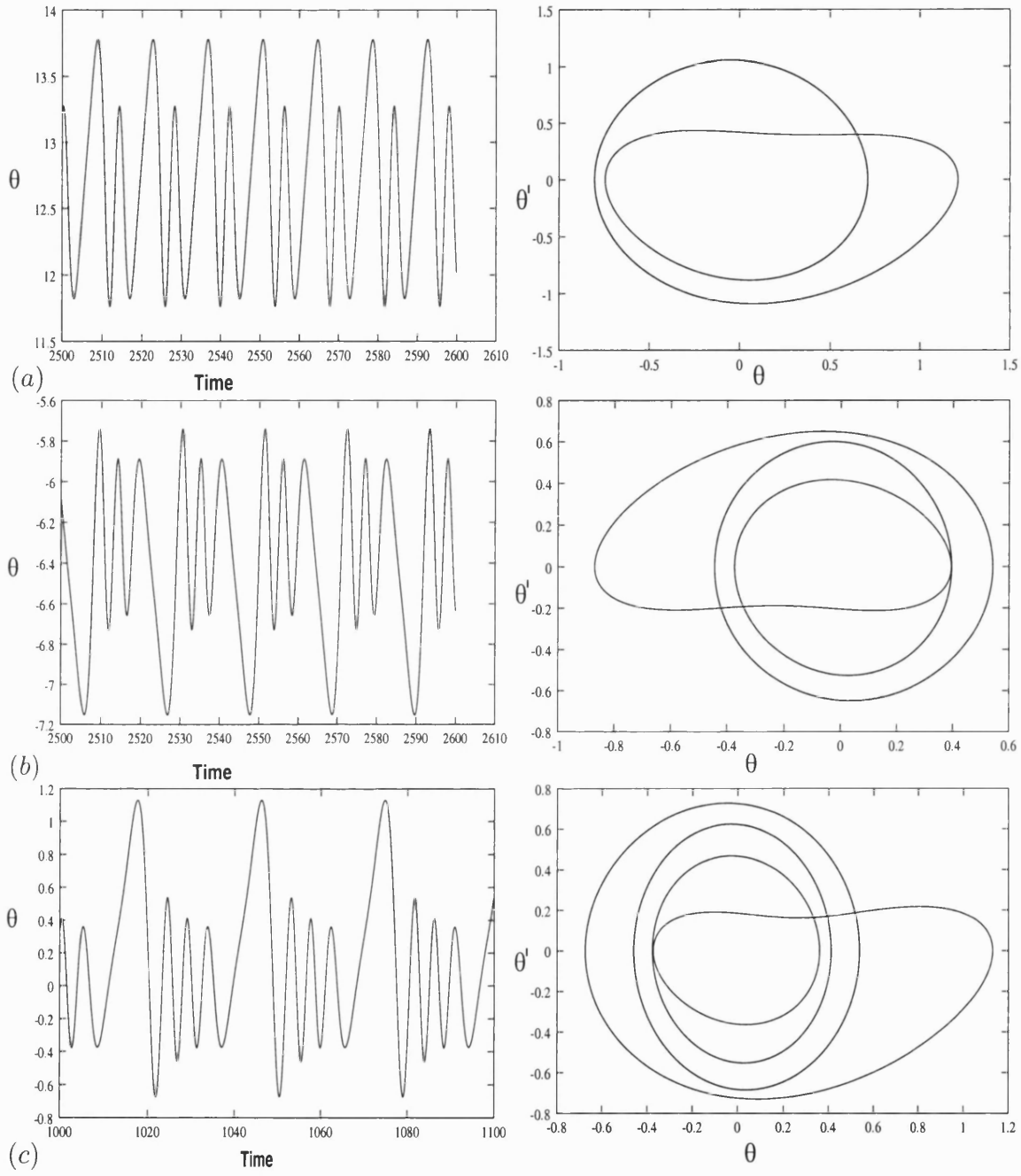

Figure 2.7: Subharmonic oscillatory orbits of the parametrically excited pendulum when n is even for $p = 1.1$: (a) Unsymmetric $1/2$ subharmonic for $\omega = 0.45$, period T (b) Unsymmetric $1/3$ subharmonic for $\omega = 0.30$, period T (c) Unsymmetric $1/4$ subharmonic for $\omega = 0.22$, period T, for initial conditions $(\theta, \theta') = (0.57, 0)$. Left: time series of the trajectories, Right: phase space plot of the trajectory.

From the results obtained we make the following observations about the significance of n:

- First, n shows the position of the resonance zone in the parameter (ω, p) space since the resonance zones in which the different harmonic and subharmonic orbits occur are located around $(\omega, p) = (2/n, 0)$, $n = 1, 2, 3, ...$ in the (ω, p) space.
- Second, n generally determines the order of the subharmonic, for example when $n = 3, 5, 7$ we have subharmonics of order $1/3$, $1/5$, and $1/7$ as shown in Figure 2.6 and when $n = 4, 6, 8$ we have subharmonics of order $1/2$, $1/3$, and $1/4$ as shown in Figure 2.7.
- Finally, n can be used to deduce the symmetry of the orbit, that is for n odd, we predominantly have symmetric orbits while for n even, we have unsymmetric orbits for which conjugate orbits exist.

2.4 Symmetry Breaking and Period Doubling Bifurcations

In this section we study the bifurcations associated with the symmetric and unsymmetric orbits of the parametrically excited pendulum as the amplitude of parametric forcing p varies. We present concrete examples of these bifurcations.

First let us consider the bifurcations associated with unsymmetric periodic orbits (that is, those found in resonance zones located around $(\omega, p) = (2/n, 0)$, were n is even number). A typical example is the bifurcation diagram shown in Figure 2.8 with $n = 6$, plotted by following an attractor. We follow stable unsymmetric $1/3$ subharmonic oscillatory period T orbit as p increases. It can be seen from Figure 2.8 that as p increases the

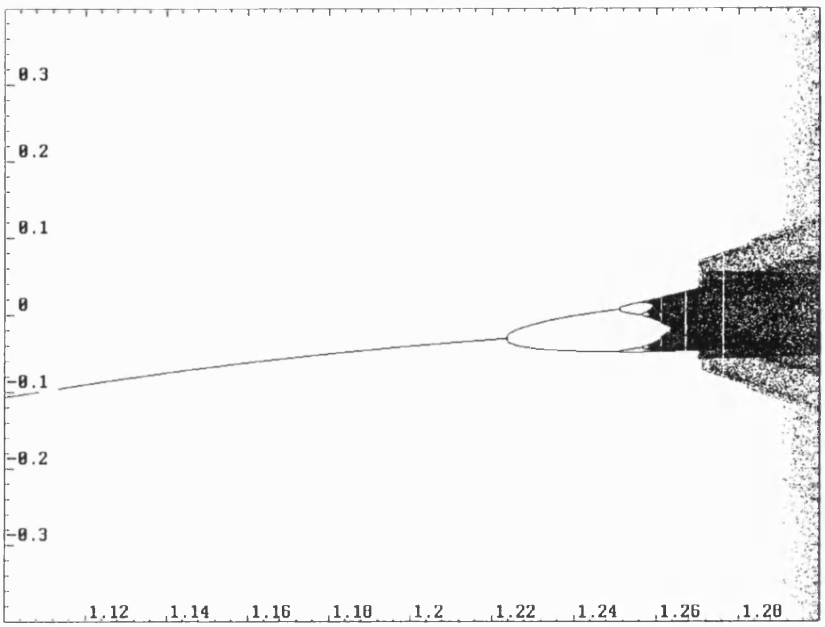

Figure 2.8: Bifurcation diagram showing transition to chaos for an unsymmetric orbit of the parametrically excited pendulum for $\omega = 0.3$, bifurcation parameter is p: Horizontal axis $p \in [1.1, 1.3]$, vertical axis $\theta \in [-0.4, 0.4]$.

unsymmetric subharmonic orbit evolves until p reaches a critical value which is about $p = 1.22$. Beyond this critical value the unsymmetric orbit undergoes a period doubling bifurcation. This period doubling bifurcation is an example of temporal symmetry breaking bifurcation because the equation of the parametrically excited pendulum is invariant under the transformation

$$[\theta, \theta', \tau] \rightarrow [\theta, \theta', \tau + T] \tag{2.17}$$

where $T = 2\pi/\omega$ is the period of the driving force. After the temporal symmetry breaking bifurcation (period doubling) a new solution appears which is period $2T$. Further increase of p results in a cascade of period doublings and transition to chaos.

Next, we consider the bifurcations associated with the symmetric orbits of the parametrically excited pendulum (that is, those found in resonance zones located at $(\omega, p) = (2/n, 0)$, where n is odd). As an example we consider the case when $n = 3$. The bifurcation diagram is shown in Figure 2.9. This diagram was plotted by following an

attractor starting with p value at $p = 1$. The symmetric $1/3$ subharmonic oscillatory orbit is period $2T$.

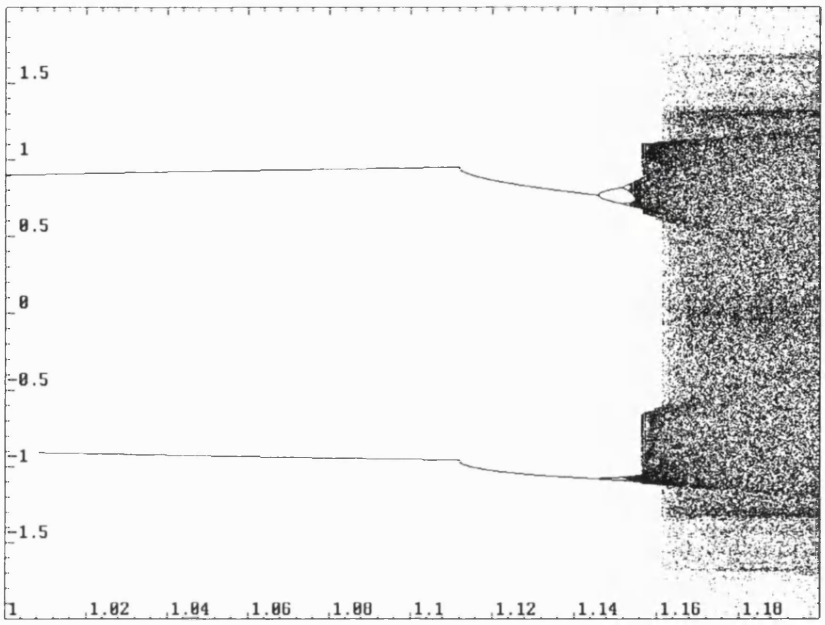

Figure 2.9: Bifurcation diagram showing transition to chaos for an symmetric orbit of the parametrically excited pendulum for $\omega = 0.6$, bifurcation parameter is p: Horizontal axis $p \in [1.0, 1.2]$, vertical axis $\theta \in [-2.0, 2.0]$.

It must be noted that in plotting this bifurcation diagram the sampling time was equal to the period of the parametric excitation, that is, $T = 2\pi/\omega$. So the $2T$ periodic attractor of the symmetric orbit is represented by two branches in this case. As p increases, the symmetric orbit undergoes a symmetry breaking bifurcation and an unsymmetric orbit appears at $p \approx 1.105$ which has the same period as the solution changing stability. After the symmetry breaking bifurcation, the unsymmetric periodic orbit undergoes a cascade of period doublings and transition to chaos as p increases.

2.5 Final Remarks

The main issues covered in this chapter include:

- A detailed study of the different harmonic and subharmonics oscillatory orbits of the parametrically excited pendulum.

- A study of the symmetry of the different harmonic and subharmonic oscillatory orbits.
- An investigation of the parameter space to show the location of the different oscillatory solutions of the parametrically excited pendulum.
- A study of the transition to chaos of the different oscillatory orbits of the parametrically excited pendulum.

Chapter 3

Rotating Orbits of the Parametrically Excited Pendulum

3.1 Introduction

In this chapter we consider rotating periodic solutions or orbits of the parametrically excited pendulum. These rotating solutions, sometimes referred to as running solutions by some authors [Bartuccelli et al., 2001; Butikov, 1999] are solutions which make complete revolutions about the pivot point. We build on the earlier work of [Clifford and Bishop, 1995] which considered rotating orbits of the parametrically excited pendulum in the first resonance zone. We shall indicate how this present work and the earlier work of [Clifford and Bishop, 1995] fit into the overall picture of the rotating motion of the parametrically excited pendulum. In this chapter we classify the steady state stable rotating solutions of the parametrically excited pendulum into four broad categories and indicate the zones in the parameter space in which the different types of rotating solutions occur. Symmetry considerations of these rotating periodic solutions will help us to distinguish between those rotating solutions which exist in conjugate pairs and those which exist as single solution.

Using the same scalings as in chapter 1, the equation governing the motion of the parametrically excited pendulum in terms of the angle θ which the pendulum makes with the vertical can be shown to be

$$\theta'' + \beta\theta' + (1 + p\cos(\omega\tau))\sin(\theta) = 0. \tag{3.1}$$

The damping coefficient is denoted by β while ω and p are the frequency of parametric forcing and amplitude of parametric forcing respectively. Several attractors exist for this simple system depending on the parameter settings and initial conditions. These include: the stationary states $(\theta, \theta') = (0, 0)$ and $(\theta, \theta') = (\pi, 0)$ (in which the pendulum simply goes up and down with the point of suspension), the oscillating solutions, the chaotic solutions and the rotating solutions which are the subject of this chapter. The stationary state $(\theta, \theta') = (0, 0)$, is generally stable except for ω, p within the tongue shaped regions shown in Figure 3.1. These tongue-shaped regions occur around the values $(\omega, p) = (2/n, 0)$, $n = 1, 2, 3, ...$ in the parameter space. The dotted lines in Figure 3.1 show the position of the resonance tongues in the (ω, p) space when $\beta = 0$. Therefore the damping acts to shift the position of the resonance zones upwards. In this chapter we shall investigate the properties of rotating orbits of the parametrically excited pendulum when the damping is fixed at a representative level of $\beta = 0.1$. The response prior to rotation corresponds to the well-known phenomenon of escape from the potential well [Clifford and Bishop, 1993, 1994; Stewart and Faulkner, 2000] which occurs in a wide variety of non-linear oscillators when a system's response crosses the maximum value of the potential energy.

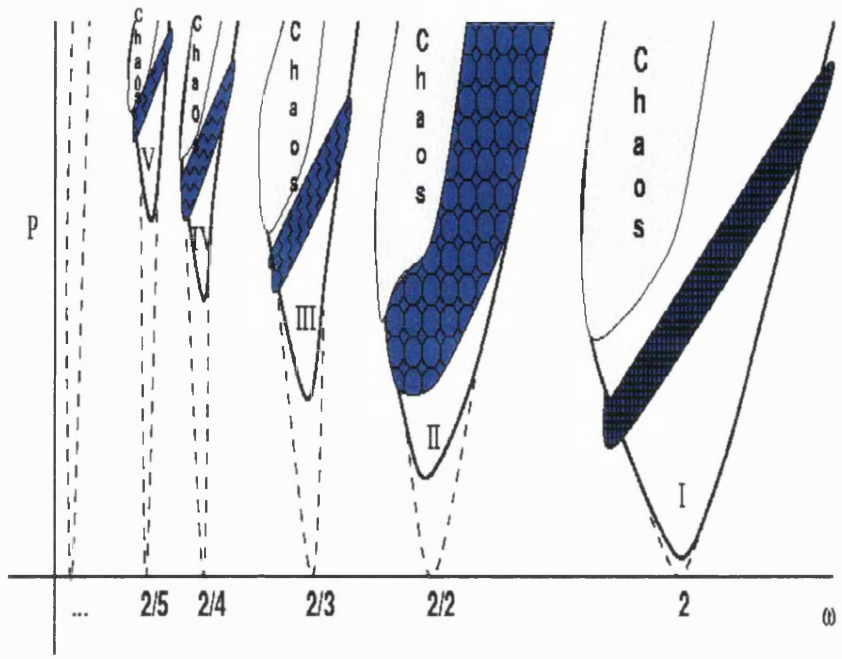

Figure 3.1: Schematic stability diagram showing the resonance zones marked **I**, **II**, **III**, **IV**, **V**, etc. Inside these resonance zones the stationary state $(\theta, \theta') = (0, 0)$ is unstable. Typically stable solutions within these zones are oscillatory, rotating and chaotic. Most rotating solutions occur within the blue narrow strips. The dashed lines indicate the position of the resonance zones in the absence of damping. Rotating solutions occur within the blue stripes.

For (ω, p) values inside these zones the parametrically excited pendulum is said to be in parametric resonance. Inside the resonance zones different types of oscillating, rotating and chaotic solutions are realised. Our focus in this chapter is explicitly on rotating solutions. With increasing p each resonance zone is twisted to the right and lies above the other so that the resonance zones may possibly merge for arbitrarily large values of p. We classify the steady state rotating orbits of the parametrically excited pendulum into four categories (see Figure 3.2 for visualisation of these solutions) as follows:

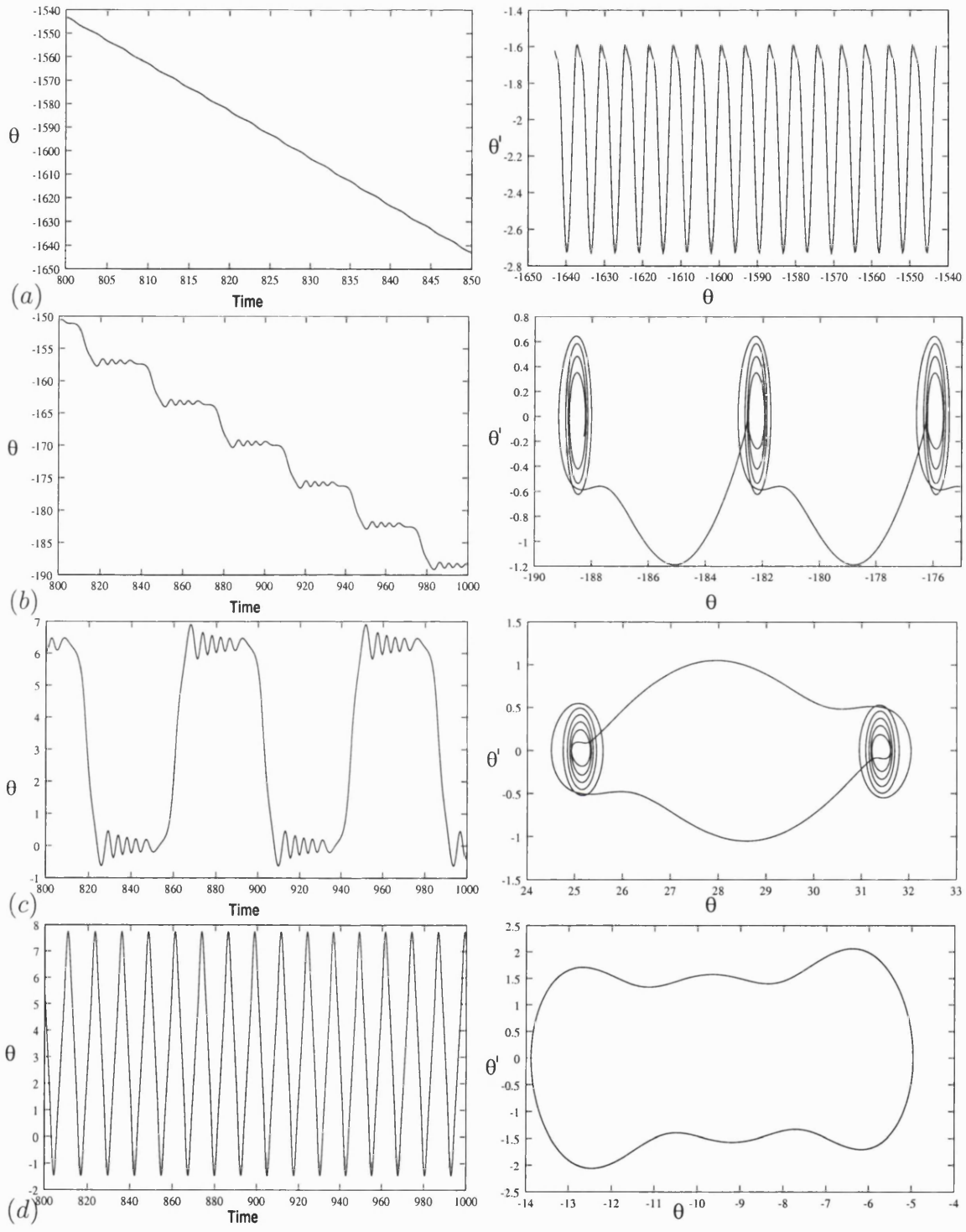

Figure 3.2: The four basic types of rotating orbits: (a) Purely rotating orbit of period T, for $\omega = 2.0$, $p = 1.17$ in zone **I**. (b) Oscillating rotating orbit of period T, for $\omega = 0.19$, $p = 1.5$ in zone **IX**. (c) Straddling rotating orbit of period $2T$, for $\omega = 0.15$, $p = 1.4$ in zone **X**. (d) Large amplitude rotating orbit of period $2T$, for $\omega = 1.0$, $p = 1.7$ in zone **II**. Left: time series of the trajectory. Right: phase space plot of the trajectory.

In Figure 3.2, transients have been allowed to decay so that, for the level of damping considered in this work, after time $\tau = 800$ units we can only view the steady state response.

(1) **Purely rotating orbits**: These rotating solutions are such that the velocity is single signed for all time, that is, either $\theta'(\tau) > 0 \ \forall\tau$ or $\theta'(\tau) < 0 \ \forall\tau$. They are the dominant type of stable rotating motion in the first resonance zone, that is, they occur around $(\omega, p) = (2/n, 0)$, $n = 1$. A typical purely rotating orbit is shown in Figure 3.2(a). These rotating orbits exist in conjugate pairs: one rotating clockwise and another rotating anti-clockwise.

(2) **Oscillating rotating orbits**: These rotating solutions are such that either average $\theta'(\tau) > 0$ or average $\theta'(\tau) < 0$. For these rotating solutions a trajectory completes a fixed number of oscillations within a potential energy well before transversing a potential maximum into the next potential energy well through rotating motion. They are the dominant stable rotating attractors within the resonance zones located around $(\omega, p) = (2/n, 0)$, $n > 2$, n odd. A typical oscillating rotating orbit is shown in Figure 3.2(b) which makes 5 oscillations before transversing into the next well through rotating motion.

(3) **Straddling rotating orbits**: These have a similar property as oscillating rotating solutions of experiencing oscillations and rotations but differ in that their response only straddles one or two or three wells. The straddling rotating solutions are the dominant stable rotating attractors within the resonance zones located around $(\omega, p) = (2/n, 0), n > 2$, n even. Figure 3.2(c) shows a typical straddling rotating solution which straddles two wells.

(4) **Large amplitude rotating orbits**: These also have similar properties as the straddling rotating solutions in that they straddle one, two or three wells but differ in that they do not make oscillations within the potential wells. They are the dominant stable rotating motions within the second resonance zone, that is the zone

located at $(\omega, p) = (2/n, 0)$, $n = 2$. A typical large amplitude rotating orbit is shown in Figure 3.2(d).

The rotating solutions occur within narrow strips shown in blue colour inside the resonance zones whose schematic representation is shown in Figure 3.1. These narrow strips are bound by lines of global bifurcations [Clifford and Bishop, 1995] and extend outside the parametric resonance zones. The study of these global bifurcations will be subject of the next chapter.

3.2 The Different Types of Rotating Orbits

In the (ω, p) parameter space the resonance zones in which the pendulum is in parametric resonance occur around $\omega = 2/n$, $n = 1, 2, 3, ...$ A schematic version of these resonance zones was shown in the previous section in Figure 3.1. As mentioned earlier on in chapter 2 the zones located around $\omega = 2/n$, $n = 1, 3, 5, ...$ are bound by period doubling bifurcations which are subcritical to the left and supercritical to the right and the zones located around $\omega = 2/n$, $n = 2, 4, 6, ...$ are bound by symmetry breaking bifurcations which are subcritical to the left and supercritical to the right.

We now consider in detail the rotating motions that occur in the blue coloured narrow strips within the resonance zones. A characteristic feature of some of the rotating motions discussed in this chapter as shown in Figure 3.2 is that they always exist in pairs: one rotating clockwise and another rotating anticlockwise. For some rotating motions there is no preferred direction of rotation. In an attempt to explain these different features of the rotating motions we will briefly consider the symmetry of the system described by equation (3.1) in this section.

First let us consider the purely rotating and the oscillating rotating solutions. A common feature of the purely rotating and the oscillating rotating solutions is that they occur in conjugate pairs which are mirror images of each other under the transformation

$$[\theta, \theta', \tau] \rightarrow [-\theta, -\theta', \tau + T/2]. \tag{3.2}$$

These conjugate pairs are such that one rotates clockwise and another rotates anticlockwise. In the case of the parametrically excited pendulum, we would expect the symmetry with respect to the transformation $[\theta, \theta', \tau] \rightarrow [-\theta, -\theta', \tau + T/2]$ to be generally broken for arbitrary ω and p because

$$\cos(\omega\tau) \neq \cos[\omega(\tau + T/2)]. \tag{3.3}$$

Numerical results show that for the parametrically excited pendulum the symmetry defined by the transformation $[\theta, \theta', \tau] \rightarrow [-\theta, -\theta', \tau + T/2]$ survives in some of the resonance zones located around $(\omega, p) = (2/n, 0)$. This accounts for the observation that the large amplitude rotating solutions and the straddling rotating solutions are symmetric with respect to this transformation and the symmetry is only broken for arbitrarily large values of p.

The purely rotating and the large amplitude rotating solutions share a common feature in that they do not involve oscillations. These solutions are the dominant stable rotating solutions in the first and second resonance zones respectively. The properties of purely rotating solutions and their subharmonics were studied in detail in [Clifford and Bishop, 1995]. The large amplitude rotating solutions are symmetric with respect to the transformation $[\theta, \theta', \tau] \rightarrow [-\theta, -\theta', \tau + T/2]$. This symmetry property is only broken for large values of the amplitude of forcing p. We want to illustrate the special features of the oscillating rotating (unsymmetric) and straddling rotating (symmetric) solutions. These two types of rotating solutions occur in the resonance zones located at values around $(\omega, p) = (2/n, 0)$, $n > 2$, in the (ω, p) space. We will verify a conjecture that in general, symmetric rotating solutions occur within the resonance zones located at $(\omega, p) = (2/n, 0)$, n even, while the unsymmetric rotating solutions occur within the resonance zones located at $(\omega, p) = (2/n, 0)$, n odd, in the (ω, p) space. For the

symmetric rotating solutions, their symmetry is only broken for p arbitrarily large.

We are interested in locating solutions in the (ω, p) space for which the symmetry property defined by the transformation $[\theta, \theta', \tau] \rightarrow [-\theta, -\theta', \tau + T/2]$ survives when the dynamics is rotational. Within these zones where this property holds, we have symmetric rotating solutions of the parametrically excited pendulum which are defined by $[\theta, \theta', \tau] = [-\theta, -\theta', \tau + T/2]$. Figure 3.3 shows typical symmetric rotating orbit of straddling type. Within the zones where the symmetry defined by the transformation $[\theta, \theta', \tau] \rightarrow [-\theta, -\theta', \tau + T/2]$ is broken we have unsymmetric rotating solutions which are defined by $[\theta(\tau), \theta'(\tau)]$ and $[-\theta(\tau + T/2), -\theta'(\tau + T/2)]$ where $[\theta(\tau), \theta'(\tau)] \neq [-\theta(\tau + T/2), -\theta'(\tau + T/2)]$. Thus, the unsymmetric rotating orbits occur in conjugate pairs. Figure 3.4 shows typical unsymmetric rotating conjugate orbits of oscillating rotating type. In this case if $[\theta(\tau), \theta'(\tau)]$ is an oscillating rotating solution of the parametrically excited pendulum with clockwise rotations, then $[-\theta(\tau+T/2), -\theta'(\tau+T/2)]$ is another oscillating rotating solution of the parametrically excited pendulum with counter-clockwise rotations. It is obvious in from the example given in Figure3.4 that $[\theta(\tau), \theta'(\tau)] \neq [-\theta(\tau + T/2), -\theta'(\tau + T/2)]$.

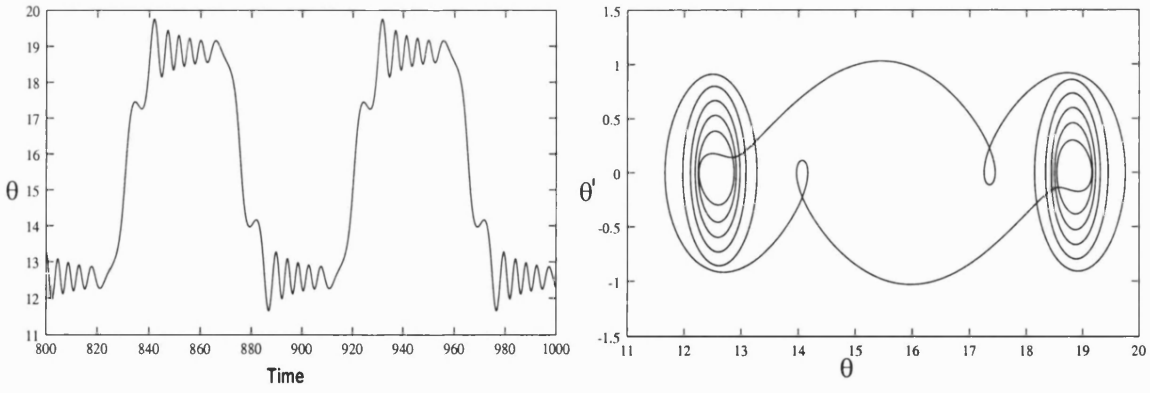

Figure 3.3: Symmetric straddling rotating orbits period $2T$, for $\omega = 0.14$, $p = 1.4$. Left: time series of the trajectory. Right: phase space plot of the trajectory.

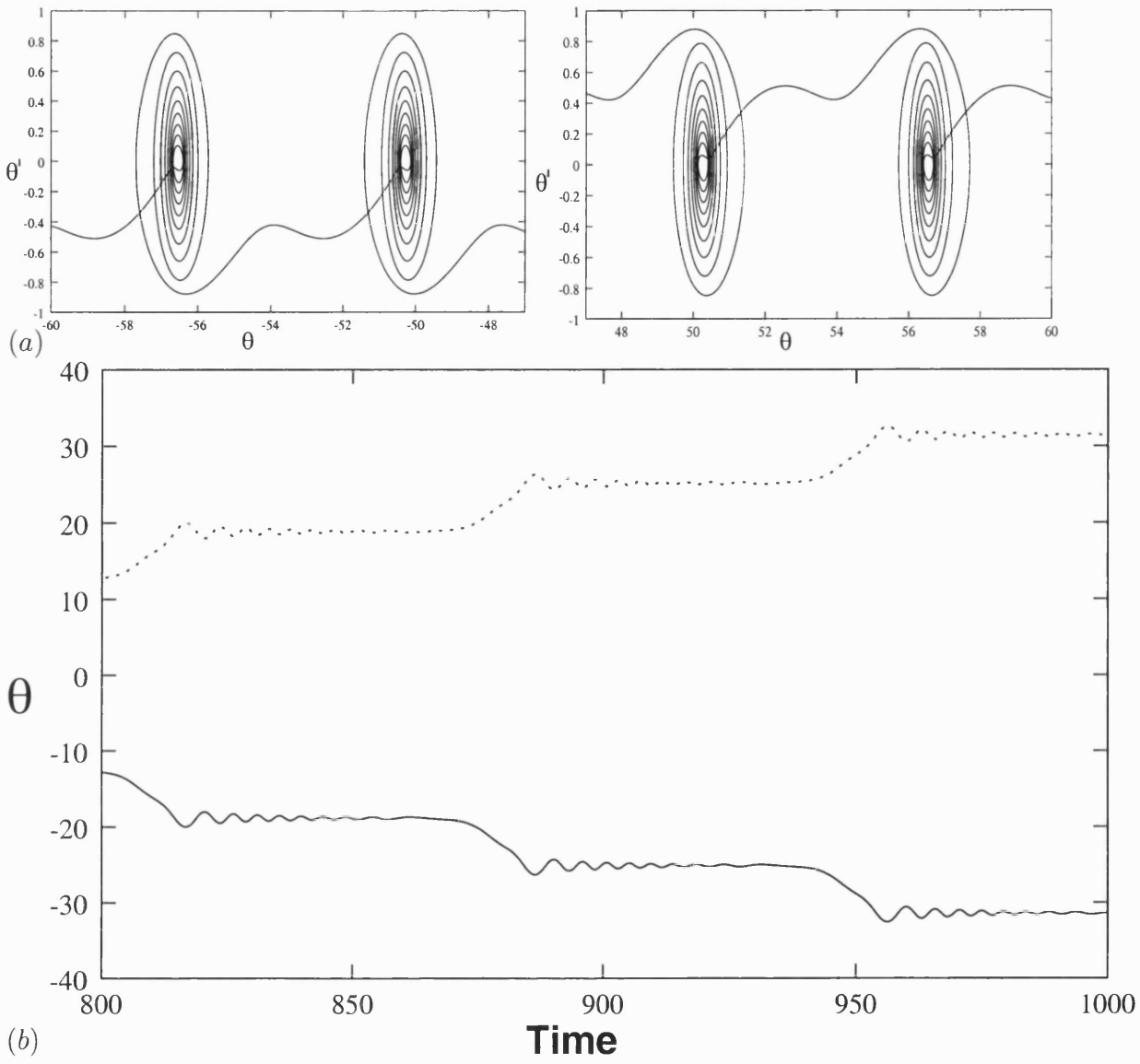

Figure 3.4: Conjugate oscillating rotating orbits period T, for $\omega = 0.09$, $p = 1.16$. (a) phase space plot of the trajectories . (b) Time series of the trajectories.

The purely rotating and the large amplitude rotating solutions share a common feature in that they do not involve oscillations. These solutions are the dominant stable rotating solutions in the first and second resonance zones respectively.

Much of the rest of this chapter will be about oscillating rotating and straddling rotating solutions. These two types of rotating solutions occur in the resonance zones located at values around $(\omega, p) = (2/n, 0)$, $n > 2$, in the (ω, p) space. Within these

resonance zones the dominant stable rotating solutions are the straddling rotating (symmetric) and the oscillating rotating (unsymmetric) solutions. We will verify a conjecture that in general, symmetric rotating solutions occur within the resonance zones located at $(\omega, p) = (2/n, 0)$, n even, while the unsymmetric rotating solutions occur within the resonance zones located at $(\omega, p) = (2/n, 0)$, n odd, in the (ω, p) space.

First let us consider the straddling rotating orbits. These occur within the zones located around $(\omega, p) = (2/n, 0)$, $n > 2$, n even. Typical examples of these symmetric orbits for n even are shown in Figure 3.5. These straddling rotating orbits were numerically calculated for values of (ω, p) in the $\mathbf{IV}^{th}$ (Figure 3.5(a)), $\mathbf{VI}^{th}$ (Figure 3.5(b)) and $\mathbf{VIII}^{th}$ (Figure 3.5(c)) resonance zones (i.e. inside the zones located around $(\omega, p) = (2/n, 0)$, $n = 4, 6, 8$).

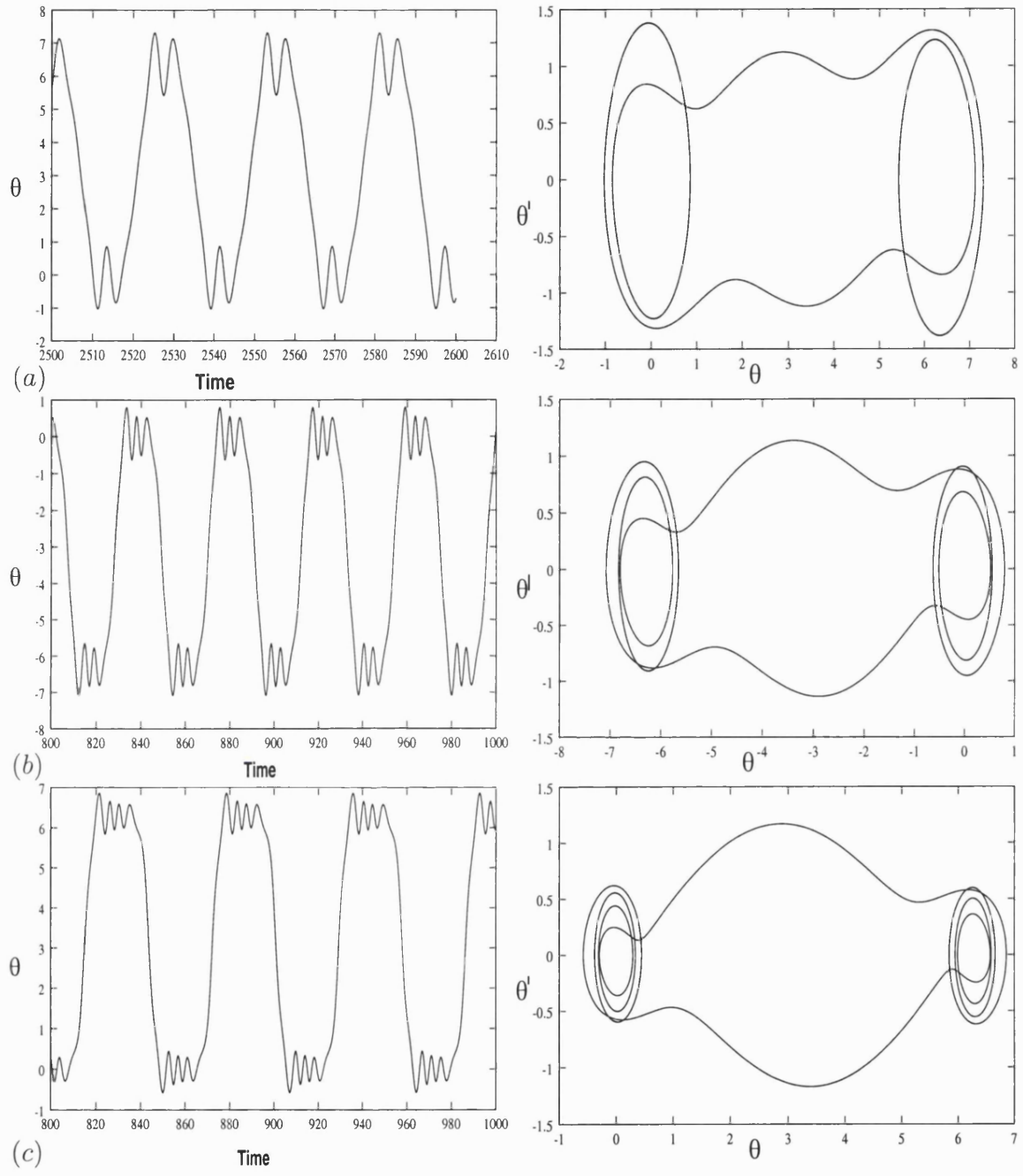

Figure 3.5: Straddling rotating orbits of the parametrically excited pendulum for $p = 1.5$ with frequency of forcing (a) $\omega = 0.45$, (b) $\omega = 0.30$, (c) $\omega = 0.22$ for initial conditions $(\theta, \theta') = (0.57, 0)$. Left: time series of the trajectories, Right: phase space plot of the trajectory. All the orbits are period $2T$. Here the two potential-wells are located at points $(\theta, \theta') = (\pm 2m\pi, 0)$, $m = 0, 1, 2, ...$ in the phase plane.

It is evident from Figure 3.5 that as ω decreases, the number of oscillations within each well decreases for the straddling rotating attractors. For example in Figure 3.5 we have 2 oscillations in the local potential energy well for $\omega = 0.45$, three oscillations for $\omega = 0.30$ and 4 oscillations for $\omega = 0.22$. These rotating solutions are symmetric with respect to the transformation formation $[\theta, \theta', \tau] \rightarrow [-\theta, -\theta', \tau + T/2]$, and the symmetry is only broken for large values of p.

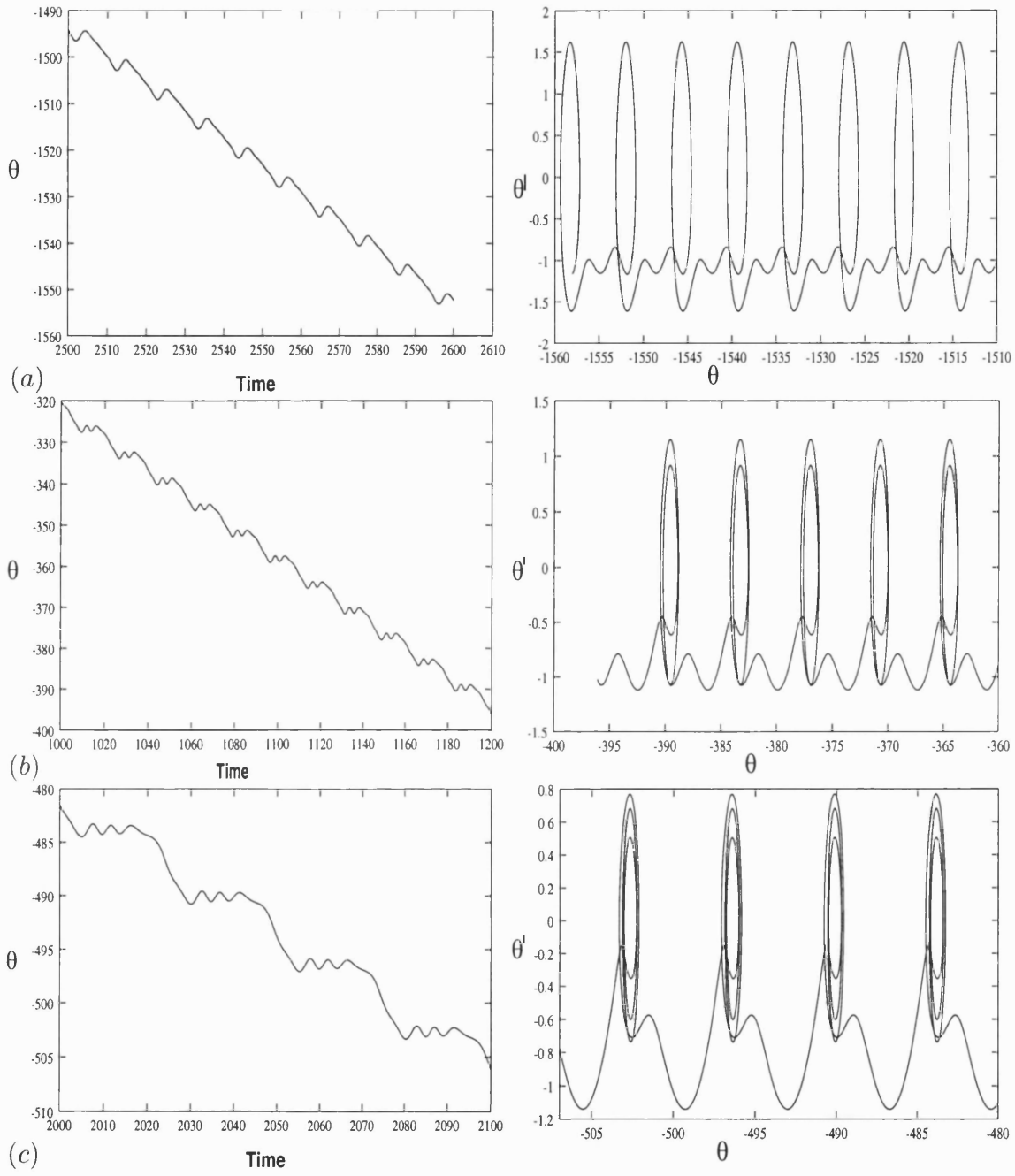

Figure 3.6: Oscillating rotating solutions for $p = 1.5$ with frequency of forcing (a) $\omega = 0.60$, (b) $\omega = 0.36$, (c) $\omega = 0.25$ for initial conditions $(\theta, \theta') = (1.57, 0)$. Left: time series of the trajectories, Right: phase space plot of the trajectory. Here all the rotating orbits are period T.

Let us consider rotating solutions which occur in the resonance zones located at $(\omega, p) = (2/n, 0)$, $n > 2$, n odd. Numerical simulations also show that when n is odd we have

unsymmetric rotating solutions (oscillating rotating type) of period T. Examples of these unsymmetric rotating orbits are shown in Figure 3.6. These oscillating rotating orbits were numerically calculated for values of (ω, p) in the $\mathbf{III}^{th}$ (Figure 3.6(a)), $\mathbf{V}^{th}$ (Figure 3.6(b)) and $\mathbf{VII}^{th}$ (Figure 3.6(c)) resonance zones (i.e. inside the zones located at $(\omega, p) = (2/n, 0)$, $n = 3, 5, 7$). It can be seen from Figure 3.6 that the number of oscillations in each well before rotation takes place increases as ω decreases (one oscillation in the well for $\omega = 0.6$, two oscillations for $\omega = 0.36$ and three oscillations for $\omega = 0.25$). These rotating solutions occur in conjugate pairs: one for which the average $\theta'(\tau) > 0$ and another for which average $\theta'(\tau) < 0$.

3.3 Other Rotating Orbits

The rotating solutions we have discussed so far are the dominant stable periodic rotating attractors of the parametrically excited pendulum in the (ω, p) space for lower values of p (typically $p < 2$). In this case we have seen that the lower resonance zones (those located around $(\omega, p) = (2/n, 0)$, $n > 2$) are alternating regions of stable oscillating rotating and straddling rotating solutions. The most obvious change for higher values of p (typically $p > 2$) is that new variants of straddling rotating solutions (those which straddle one or two wells) are realised and those which straddle two well (in the case of $p < 2$) become unstable.

For lower values of the amplitude of parametric forcing $p < 2$, the resonance zones are separated by regions in which the stationary solution is stable. In this case the boundaries between the different resonance zones are distinct. However, for higher values of $p > 2$ the stationary solution becomes unstable and the boundaries between the different resonance zones become less distinct. In this case it becomes difficult to designate a particular rotating solution as belonging to a particular resonance zone. For these higher values of p, it becomes more convenient to treat the whole parameter space as a continuous single resonance zone with different regions representing different

dynamical behaviours.

For $p > 2$ different new types of straddling rotating attractors become stable. Figure 3.7 shows straddling rotating solutions which only straddle one well. Just as in the case of $p < 2$, it can be seen from Figure 3.7 that the number of oscillations increase as ω decreases (3 oscillations in the well for $\omega = 0.6$, 5 oscillations for $\omega = 0.36$ and 7 oscillations in the well for $\omega = 0.25$).

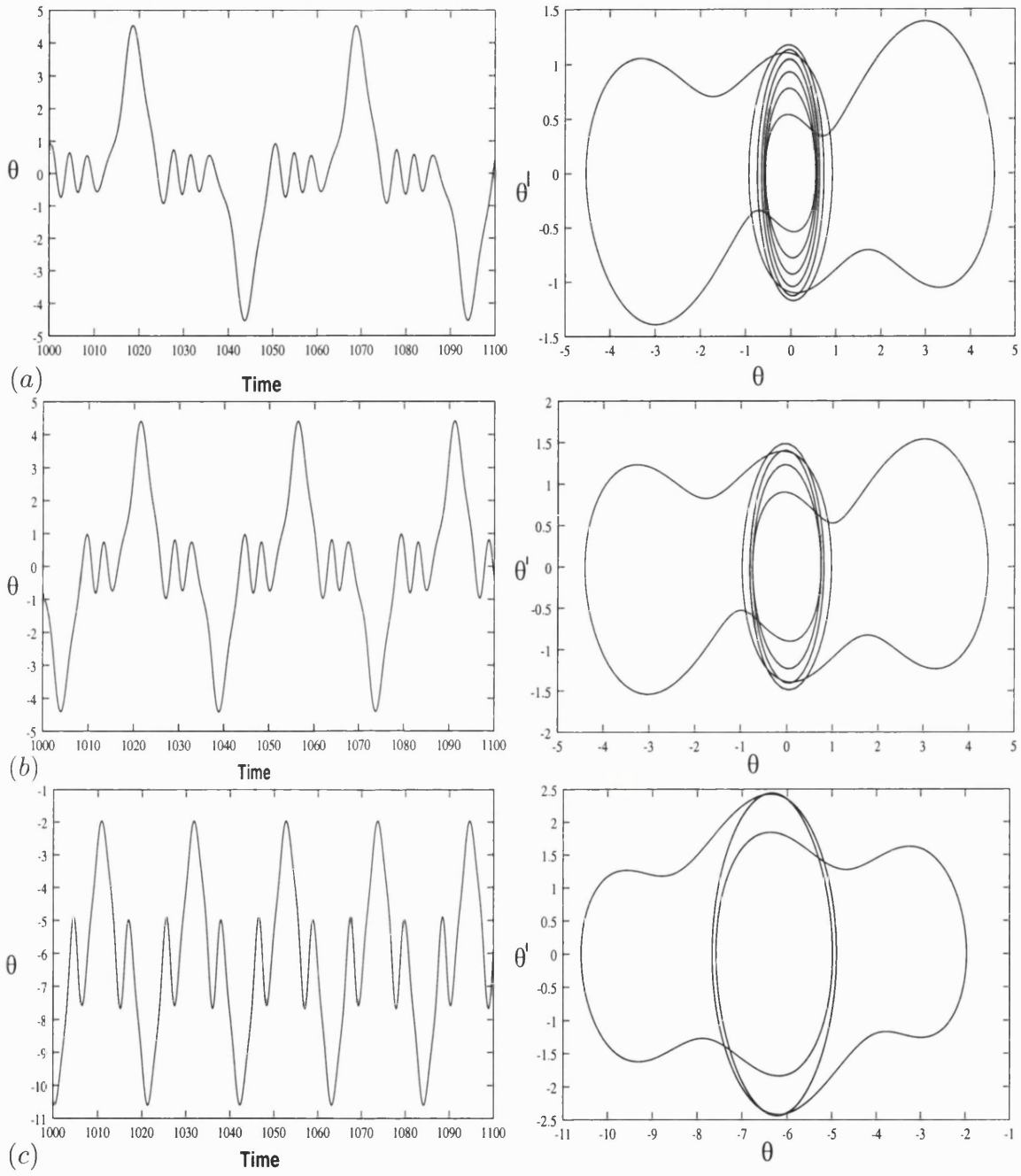

Figure 3.7: Straddling rotating motion with frequency of forcing (a) $\omega = 0.25$, $p = 2.0$, (b) $\omega = 0.36$, $p = 2.5$, (c) $\omega = 0.60$, $p = 3.0$ for initial conditions $(\theta, \theta') = (1.57, 0)$. Left: time series of the trajectories, Right: phase space plot of the trajectory. All the examples here are period $2T$.

Other straddling rotating solutions which can also be realised for higher values of are shown in Figure 3.8. Here the solutions straddle three wells.

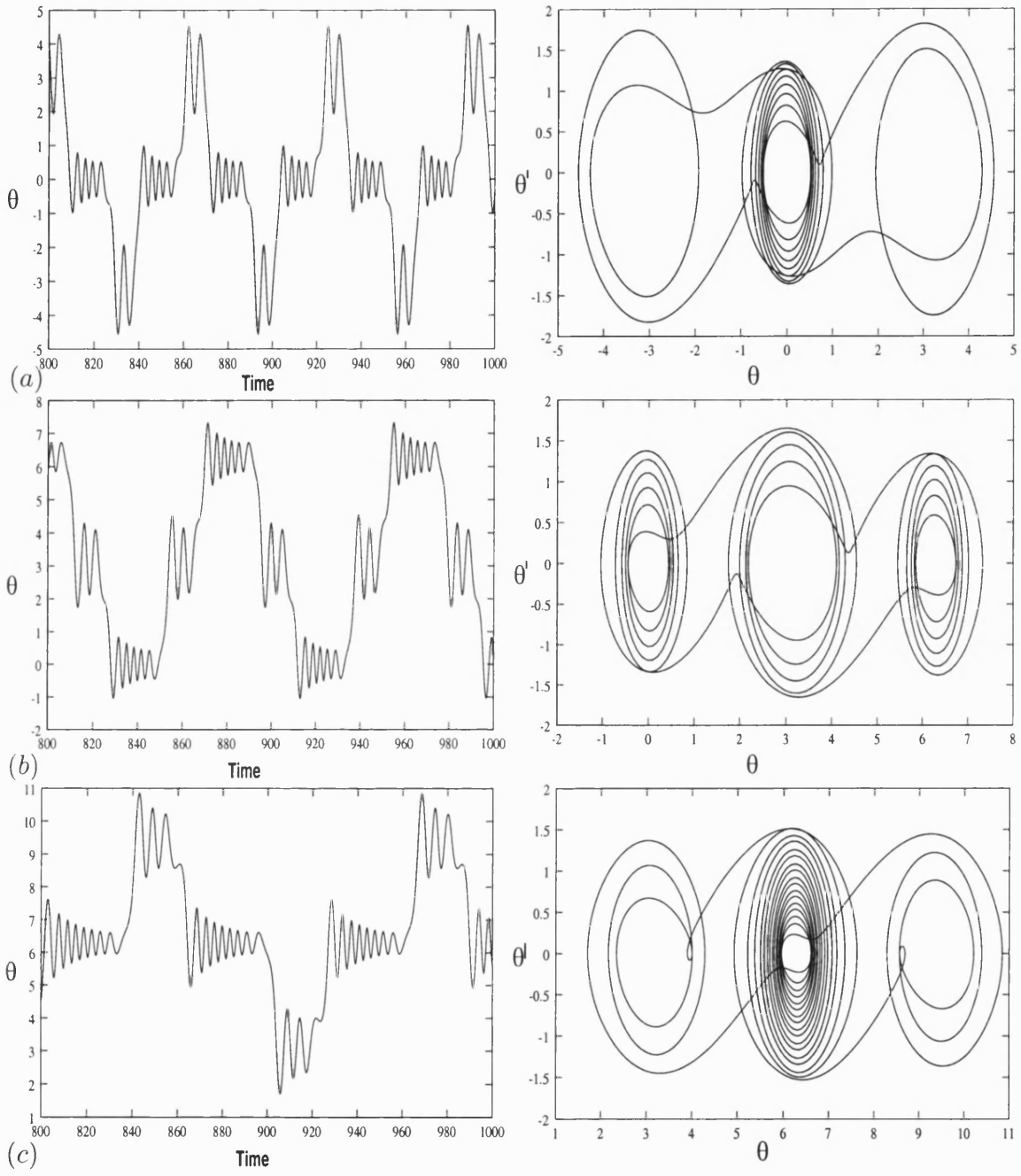

Figure 3.8: Other straddling rotating solutions (a) $\omega = 0.20$, $p = 3.1$, (b) $\omega = 0.15$, $p = 3.0$, (c) $\omega = 0.1$, $p = 2.5$. $(\theta, \theta') = (0.57, 0)$. Left: time series of the trajectories, Right: phase space plot of the trajectory. All the examples here are period $2T$.

3.4 Final Remarks

We have considered the different types of rotating periodic motions of the parametrically excited pendulum in the parameter space. We have seen that within the first two resonance zones the dominant stable rotating solutions do not involve oscillations in the local potential energy wells while in all other resonance zones the rotating solutions involve oscillations within local potential energy wells. Numerical evidence has been presented which shows that the lower resonance zones are alternating regions in which we realise symmetric and nonsymmetric rotating solutions.

The main issues covered in this chapter are:

- A classification of the different rotating solutions of the parametrically excited pendulum .
- An investigation of symmetry of the different rotating solutions.
- A study of the parameter space to determine the location of the different rotating solutions.

Chapter 4

Chaos in the Parametrically Excited Pendulum

4.1 Introduction

Chaotic solutions represent another class of response of dynamical systems. In this chapter we explore different chaotic solutions of the parametrically excited pendulum. It is not easy to prove that a given dynamical response is indeed chaotic, in the technical sense of the word as defined for example in [Wiggins, 1990; Devaney, 1992]. Over the past few years the Melnikov method [Koch and Leven, 1985; Nayfeh and Balachandran, 1995; Wiggins, 1988] has been used to analyse if chaotic responses may occur in a particular dynamical system. In connection with this Lyapunov exponents [Jackson, 1991; Sano et al., 1985] have been used to evaluate if an observed dynamical response is indeed chaotic. The rule of thumb here is that one can regard the dynamics on a bounded set as chaotic if there is a positive Lyapunov exponent [Thompson and Stewart, 2002; Sano et al., 1985]. But the mere positivety of Lyapunov exponents is only necessary but not sufficient condition.

In the study of chaos one area of research which has been actively pursued by scientists is how nonlinear dynamical systems may evolve toward the chaotic dynamical state. At the centre of this problem is the following question: Given a dynamical system with only nonchaotic, stable, time-asymptotic states, how do chaotic attractors arise from

these states as some parameter of the system is varied? It has since been shown that there are many different scenarios for transition to the chaotic state [Devaney, 1992] for dynamical systems when an appropriate parameter is varied. These scenarios include:

(a) **The period-doubling sequence**: The period doubling transition to chaos is the most easily identifiable route to chaos for a dynamical system. For this reason experimental researchers attempting to identify and study chaos in real systems are often drawn to look for period doubling cascades [Lepers et al., 1991; Arecchi et al., 1982; Bielawski et al., 1993; Kocarev et al., 1993]. In the period doubling scenario, as a parameter is gradually varied, we proceed from a periodic solution to a chaotic solution through a sequence of period-doubling bifurcations. This type of transition to chaos is associated with local bifurcations. In the period doubling transition to chaos, the bifurcations become more and more closely spaced, the ratio of successive parameter intervals tending to the Feigenbaum number $\delta_\infty = 4.669201$ [Feigenbaum, 1978]. This number is universal in the sense that it arises in a wide class of problems.

(b) **The intermittency mechanism**: Another route to chaos which is observed frequently in physical experiments is the onset of chaos via intermittency. It is a complex steady-state motion involving irregular switchings between periodic and chaotic behaviour [Sen, 2001; Kim et al., 1997]. In this case the dynamical system is periodic for long stretches but is subjected to seemingly random chaotic outbursts at irregular intervals. In between these chaotic bursts the system resumes its periodic behaviour. Thus even though the system drifts away from the periodic state, it is quickly re-injected into it.

(c) **The quasiperiodic route**: There are several types of quasiperiodic routes to chaos [Nayfeh and Balachandran, 1995], some of them not yet fully understood [Yang, 2000; Pazó et al., 2001]. They occur when a multi-frequency quasiperiodic flow destabilises. For example, if a flow arises with a two-frequency

quasiperiodicity, the destabilisation of a third incommensurate frequency is supposed instantly to create a chaotic flow [Grebogi et al., 1983a].

(d) **Crises**: In some cases the period doubling route to chaos may also involve a crisis bifurcation. Three types of crises are described in [Grebogi et al., 1986, 1983b]. In the first type, a chaotic attractor is suddenly destroyed as the parameter passes through its critical value. In the second type, the size of the chaotic attractor in phase space suddenly increases. This type of crises was later on called an explosion [Thompson and Stewart, 2002] to emphasise the fact that the change in the size of the attractor is discontinuous. In the third type, two more chaotic attractors merge to form one chaotic attractor. In [Grebogi et al., 1986] the authors note that in this third type of crises the attractors collide simultaneously with the basin boundary and that this can be expected only in systems which have symmetry or other special property.

Most of the studies on transition to chaos have been helpful to characterise the boundaries between periodic and chaotic responses. In this chapter we take a different approach and characterise the boundaries, not only between periodic and chaotic responses, but also between different types of chaotic response. From an engineering point of view this is a very attractive viewpoint because this might lead to applications making use of multiple types of chaos arising in a system, such as a vibration machine that can provide various chaotic vibrations without significant change of its mechanical structure. The distinct chaotic responses of the parametrically excited pendulum were identified by [Bishop and Clifford, 1996a]. These are:

(1) **Oscillating chaos**: This is chaotic motion in which the parametrically excited pendulum undergoes non-periodic oscillations whose amplitude is less that 2π, that is, $\mid \theta \mid < \pi$. See Figure 4.11 for a typical oscillating chaotic trajectory and the associated attractor.

(2) **Rotating chaos**: This is chaotic motion in which the parametrically excited pendulum undergoes continuous rotating motions with different angular velocities.

Here the rotating chaos is such that the velocity is single signed for all time, that is, either $\theta'(\tau) > 0\ \forall t$ or $\theta'(\tau) < 0\ \forall \tau$, but its value changes chaotically as the pendulum goes through one rotation to the next. Thus due to symmetry we can have clockwise rotating chaos or anticlockwise rotating chaos. See Figure 4.5 for a typical rotating chaotic trajectory and the associated attractor.

(3) **Tumbling chaos**: This is chaotic motion in which the parametrically excited pendulum undergoes a complicated combination of oscillations and rotations. See Figure 4.6 for a typical tumbling chaos trajectory and the associated attractor.

We do not claim to have proved that these three types of dynamical response of the parametrically excited pendulum are indeed chaotic in the technical sense of the word such as for example in [Wiggins, 1990]. By the word chaos here we mean bounded limit sets on which the dynamics is not asymptotically periodic or quasiperiodic. In any case the results of this chapter still hold.

4.2 Transition to Tumbling Chaos

For the parametrically excited pendulum the tumbling chaos exits in a reasonably large region of the parameter space. In the parameter space the regions of chaotic dynamics are within the resonance zones located around $(\omega, p) = (2/n, 0)$, $n = 1, 2, 3, ...$ Figure 4.1 shows the numerically determined resonance zones using the software [Nusse and Yorke, 1998].

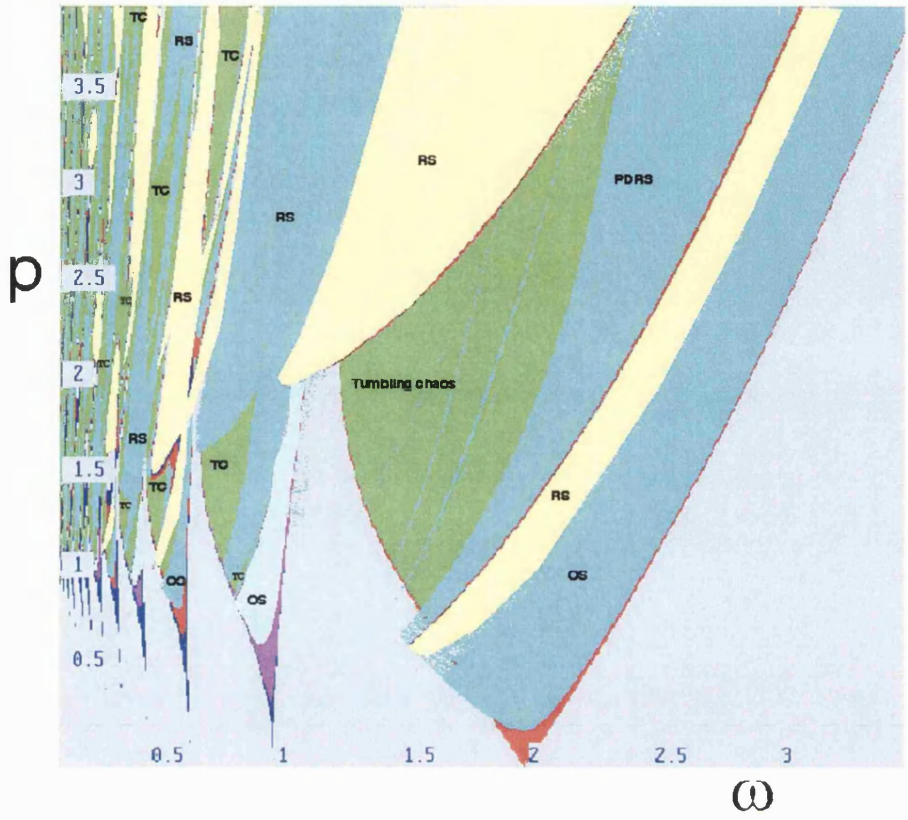

Figure 4.1: Regions of tubling chaos are coloured green and are marked **TC**. Other regions are zones of rotating and oscillating periodic solutions. In the first resonance zone the region of period doubled rotating solutions is marked **PDRS**. The regions in yellow marked **RS** represents the parameter space where rotating solutions are realised. The regions marked **OS** is where oscillating solutions are realised.

Within the resonance zones, regions of chaos are coloured green and are marked **TC**. Regions coloured otherwise are for rotating and oscillating periodic solutions (marked **RS** and **OS** respectively). The region in the first resonance zone marked **PDRS** is the zone of period doubled rotating solutions.

The robust feature of the chaotic solutions of tumbling type was confirmed by [Doreen, 1997] in the relevant zone in the parameter space by a numerical computation of the Lyapunov dimension, which is a measure of the fractal nature of the corresponding attractor. More recently [Szemplińska-Stupnicka et al., 2000] considered transient tumbling

chaos. Using the same scaling as in chapter 1 the equation governing the motion of the parametrically excited pendulum in terms of the angle θ which defines its configuration can be shown to be

$$\theta'' + \beta\theta' + (1 + p\cos(\omega\tau))\sin(\theta) = 0. \tag{4.1}$$

In this equation β is the damping while ω and p are the frequency of parametric forcing and amplitude of parametric forcing respectively. We use a representative value of β fixed at $\beta = 0.1$.

In this chapter we investigate the transition from periodic solutions to tumbling chaos in the parametrically excited pendulum. The periodic solutions could be oscillating or rotating. We define oscillating periodic solutions to mean those for which $\mid \theta \mid \leq \pi$ (oscillation about the downward equilibrium), and rotating periodic solutions to mean those for which $\mid \theta \mid \geq \pi$. As the driving amplitude, p is increased two routes to tumbling chaos are shown to exist. These two routes to tumbling chaos take place in stages and are related to the initial periodic solutions. For an initial rotating periodic solution the transition to tumbling chaos involves two stages: The first stage is transition from period doubled rotating solution to rotating chaos. The second stage involves transition from rotating chaos to tumbling chaos. This latter transition takes place as a result of an explosion of the attractor [Robert et al., 2000; Endo et al., 2000] of rotating chaos. These stages of transition to tumbling chaos are shown schematically in Figure 4.2.

If an initial periodic solution is oscillatory the transition to tumbling chaos involves three stages: The first stage involves transition from period doubled oscillations to unsymmetric oscillating chaos with a small attractor. The second stage involves transition from small attactor unsymmetric oscillating chaos to unsymmetric oscillating chaos with a larger attractor. This stage will be shown to occur as a result of attractor collision of the

conjugate attractors [Dellnitz and Heinrich, 1995; Grebogi et al., 1987] of the unsymmetric oscillating chaos. It is manifested by a sudden increase in the size of the chaotic attractor to more or less the size of the two conjugate attractors. The third and final stage involves transition from oscillating chaos to tumbling chaos. This latter transition again arises as a result of attractor explosion.

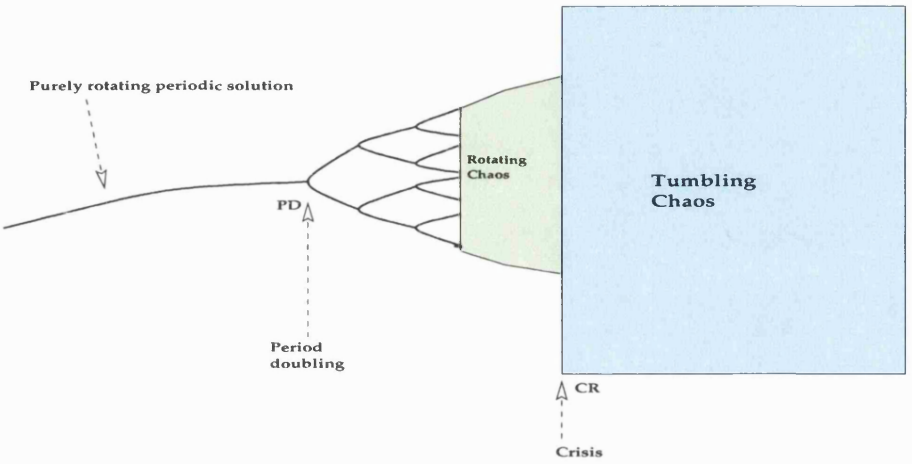

Figure 4.2: Schematic diagram showing transition to tumbling chaos for an initially purely rotating solution.

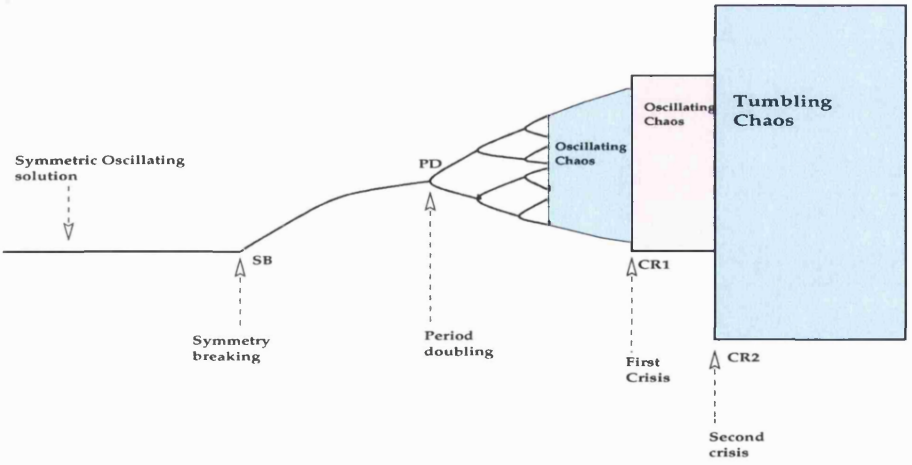

Figure 4.3: Schematic diagram showing transition to tumbling chaos for an initially oscillatory solution.

The three stages when an oscillatory solution is in transition to tumbling chaos are shown schematically in Figure 4.3.

At the heart of this chapter is the observation that both oscillating chaos and rotating chaos are generally unsymmetric chaos while tumbling chaos is symmetric chaos and that the two types of unsymmetric chaos lose stability at an attractor explosion, which is a symmetry restoring bifurcation. The rest of this chapter is organised as follows: In section 4.3 we discuss the concept of symmetry of a chaotic attractor. Results on transition to tumbling chaos of rotating periodic solutions are presented in section 4.4. In section 4.5 we discuss the results on transition of oscillating solutions to tumbling chaos. We give concluding remarks in section 4.6.

4.3 Symmetry of Chaotic Attractors of the Parametrically Excited Pendulum

In this section we define the concept symmetry of chaos or of a chaotic attractor. Our approach in seeking to define a symmetric and unsymmetric chaotic attractor is to consider first some suitable maps generated by the equation of the parametrically excited pendulum and then use these maps to define the symmetry of their ω-limit sets. We will assume that if these ω-limit sets are attracting then they correspond to attractors (including the chaotic attractors which are the subject of this chapter) of the equation of the parametrically excited pendulum. The second-order differential equation (4.1) for the parametrically excited pendulum can be transformed to a system of first-order differential equations:

$$\frac{d}{d\tau}\begin{bmatrix}\theta\\ \theta'\end{bmatrix} = \begin{bmatrix}\theta'\\ -\beta\theta' - (1 + p\cos(\omega\tau))\sin(\theta)\end{bmatrix} = F(\mathbf{x}, \boldsymbol{\lambda}, \tau), \qquad (4.2)$$

where $\mathbf{x} = \{\theta, \theta'\}^T$, $\boldsymbol{\lambda} = \{\beta, p, \omega\}^T$ and $F(\mathbf{x}, \boldsymbol{\lambda}, \tau) = \{\theta', -\beta\theta' - [1 + p\cos(\omega\tau)]\sin(\theta)\}^T$.

A periodic solution of period $T = 2\pi/\omega$, of the parametrically excited pendulum is said to be symmetric if $\mathbf{x}(\tau) = -\mathbf{x}(\tau + T/2)$. Otherwise it is unsymmetric in which case there exists a pair of the unsymmetric orbits defined by $\mathbf{x}(\tau)$ and $-\mathbf{x}(\tau + T/2)$ such that $\mathbf{x}(\tau) \neq -\mathbf{x}(\tau + T/2)$. Note that for the equation of the parametrically excited pendulum (4.2) we would expect the symmetry defined by the transformation $\mathbf{x}(\tau) \rightarrow -\mathbf{x}(\tau + T/2)$ to be generally broken because $\cos(\omega t) \neq \cos[\omega(\tau + T/2)]$. But this symmetry survives in some resonance zones and is only broken for arbitrarily large values of p. This behaviour was encounterd in chapter 2 and chapter 3 of this thesis in relationship to oscillating and rotating soltions of the parametrically excited pendulum where in some regions of the parameter space the solutions possessed symmetry which is not present in the governing equations.

When considering symmetry of periodic solutions it is enough to consider the behaviour of a single trajectory. However, for chaotic solutions, we can consider their symmetry by studying their attractors, which are limit sets. In order to do that we need to consider the limit sets of maps generated by the differential equation (4.2). One of the maps generated the above equation is the Poincaré map, denoted here as $P(\mathbf{x})$ where:

$$P(\mathbf{x}) : \mathbb{R}^2 \rightarrow \mathbb{R}^2; \quad \mathbf{x}(\tau_0) \rightarrow \mathbf{x}(\tau_0 + T), \quad T = 2\pi/\omega. \tag{4.3}$$

Because of the symmetry condition (which requires that $\mathbf{x}(\tau) = -\mathbf{x}(\tau + T/2)$ in order for a single periodic orbit to be symmetric) we can define another map of the parametrically excited pendulum to be $S(\mathbf{x})$ where

$$S(\mathbf{x}) : \mathbb{R}^2 \rightarrow \mathbb{R}^2; \quad \mathbf{x}(\tau_0) \rightarrow -\mathbf{x}(\tau_0 + T/2), \quad T = 2\pi/\omega. \tag{4.4}$$

Under the map $S(\mathbf{x})$, a symmetry breaking bifurcation of a symmetric solution looks like a period doubling bifurcation. We adopt the following definition of ω-limit sets of these two maps:

Definition 4.1 *[Melbourne et al., 1993] If X is a finite-dimensional Euclidean space, $h : X \to X$ is a continuous mapping and $\mathbf{x} \in X$ then the ω-limit set of $\mathbf{x}$ is the set $\omega(\mathbf{x})$ consisting of points $\mathbf{y} \in X$ for which there is an increasing sequence $\{n_k\}$ of positive integers such that $h^{n_k}(\mathbf{x}) \to \mathbf{y}$.*

Let us denote $\omega_S(\mathbf{x})$ and $\omega_P(\mathbf{x})$ to be the ω-limit sets of $\mathbf{x}$ generated by the maps S and P respectively. A lot is known about properties of ω-limit [Alligood et al., 1996]. Here we will discuss only two because of their relevance to our situation.

Proposition 4.1 $\omega_S(\mathbf{x}) = \omega_P(\mathbf{x}) \cup \omega_P(S(\mathbf{x}))$.

Proposition 4.2 $S(\omega_P(\mathbf{x})) = \omega_P(S(\mathbf{x}))$.

In order for this last proposition to hold, we assume that the discrete maps $P(\mathbf{x})$ and $S(\mathbf{x})$ are continuous and invertible with a continuous inverse. These properties follow from the continuity of the flow. These two propositions will now enable us to define a symmetric attractor. First proposition 1 makes it clear that the ω-limit set under the map $S(\mathbf{x})$ is the union of two conjugate ω-limit sets: $\omega_P(\mathbf{x})$ and $\omega_P(S(\mathbf{x}))$ and from proposition 2 we see that by applying the map S to one of the two conjugate sets the other set can be obtained. We can now define the symmetry of an ω-limit set of our maps:

Definition 4.2 *$\omega_P(\mathbf{x})$ is symmetric if $\omega_P(\mathbf{x}) = \omega_P(S(\mathbf{x}))$.*

This means that an ω-limit set is symmetric if it is equal to its conjugate set. If we now assume the ω-limit sets to be attracting then we can define a symmetric chaotic attractor as follows:

Definition 4.3 *A chaotic attractor is symmetric if its ω-limit set denoted as $\omega_P(\mathbf{x})$ is such that $\omega_P(\mathbf{x}) = \omega_P(S(\mathbf{x}))$. Otherwise it is unsymmetric in which case there exists a pair of conjugate attractors $\omega_P(\mathbf{x})$ and $\omega_P(S(\mathbf{x}))$ such that $\omega_P(\mathbf{x}) \neq \omega_P(S(\mathbf{x}))$.*

Based on this definition of symmetry of a chaotic attractor, we consider the various chaotic attractors of the parametrically excited pendulum in the following section. We show that in the case of the parametrically excited pendulum, oscillatory and rotating chaotic attractors are generally unsymmetric. The symmetry of these two chaotic attractors is restored at a symmetry restoring bifurcation [Sanjuań, 1996; Kim, 1998], which in this case occurs at attractor explosion. In line with the given definition of a symmetric attractor, we adopt the following definition of a symmetry restoring bifurcation:

Definition 4.4 *There is a symmetry restoring bifurcation at* $(\mathbf{x}, p_E)$ *if for any sufficiently small neighbourhood* U *of* $(\mathbf{x}, p_E)$*, there exists* $(\mathbf{x}, p)$, $(\mathbf{y}, \bar{p}) \in U$ *where* $\bar{p} < p_E < p$ *or* $\bar{p} > p_E > p$*, such that, on one side of the symmetry restoring bifurcation,* $\omega_P(\mathbf{x}) \neq \omega_P(S(\mathbf{x}))$, $\omega_P(\mathbf{x}) \cap U \neq \emptyset$ *and* $\omega_P(\mathbf{x})$ *is not contained in a larger limit set (that is there is not* $\omega_P(\mathbf{z})$ *such that* $\omega_P(\mathbf{x}) \subset \omega_P(\mathbf{z})$*), and on the other side of the symmetry restoring bifurcation* $\omega_P(\mathbf{y}) = \omega_P(S(\mathbf{y}))$, $\omega_P(\mathbf{x}) \cap U \neq \emptyset$ *and* $\omega_P(\mathbf{y})$ *is not contained in a larger limit set.*

In the following two sections we consider the different chaotic attractors of the parametrically excited pendulum and then classify them according to their symmetry.

4.4 Numerical Illustrations of Explosions of Rotating Chaotic Attractors

In this section we study the transition of rotating periodic solutions to tumbling chaos. In the first and second resonance zones the explosion of rotating chaotic attractors is the main mechanism by which tumbling chaos is induced. In this section we give two examples to illustrate the different stages of transition from rotating periodic solutions to tumbling chaos. Our first example will be for parameter values fixed in the first resonance zone and the second with $\omega = 2$ and our second example will be from the second resonance zone with $\omega = 0.9$. The transition of rotating periodic solutions to tumbling chaos involves two principal stages: The transition from period doubled

rotating solutions to rotating chaos. Then the transition from rotating chaos to tumbling chaos.

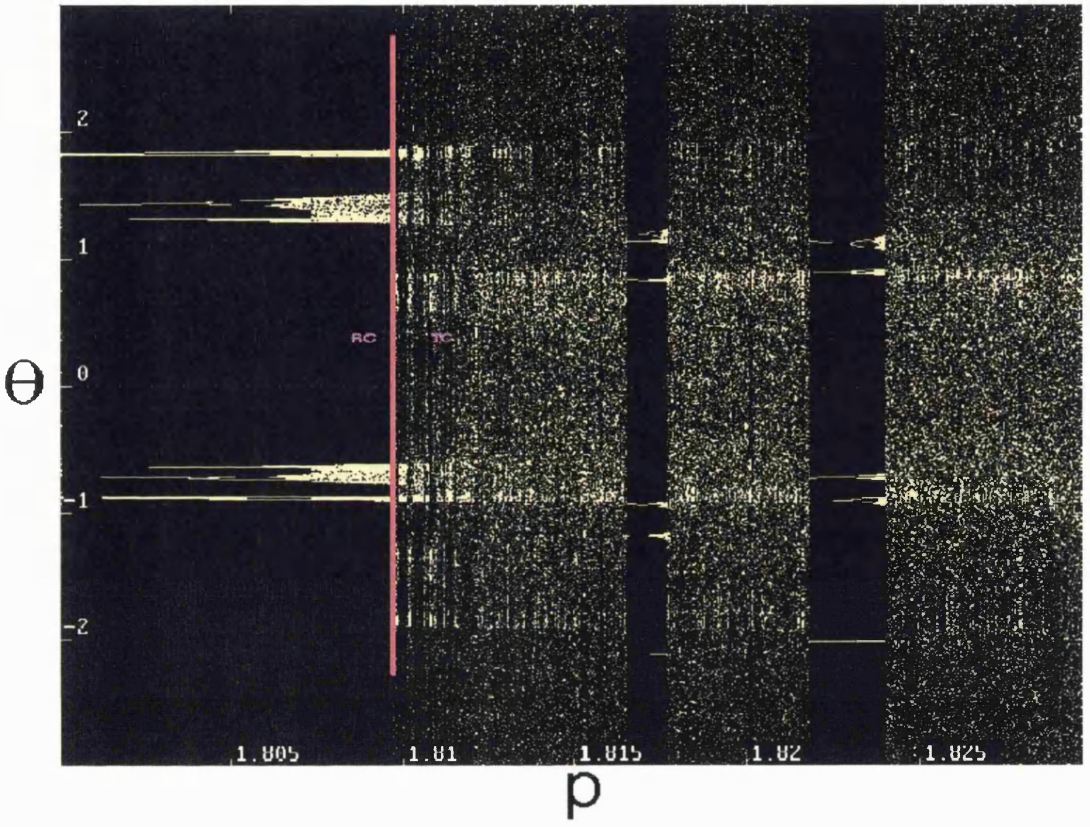

Figure 4.4: Boundary of transition from rotating chaos to tumbling chaos marked in thick red line for $\omega = 2.0$. The red line corresponds to the point of attractor explosion ($p = p_E = 1.8094$) which induces tumbling chaos. In this bifurcation diagram $\theta = \theta \text{mod}[2\pi]$.

Figure 4.4 shows the bifurcation diagram which illustrates the transition of a purely rotating period $2T$ solution to tumbling chaos as the amplitude of parametric forcing increases when ω is fixed at $\omega = 2$. For $p < P_E = 1.8094$, we have rotating chaos due to period doubled rotating solution. At $p = p_E$, there is a sudden widening of the bifurcation diagram. This corresponds to the point of attractor explosion. Figure 4.5 shows the unsymmetric attractor of the rotating chaos together with a plot of time history of the angular coordinate and the associated phase space trajectory just before the explosion ($p = 1.809$

marks the point of attractor explosion. For $p > p_E$, we have tumbling chaos. After the attractor explosion (that is, $p > p_E$) we have a different form of chaos, the tumbling chaos. The tumbling chaos is symmetric chaos, and so the chaotic attractor explosion which occurs at $p = p_E = 1.8094$ is a symmetry restoring bifurcation. The symmetric attractor of tumbling chaos which occurs just after this symmetry restoring bifurcation ($p = 1.81 > p_E$) is shown in Figure 4.6 together with a plot of the time history of the angular coordinate and the associated phase space trajectory. From the definition of a symmetry restoring bifurcation given in the previous section, it means that before the symmetry restoring bifurcation (chaotic attractor explosion), we have two conjugate attractors defined by $\omega_P(\mathbf{x})$ and $\omega_P(S(\mathbf{x}))$ such that $\omega_P(\mathbf{x}) \neq \omega_P(S(\mathbf{x}))$. In Figure 4.5, one of these conjugate attractors of rotating chaos is shown as a 2-band attractor. After the symmetry restoring bifurcation, we only have one attractor defined by $\omega_P(\mathbf{x})$ such that $\omega_P(\mathbf{x}) = \omega_P(S(\mathbf{x}))$. This single attractor of symmetric chaos is shown in Figure 4.6.

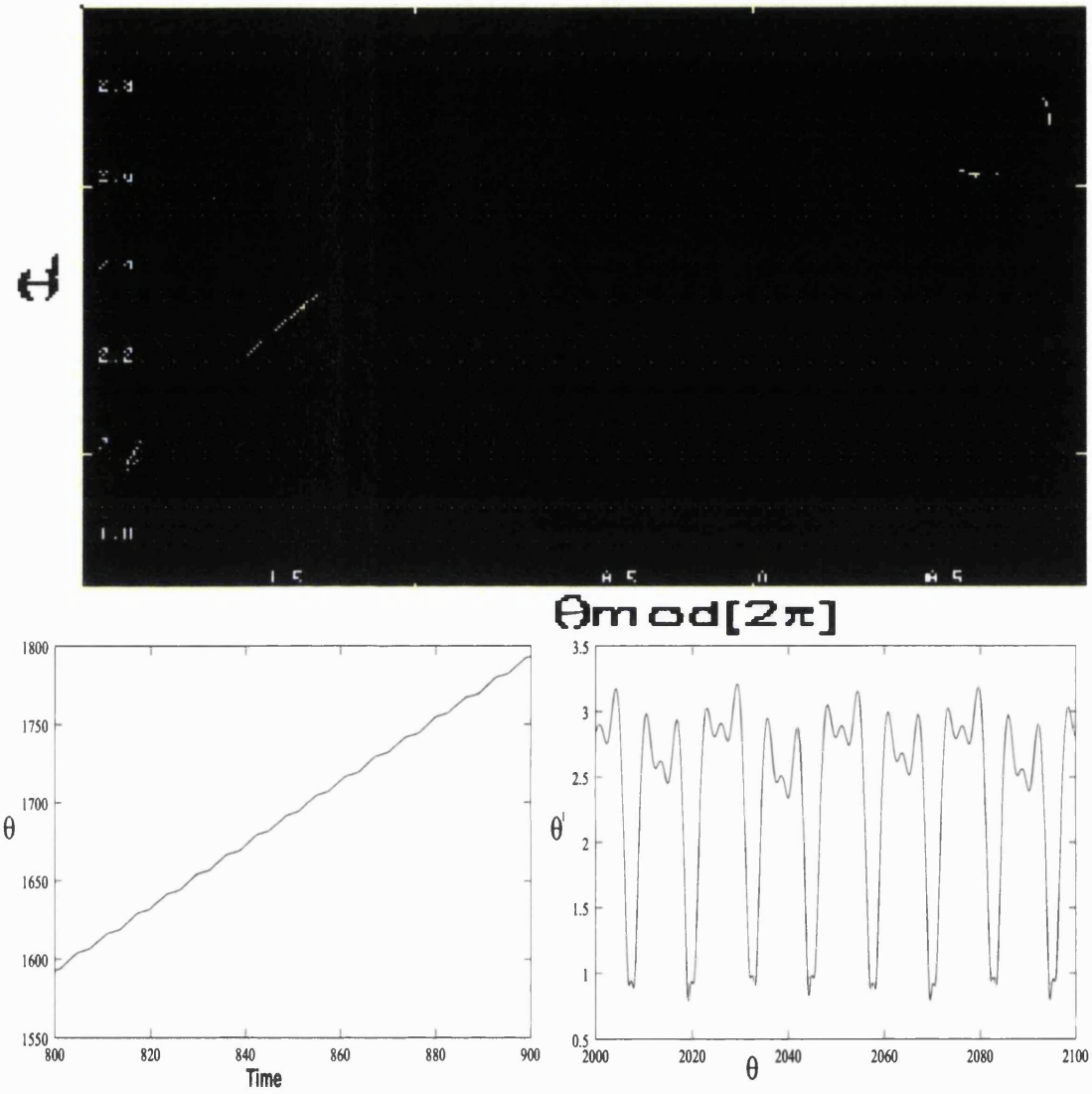

Figure 4.5: **Top**: The unsymmetric attractor of the rotating chaos just before the attractor explosion, $\omega = 2.0$, $p = 1.809$. **Bottom**: Left: Time series of the trajectory, Right: phase space plot of the trajectory.

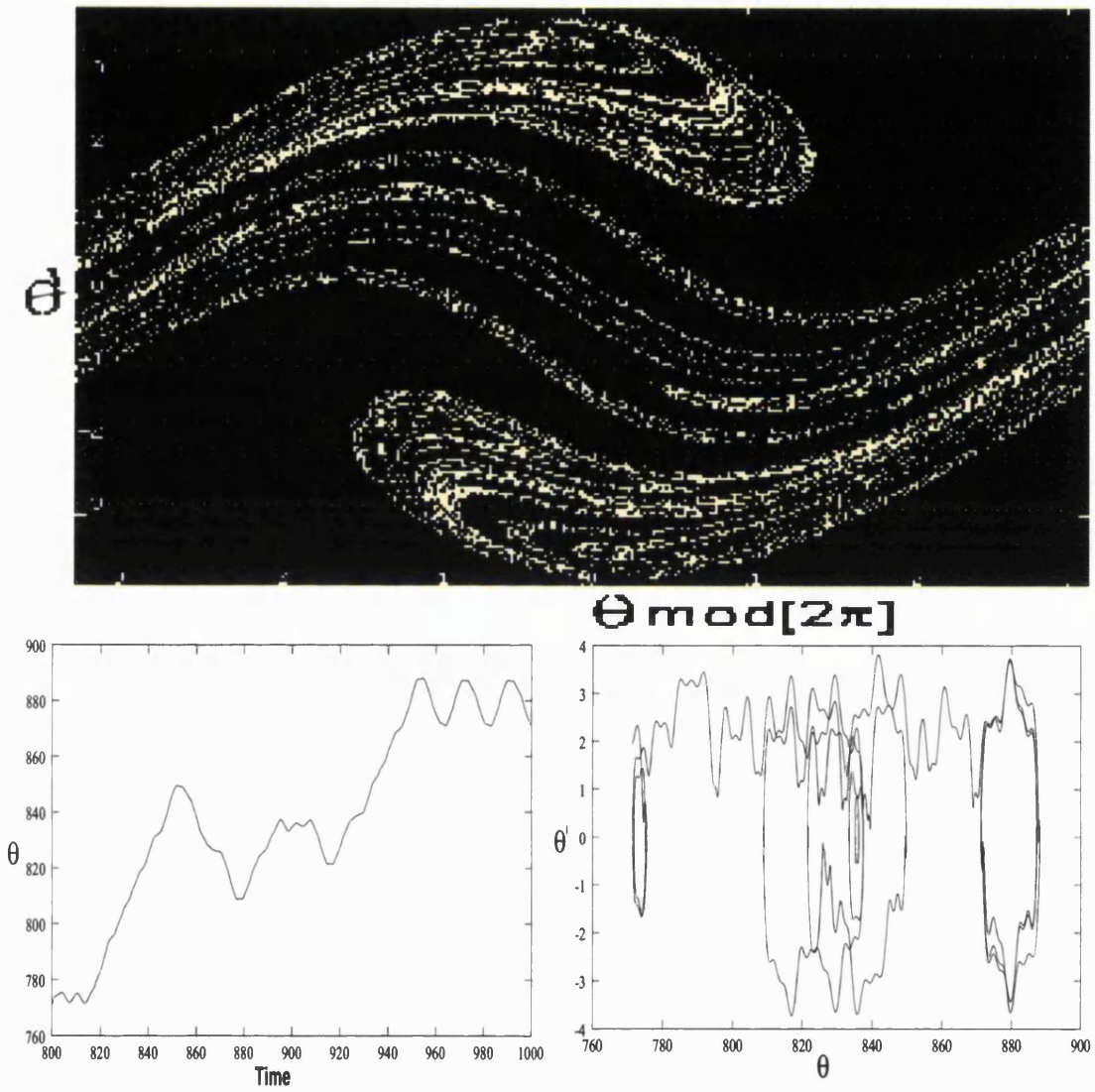

Figure 4.6: **Top**: The symmetric attractor of the tumbling chaos just after the attractor explosion, $\omega = 2.0$, $p = 1.810$. **Bottom**: Left: Time series of the trajectory, Right: phase space plot of the trajectory.

Now we consider the transition to tumbling chaos of another type of rotating motion. This time we consider an example from the second resonance zone, that for (ω, p) located around $(2/n, 0)$, $n = 2$. More specifically we consider the transition to tumbling chaos when $\omega = 0.9$. The initial rotating solution considered in this example can be viewed as an oscillation of amplitude 2π. But because it makes a complete revolution, we classify it as a rotating periodic solution. Figure 4.7 shows the bifurcation

diagram which illustrates the transition of this type of rotating periodic solution to tumbling chaos as the amplitude of parametric forcing increases. Again as in the previous case, as the amplitude of parametric forcing, p increases we have the period doubled rotating solution becoming rotating chaos (unsymmetric chaos) first as a transitional behaviour to tumbling chaos (symmetric chaos). In Figure 4.7 the point of attractor explosion at which the bifurcation suddenly widens is marked by a thick red line at $p = p_E = 1.73971$.

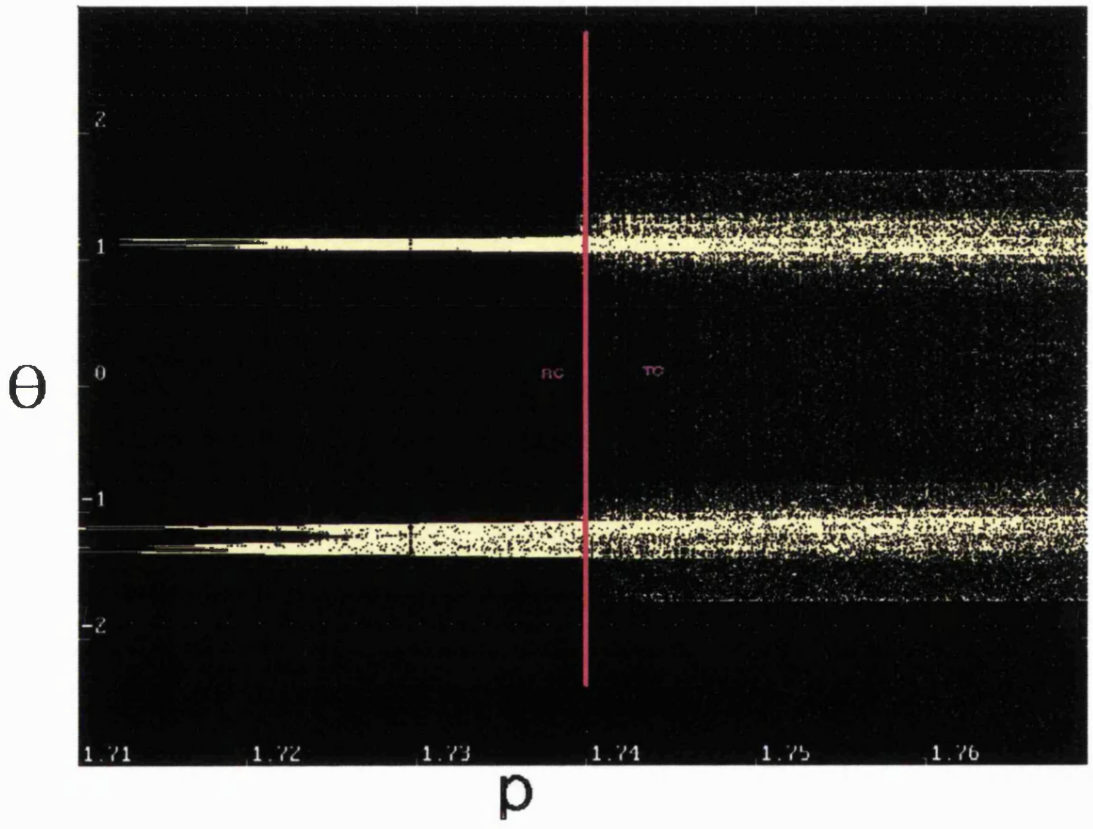

Figure 4.7: Boundary of transition from rotating chaos to tumbling chaos marked in thick red line for $\omega = 0.9$. The red line at $p = p_E = 1.73971$ marks the point of attractor explosion which induces tumbling chaos. In this bifurcation diagram $\theta = \theta \text{mod}[2\pi]$.

The unsymmetric attractor for the rotating chaos together with a typical time series of the trajectory and the associated phase space trajectory just before the attractor explosion ($p = 1.735 < p_E$ is shown in Figure 4.8. The extinction of this rotating attractor occurs at the point of attractor explosion at $p = p_E = 1.73971$, where the rotating

chaos becomes tumbling chaos. Again this attractor explosion is a symmetry restoring bifurcation in which the non-symmetric rotating chaos becomes symmetric tumbling chaos. The symmetric attractor as well as a typical trajectory both as time series and in phase space of the tumbling chaos just after the symmetry restoring bifurcation is shown in Figure 4.9. Thus again, here we have two conjugate unsymmetric attractors of the parametrically excited pendulum of rotating chaos which are defined by $\omega_P(\mathbf{x})$ and $\omega_P(S(\mathbf{x}))$ such that $\omega_P(\mathbf{x}) \neq \omega_P(S(\mathbf{x}))$ before the chaotic attractor explosion. After the attractor explosion we now have one symmetric chaotic attractor defined by $\omega_P(\mathbf{x})$ such that $\omega_P(\mathbf{x}) = \omega_P(S(\mathbf{x}))$.

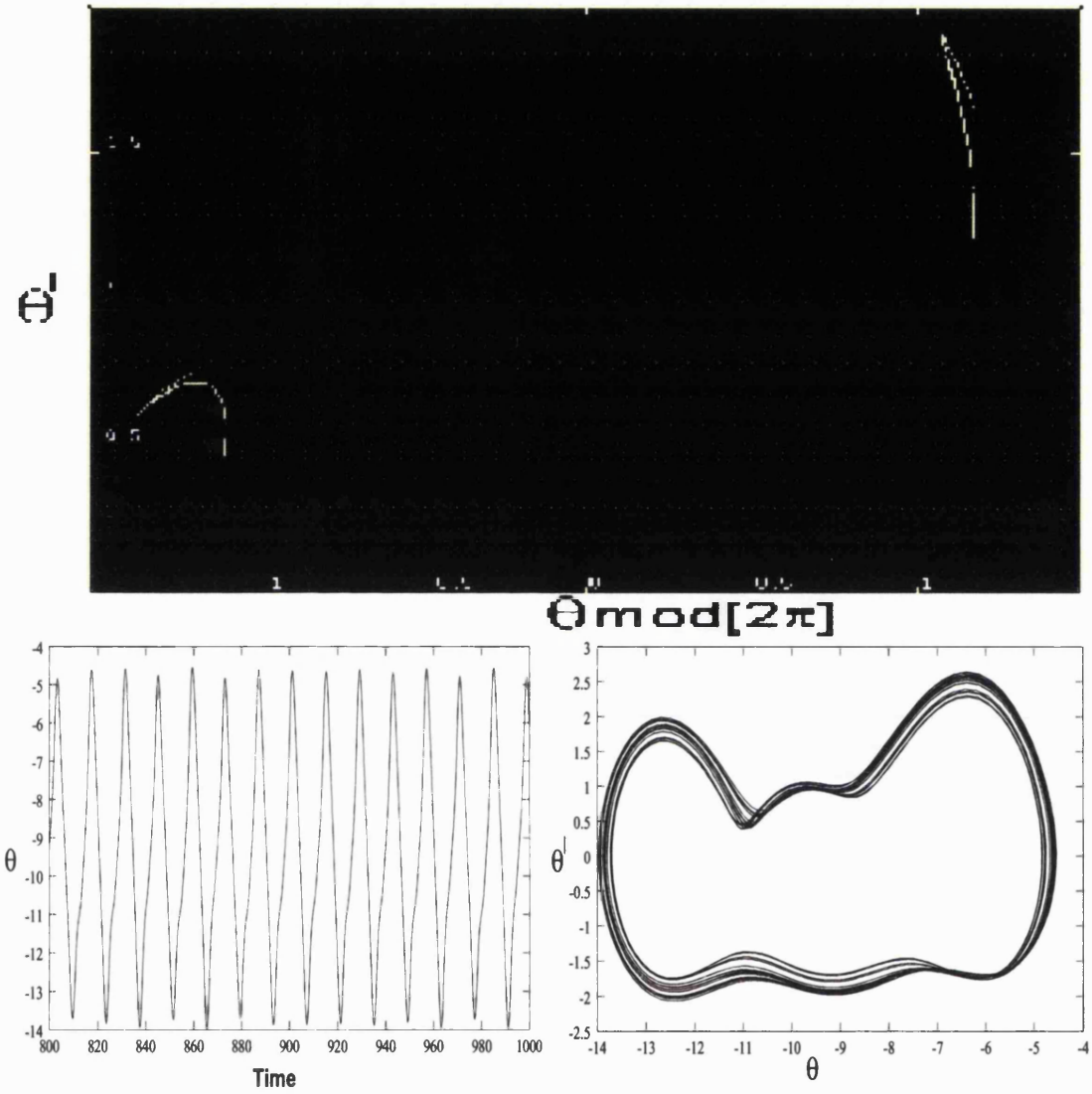

Figure 4.8: **Top**: The unsymmetric attractor of the rotating chaos just before the attractor explosion, $\omega = 0.90$, $p = 1.735$. **Bottom**: Left: Time series of the trajectory, Right: phase space plot of the trajectory.

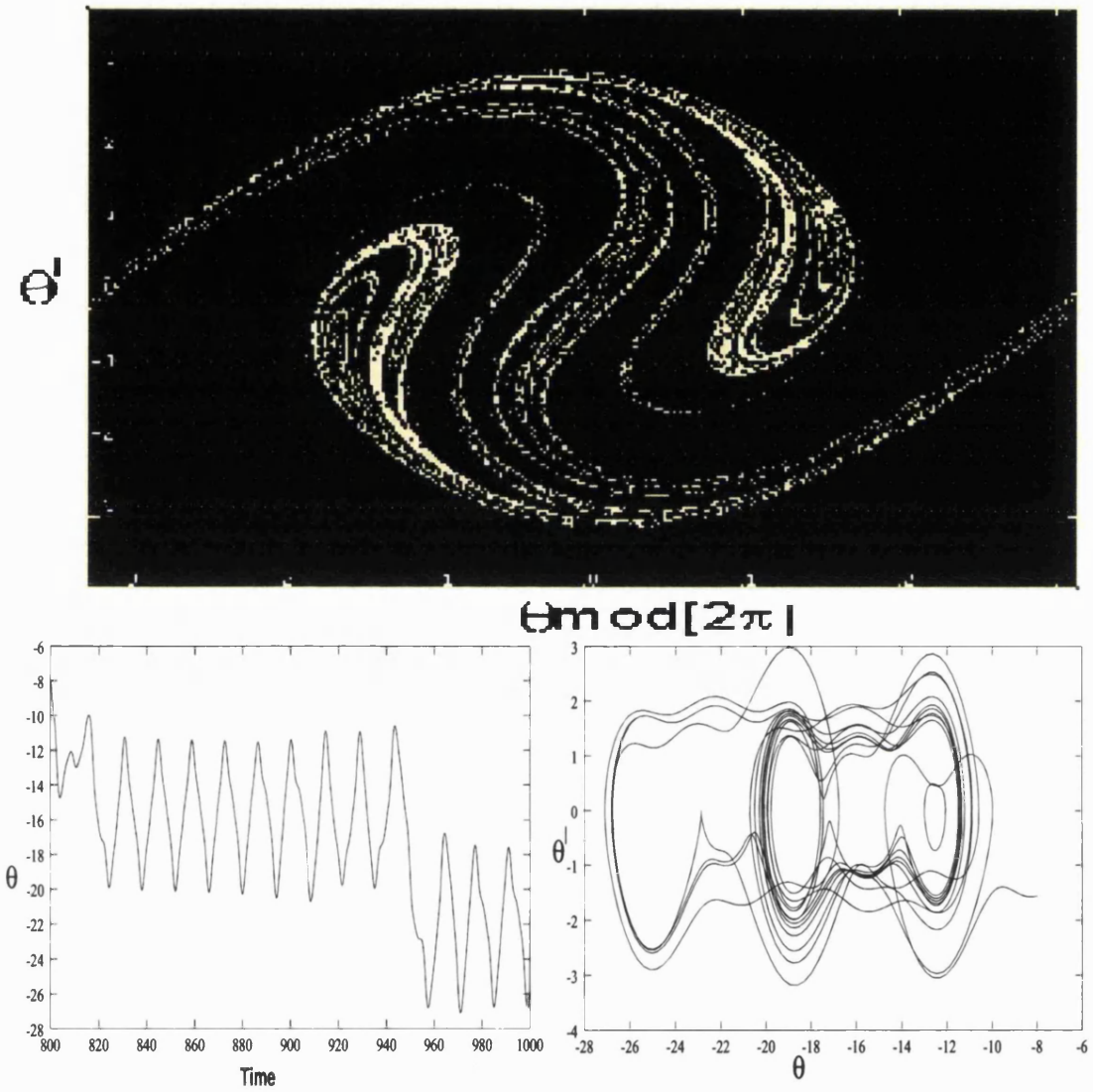

Figure 4.9: **Top**: The symmetric attractor of the tumbling chaos just after the attractor explosion, $\omega = 0.90$, $p = 1.760$. **Bottom**: Left: Time series of the trajectory, Right: phase space plot of the trajectory.

Numerical investigations confirmed that the two types of chaos here, that is the rotating chaos and the tumbling chaos do not coexist and that there is no hysterisis at the boundary of transition from rotating chaos to tumbling chaos.

4.5 Numerical Illustrations of Explosions and Collision of Oscillating Chaotic Attractors

Now we consider the transition of oscillatory solutions to tumbling chaos. We consider two examples: First an initially symmetry $1/3$ subharmonic oscillatory solution ($\omega = 0.6$) of period $2T$. This example is for parameter values fixed in the third resonance zone, that is, for parameter values around $(\omega, p) = (2/n, 0), n = 3$. Second, we consider initially unsymmetric subharmonic oscillatory solution of order $1/2$ ($\omega = 0.45$). This second example is for parameter values fixed in the fourth resonance zone, that is, for parameter values around $(\omega, p) = (2/n, 0), n = 4$. In these two different types of oscillatory solutions, we show that the actual transition from oscillatory periodic solutions to tumbling chaos takes place in three principal stages: First the period doubled oscillatory solution become unsymmetric oscillatory chaos. Second the conjugate attractors of this unsymmetric oscillatory chaos collide and form a larger oscillatory chaotic attractor. In the third and final stage, the oscillatory chaos becomes tumbling chaos. This final stage involves an attractor explosion.

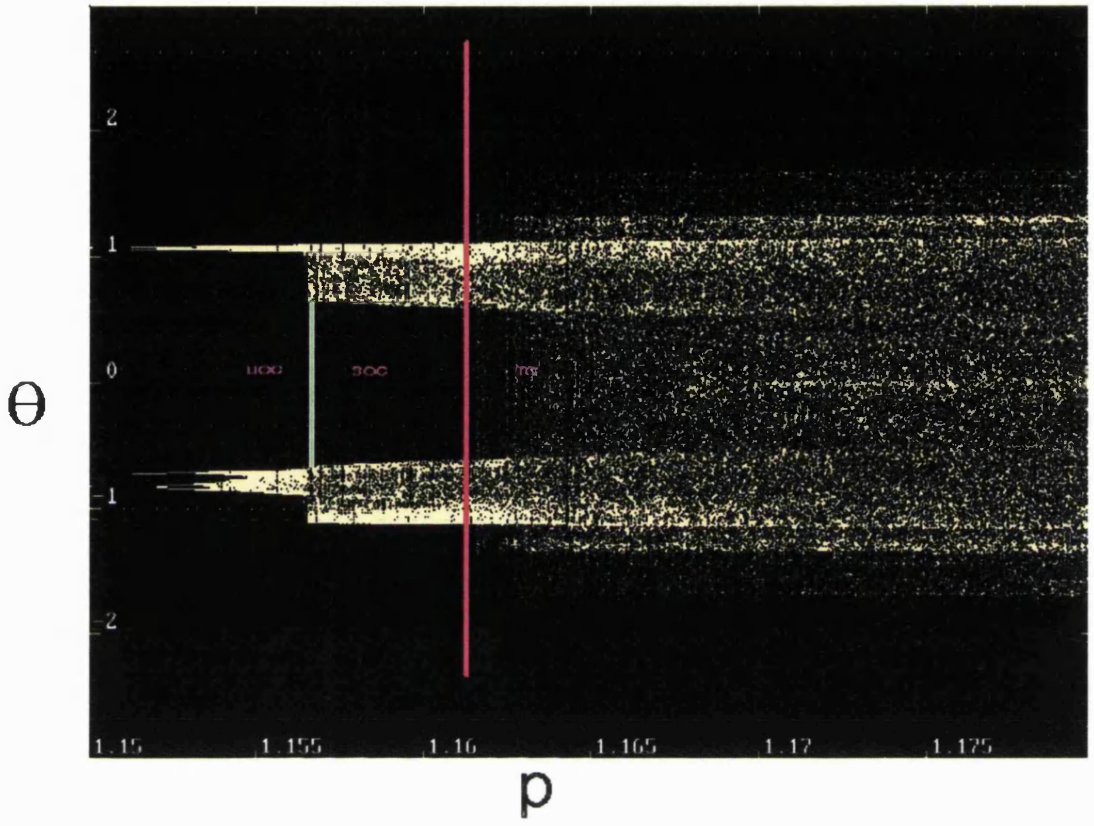

Figure 4.10: Boundary of transition from oscillating chaos to tumbling chaos marked in thick red line for $\omega = 0.6$. The green line marks the point attractor collision while the red line marks the point of attractor explosion. In this bifurcation diagram $\theta = \theta \text{mod}[2\pi]$.

Let us consider first the transition of an initially symmetric $1/3$ subharmonic oscillatory solution. Before the period doubling cascade, this solution first undergoes a symmetry breaking bifurcation. Figure 4.10 shows the bifurcation diagram which illustrates the three transition stages to tumbling chaos. First the period doubled $1/3$ subharmonic oscillatory orbit becomes unsymmetric oscillatory chaos through a cascade of period doublings of the symmetry broken oscillatory orbit. The unsymmetric attractor of this oscillatory chaos together with a plot of the time history of the angular coordinate and the associated phase space trajectory is shown in Figure 4.11. Then at $p = p_C = 1.15628$, there is a sudden enlargement of the oscillatory symmetry broken

chaotic attractor. This occurs as a result of collision of the two conjugate chaotic attractors. The result is unsymmetric oscillatory chaos with a much larger 2-band attractor. Figure 4.12 shows the unsymmetric 2-band chaotic attractor which occurs as a result of this attractor collision as well as a plot of a time history of the angular coordinate and the associated phase space trajectory. For $p = p_E = 1.16108$, we see a further sudden widening of the bifurcation resulting in tumbling chaos. This enlargement of the unsymmetric oscillatory chaotic attractor occurs as a result of attractor explosion. The result of this attractor explosion is symmetric chaos, which in this case is tumbling chaos. Figure 4.13 shows the symmetric chaotic attractor of the tumbling chaos just immediately after the attractor explosion ($p = 1.17 > p_E$) together with a time series of the trajectory and its corresponding one in phase space.

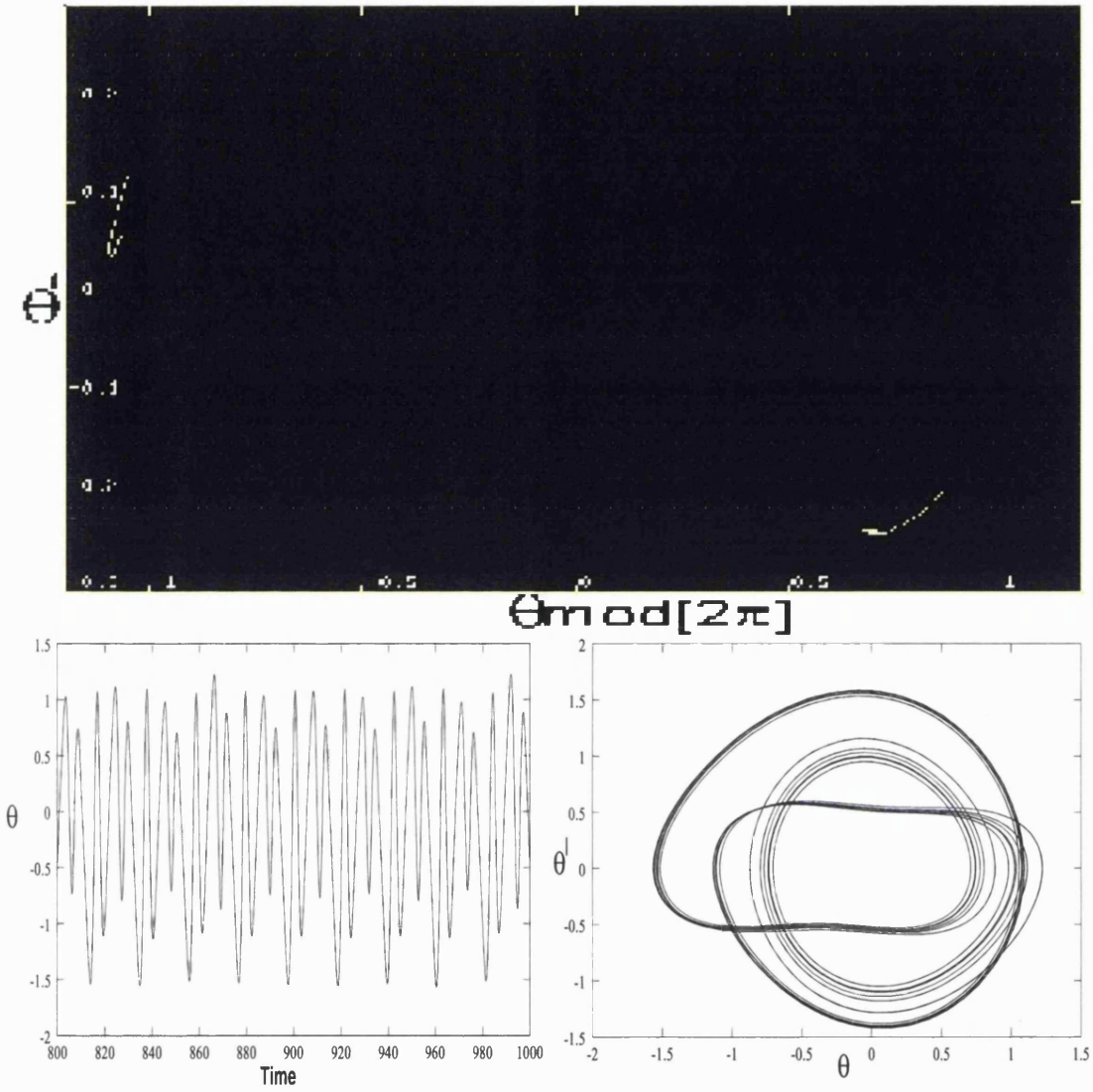

Figure 4.11: **Top**: The unsymmetric attractor of the oscillating chaos just before the attractor collision, $\omega = 0.60$, $p = 1.156$. **Bottom**: Left: Time series of the trajectory, Right: phase space plot of the trajectory.

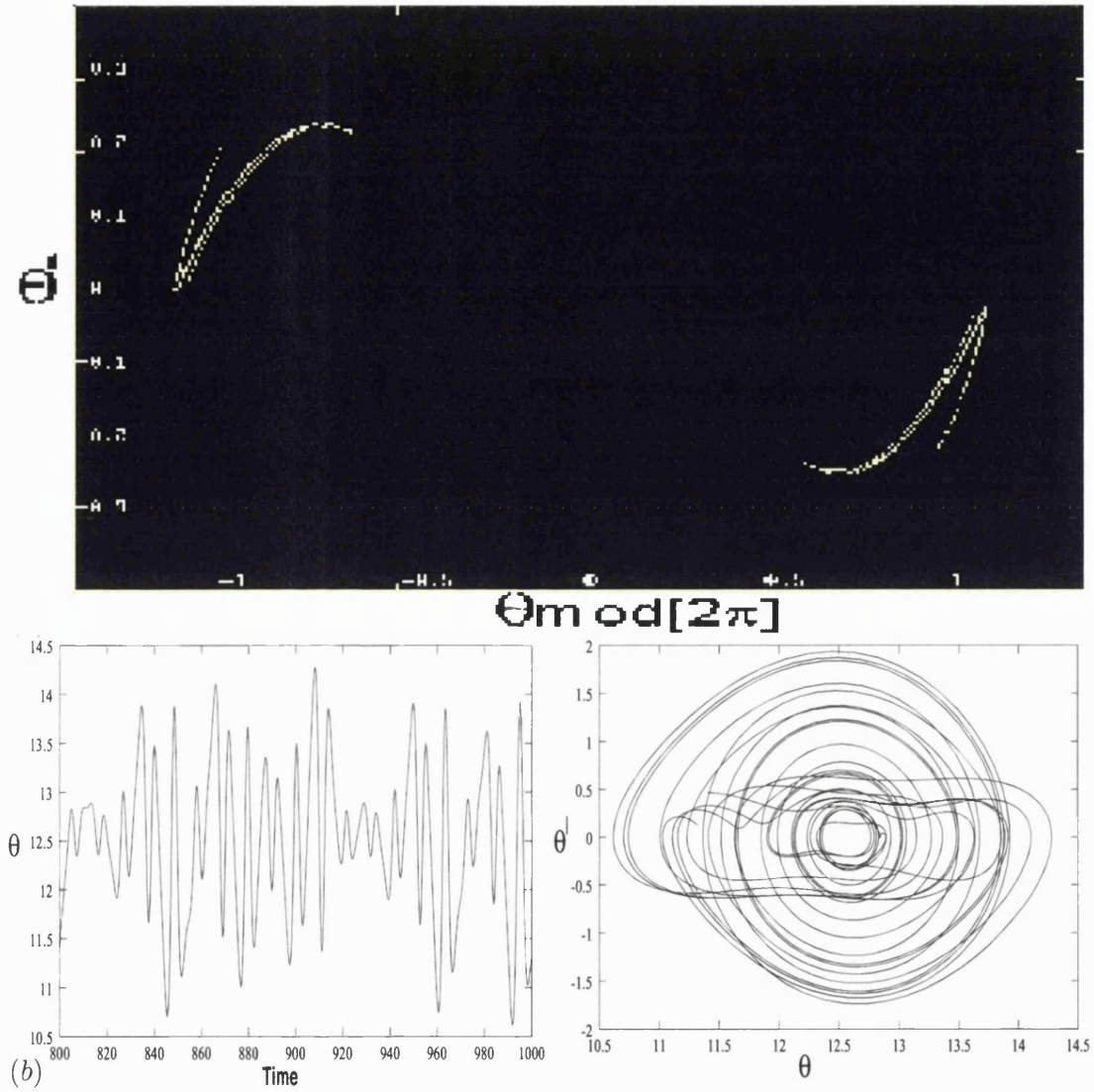

Figure 4.12: **Top**: The attractor of the oscillating chaos just after the attractor collision, $\omega = 0.6$, $p = 1.16$. **Bottom**: Left: Time series of the trajectory, Right: phase space plot of the trajectory.

Thus transition to tumbling chaos of the oscillatory solution here resembles other previous cases in that it involves a symmetry restoring bifurcation. In this case, for $p < p_E = 1.16108$, we have two conjugate unsymmetric chaotic attractors defined by $\omega_P(\mathbf{x})$ and $\omega_P(S(\mathbf{x}))$ such that $\omega_P(\mathbf{x}) \neq \omega_P(S(\mathbf{x}))$. After the attractor explosion we only have one symmetric attractor defined by $\omega_P(\mathbf{x})$ such that $\omega_P(\mathbf{x}) = \omega_P(S(\mathbf{x}))$.

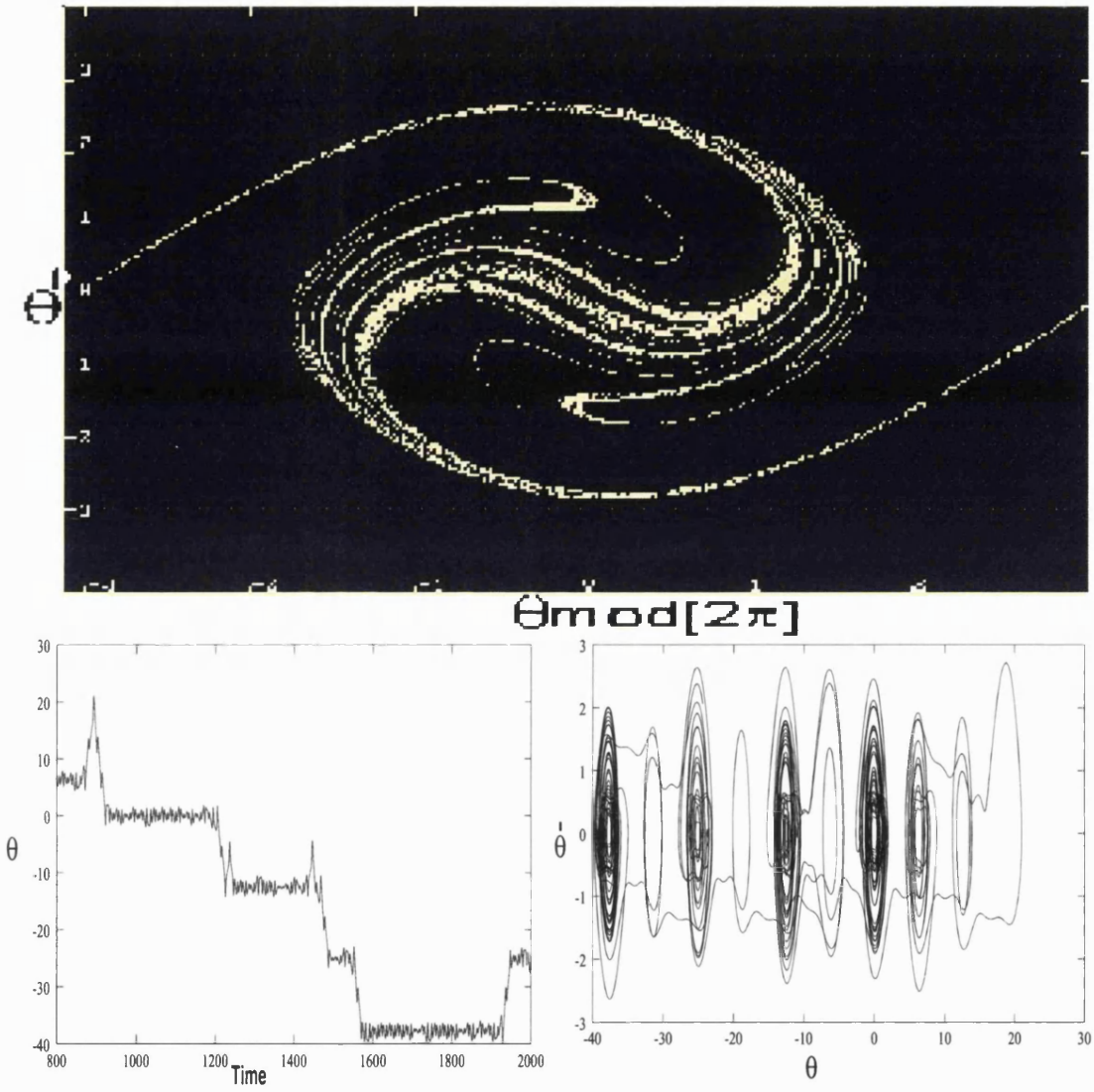

Figure 4.13: **Top**: The symmetric attractor of the tumbling chaos just after the attractor explosion, $\omega = 0.60$, $p = 1.17$. **Bottom**: Left: Time series of the trajectory, Right: phase space plot of the trajectory.

In our last example we consider the transition to tumbling chaos of a $1/2$ subharmonic oscillatory orbit of period T. Figure 4.14 shows the bifurcation diagram which depicts the different stages of the transition to tumbling chaos of this periodic solution.

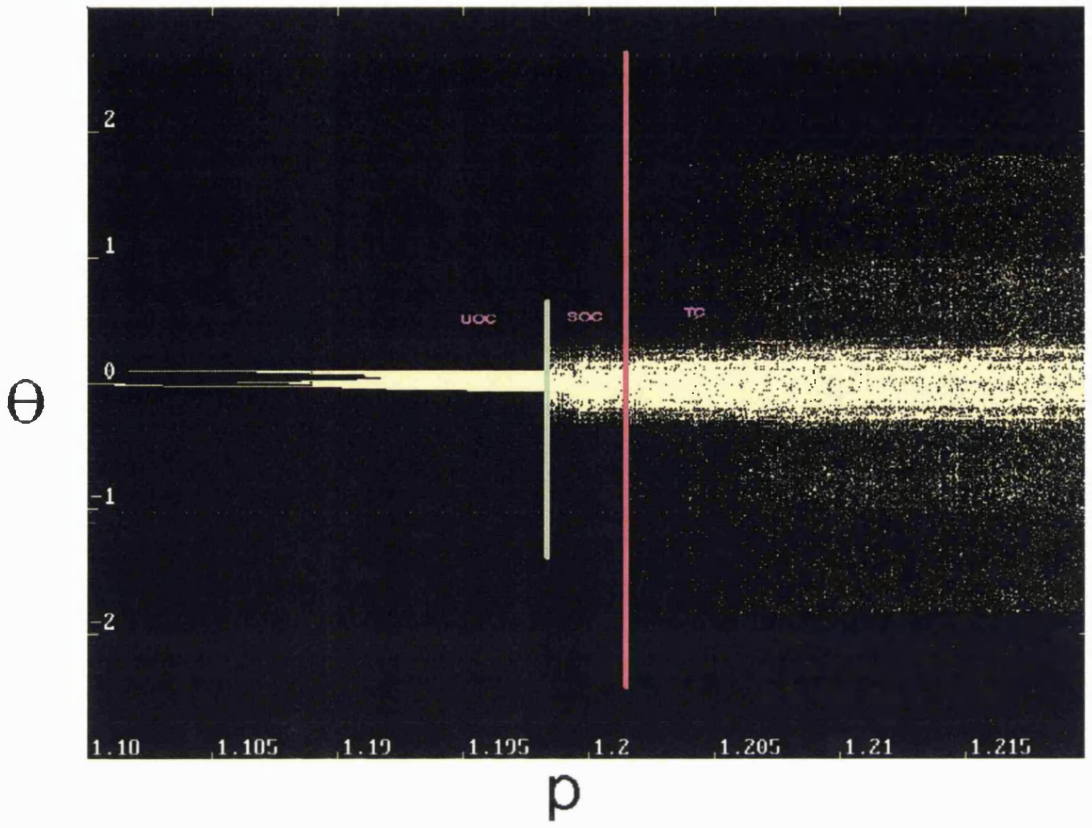

Figure 4.14: Boundary of transition from oscillating chaos to tumbling chaos marked in thick red line for $\omega = 0.45$. The green line marks the point attractor collision while the red line marks the point of attractor explosion. In this bifurcation diagram $\theta = \theta \text{mod}[2\pi]$.

The three stages of transition to tumbling chaos when an periodic trajectory is oscillatory are further confirmed. First we have small attractor oscillatory chaos shown in Figure 4.15. Then the two conjugate attractors of this nonsymmetric oscillatory chaos collide to form a larger 2-band unsymmetric oscillatory chaos. The resultant larger chaotic attractor is shown in Figure 4.16.

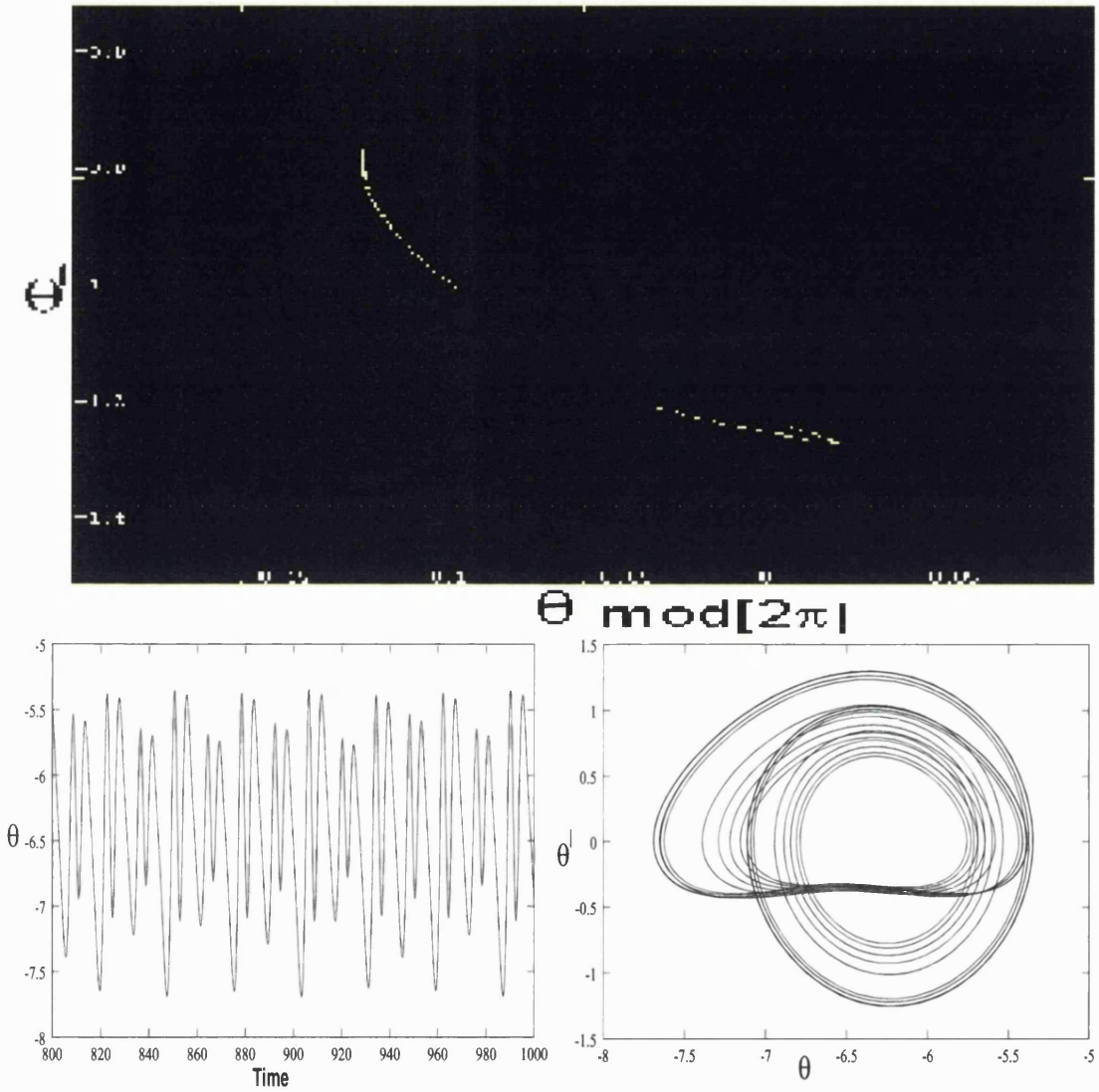

Figure 4.15: **Top**: The unsymmetric attractor of the oscillating chaos just before the attractor collision, $\omega = 0.45$, $p = 1.19$. **Bottom**: Left: Time series of the trajectory, Right: phase space plot of the trajectory.

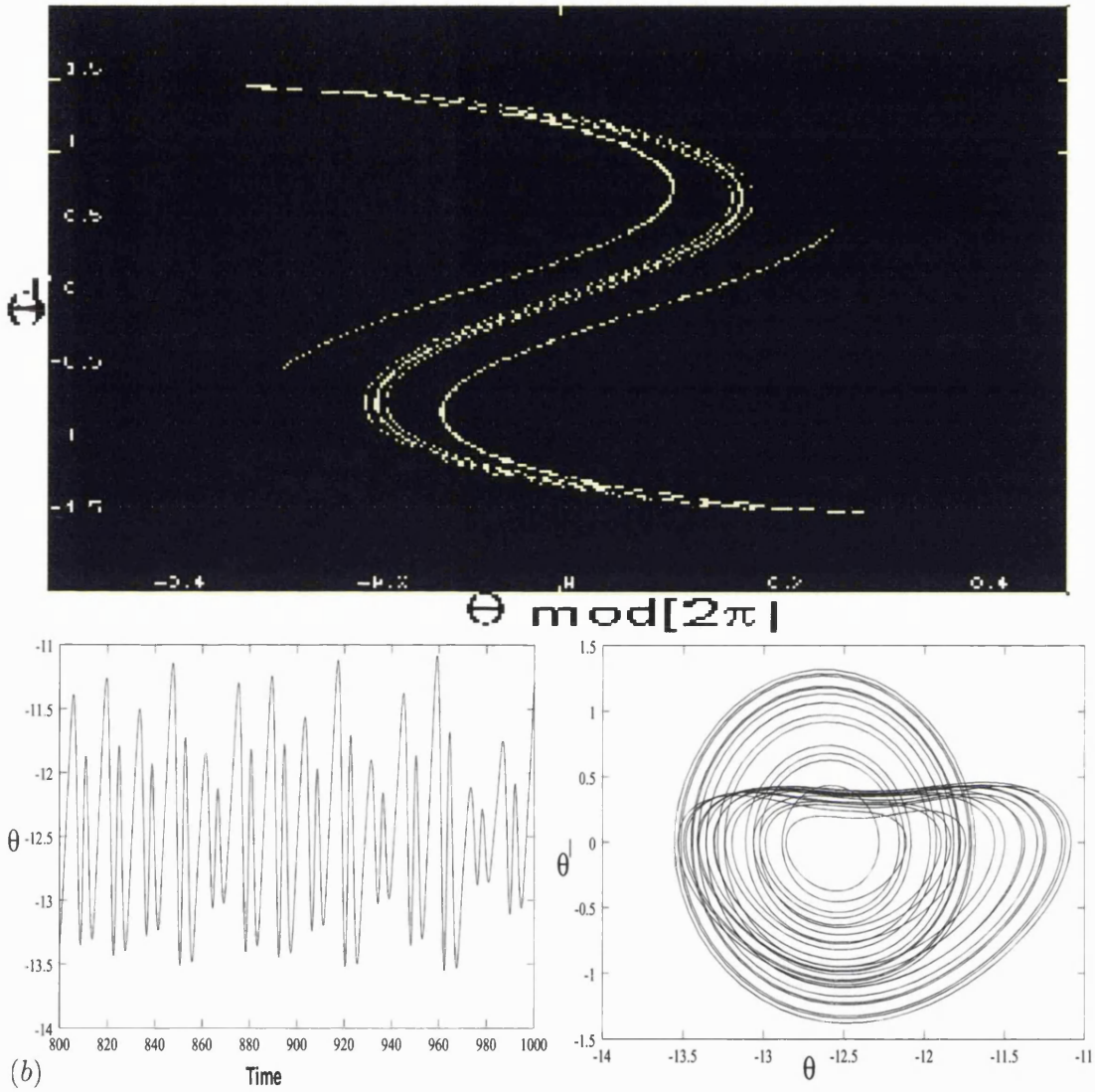

Figure 4.16: **Top**: The attractor of the oscillating chaos just after the attractor collision, $\omega = 0.45$, $p = 1.20$. **Bottom**: Left: Time series of the trajectory, Right: phase space plot of the trajectory.

A further increase in the amplitude of parametric forcing to beyond $p = p_E = 1.20181$ results in tumbling chaos. Figure 4.17 shows the resulting symmetric attractor of the tumbling chaos.

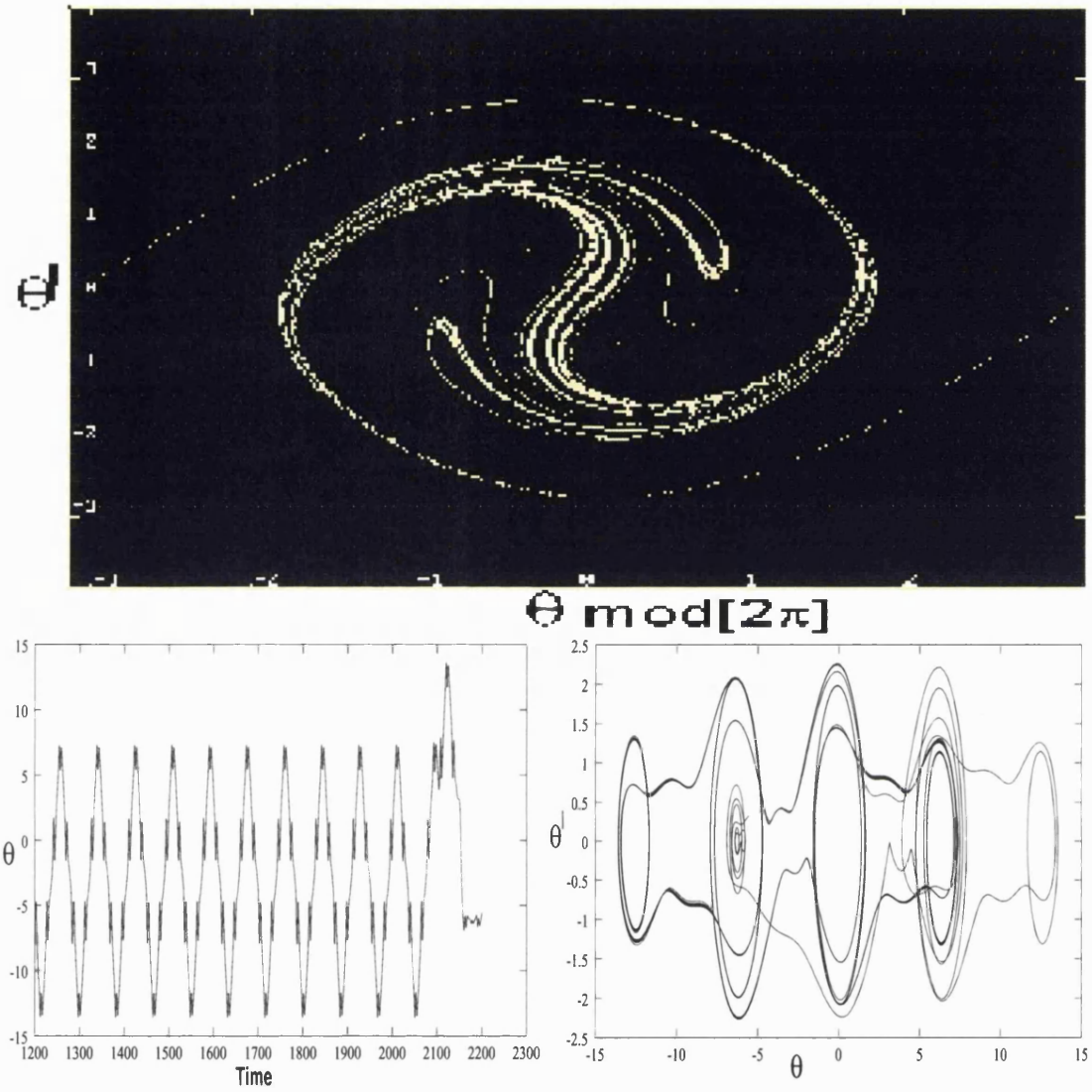

Figure 4.17: **Top**: The symmetric attractor of the tumbling chaos just after the attractor explosion, $\omega = 0.45$, $p = 1.22$. **Bottom**: Left: Time series of the trajectory, Right: phase space plot of the trajectory.

Numerical investigations also confirmed that the two types of chaos here, that is the oscillating chaos and the tumbling chaos do not coexist and that there is no hysterisis at the boundary of transition from oscillating chaos to tumbling chaos.

4.6 Final Remarks

In this chapter we have considered the transition to tumbling chaos through attractor explosion. We have established that for low values of the amplitude of parametric forcing p, small attractor oscillating and rotating chaotic states exist. When p is increased to relatively higher values, these unsymmetric chaotic states lose stability through a symmetry restoring bifurcation to symmetric large attractor tumbling chaos. We have also verified that the symmetry restoring bifurcation involves the explosion of the symmetry broken chaotic attractors of oscillating chaos and rotating chaos. In the first and second resonance zones the main mechanism by which structurally stable tumbling chaos is induced is through the explosion of symmetry broken rotating chaotic attractors. But in the lower resonance zones, we have alternating zones of tumbling chaos interspaced by periodic windows, where some of these zones are due to attractor explosion of oscillating chaos while others are due to explosion of rotating chaos attractors.

The main results of this chapter are:

- that there is no direct transition from rotating or oscillatory solutions to tumbling chaos through the period doubling sequence.
- that the rotating or oscillatory solutions first period double to either rotating or oscillatory chaos.
- that the actual transition from either oscillatory chaos or rotating chaos to tumbling chaos is through a global bifurcation.

Chapter 5

Periodic Synchronisation Regimes of Two Parametrically Excited Pendula

5.1 Introduction

In this chapter we consider the different periodic synchronisation regimes that occur in a system of two parametrically excited pendula which are bidirectionally or mutually coupled. Our emphasis is on understanding the important role that the coupling plays in changing the synchronous behaviours of the system. This deepens our understanding of the desynchronisation bifurcations which cause the system to experience different forms of periodic synchronisation as coupling increases. We are also interested in the nature of the transients before the system converges onto the synchronised state. Two kinds of periodic synchronisation are of particular interest: one in which the pendula are moving in-phase with equal amplitudes and another in which the two pendula are always moving in counter-phase, that is, out-of-phase by π radians, but still with equal amplitudes of oscillation. When there is no damping, these types of synchronised periodic motions are observed for very small values of the driving amplitude. But with damping present, these types of oscillatory motion are only realised when the amplitude of parametric forcing exceeds a certain threshold value so that the system can overcome energy losses due to damping. These two types of periodic synchronisation correspond to **1-motion** and **2-motion** as defined in section 1.5.2 of chapter 1.

The study of periodic synchronisation is not a new discipline. Scientists have known about the synchronisation of periodic oscillations since the historical observation of this phenomenon by Huygens in pendulum clocks [Hugenii, 1673]. However, recently considerable attention has been focused on the synchronisation of systems behaving chaotically beginning with the work of Fujisaka and Yamada in the 1980s [Fujisaka and Yamada, 1983, 1985; Yamada and Fujisaka, 1983, 1984], which further gained worldwide attention after Pecora and Carroll's suggestion of its use in secure telecommunications [Pecora and Carroll, 1990].

Despite this long history of the subject, fundamental issues regarding synchronisation of coupled dynamical systems have not been effectively tackled. The most basic and arguably one of the most important is sharp, sufficient conditions stating when two identical systems will synchronise. Research into this problem and others related to it have lead to the discovery of a wide variety of phenomena in the study of coupled dynamical systems, including *attractor bubbling* [Ashwin et al., 1996], *riddled basins of attraction* [Alexander et al., 1992], and *on-off intermittency* [Yu et al., 1995]. Inspite of the massive research directed at this problem, to date, the only most widely known criterion for successful synchronisation rely on the negativity of transverse Lyapunov exponents first introduced in [Fujisaka and Yamada, 1983]. When all transversal Lyapunov exponents of the coupled dynamical systems are negative then one expects that the systems synchronise. But there is now a growing body of evidence suggesting that the mere negativity of Lyapunov exponents alone is inadequate to guarantee high quality synchronisation [Varone et al., 1998]. While such conditions are necessary for synchronisation, they are by no means sufficient. Intervals of desynchronisation bursting behaviour can appear even when the largest transverse Lyapunov exponent is negative, especially as in practical settings, when there is noise in the system [Heagy et al., 1995b]. The deficiency of this criterion is perhaps not suprising since we know that exponents only give a linearized picture of the stability of the synchronous state. The 'global' stability of the synchronous state will be typically determined by the

dynamics away from the synchronisation manifold, and cannot be found by a local analysis of higher order terms in some Taylor expansion [Ashwin et al., 1996].

The focus of this chapter is on bifurcations that destroy synchronisation when the parameters of the coupled dynamical systems are varied, particularly the coupling parameter. Desynchronisation bifurcations in which increasing the coupling strength between the systems in the coupled array destabilises the synchronisation have been reported in [Heagy et al., 1995a]. This phenomenon was called a short wavelength bifurcation. In this chapter we report on desynchronisation phenomenon which occurs when the coupling strength is increased in a system of two coupled parametrically excited pendula. This bifurcation gives rise to range of synchronisation regimes of the pendula as the coupling increases.

5.2 The System of Coupled Pendula

When two parametric excited pendula are coupled, the dynamics of the system becomes richer and more complex. There are different ways of coupling two pendula. [Zhang et al., 1999], for example, describe two parametrically excited pendula coupled unidirectionally and connected through a periodical feedback. In this work the setting is continuous bidirectional or mutual coupling. This type of coupling was described in detail by [Banning and Weele, 1995; Banning et al., 1997], where both the Hamiltonian and dissipative cases are considered.

Using the same scaling as those used in chapter 1, the equations of the coupled pendula in terms of the angles θ_1 and θ_2 which define their configuration can be shown to be:

$$\begin{cases} \theta_1'' + \beta\theta_1' + (1 + p\cos(\omega\tau))\sin(\theta_1) + k(\theta_1 - \theta_2) = 0 \\ \theta_2'' + \beta\theta_2' + (1 + p\cos(\omega\tau))\sin(\theta_2) - k(\theta_1 - \theta_2) = 0 \end{cases} \tag{5.1}$$

where k is the coupling parameter and β, p, ω are the damping, amplitude of parametric forcing and the frequency of parametric forcing of the pendula respectively. In these

equations the natural frequency is now scaled to 1.

First let us consider the zones in the parameter space in which the in-phase and out-of-phase periodic synchronisation occur.

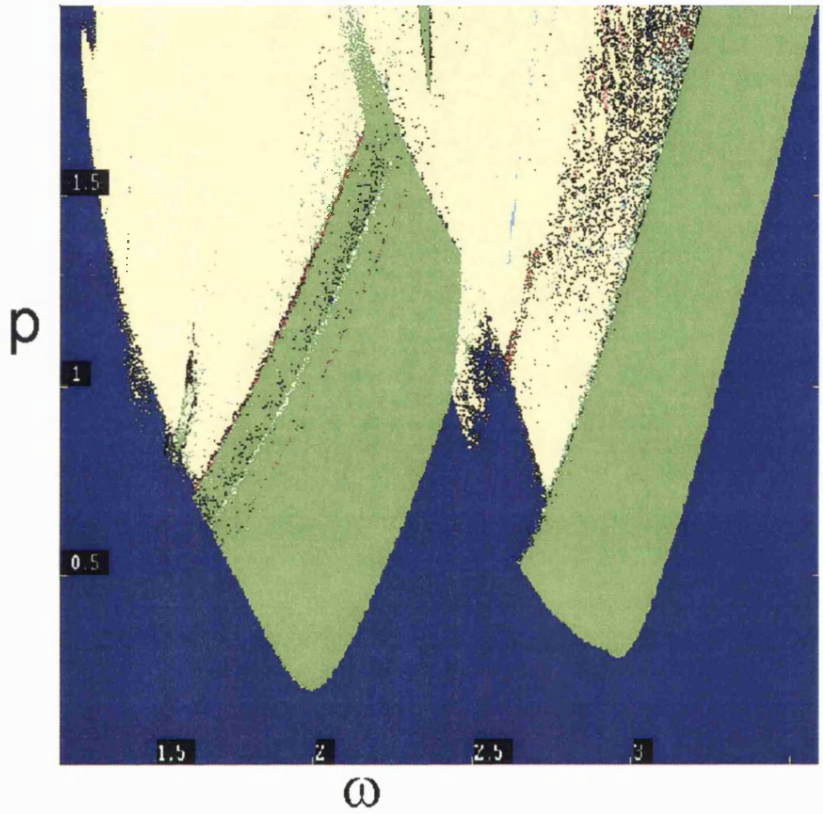

Figure 5.1: Regions of in-phase, out-of-phase and chaotic motion in the (ω, p) space for $k = 0.6$. In the first resonance zone (located around $\omega = 2$) green colour represents the parameter space in which in-phase motion is realised and in the second resonance zone (located around $\omega = 3$) the same colour represents region of out-of-phase motion. The yellow colour represents regions of chaos while blue colour represent regions of stability of the downward equilibrium.

Figure 5.1 shows the resonance zones of in-phase and out-of-phase periodic synchronisation which were numerically determined for the full nonlinear equations using the software [Nusse and Yorke, 1998]. It is important to notice from Figure 5.1 that now we have another resonance zone around $\omega = 3$ which is not there for the single

parametrically excited pendulum. Within the first resonance zone (located around $(\omega, p) = (2, 0)$), the region in green colour represents the parameter space for which in-phase periodic synchronisation is realised while in the second zone the same colour represents the parameter space for which out-of-phase synchronisation occurs. In both resonance zones yellow colour represent regions of tumbling chaos while the blue colour represents regions of stability of the downward equilibrium for both pendula. We will discuss the synchronisation of chaos within the yellow region in the next chapter.

Within these zones shown in Figure 5.1, small perturbations from the downward hanging equilibrium do not die out but can be excited into in-phase and out-phase synchronisation for sufficiently large k. Realistically, the perturbations can be excited into a plethora of different types of motions, even chaotic ones in these zones, but our interest here is in those which are periodic and oscillatory. The main resonance zone for the in-phase periodic synchronisation occurs around $(\omega, p) = (2, 0)$, that is, at twice the natural frequency of the pendula. As a consequence, for in-phase synchronisation, the most important motions of this type have period $2T$, where $T = 2\pi/\omega$ is the period of the driving force. Similarly, the main resonance zone for out-of-phase periodic synchronisation occurs around $\omega = 2\sqrt{1+2k}$ in the (ω, p). However, for both in-phase and out-of-phase periodic synchronisation higher order resonance zones of in-phase and out-of-phase motion are centred around $(\omega, p) = (2/n, 0)$ and $(\omega, p) = (2/n\sqrt{1+2k}, 0)$ respectively in the (ω, p) space with $n = 2, 3, 4, ...$, but these are of lesser significancy because for small values of the amplitude of forcing they occupy a small region in the parameter space.

It must be noted that as the coupling increases the second resonance zone, in which out-of-phase synchronisation occurs shifts to the right. The occurrence of in-phase and out-of phase oscillations can be illustrated more clearly by using normal co-ordinates.

Let us indicate the periodic forcing term with $F(\tau)$. The equations of motion of the two coupled parametrically excited pendulums (Latin spelling pendula) are written as

$$\begin{cases} \theta_1'' + \beta\theta_1' + F(\tau)\sin\theta_1 + k(\theta_1 - \theta_2) = 0 \\ \theta_2'' + \beta\theta_2' + F(\tau)\sin\theta_2 - k(\theta_1 - \theta_2) = 0. \end{cases} \tag{5.2}$$

Define the normal co-ordinates by

$$\begin{cases} \phi_1(\tau) = (\theta_1(\tau) + \theta_2(\tau))/2 \\ \phi_2(\tau) = (\theta_1(\tau) - \theta_2(\tau))/2 \end{cases} \longrightarrow \begin{cases} \theta_1(\tau) = \phi_1(\tau) + \phi_2(\tau) \\ \theta_2(\tau) = \phi_1(\tau) - \phi_2(\tau). \end{cases} \tag{5.3}$$

With this change of co-ordinates the in-phase motion ($\theta_1(\tau) = \theta_2(\tau)$) is now expressed as $\phi_2(\tau) = 0$, while for the out-of-phase motion ($\theta_1(\tau) = -\theta_2(\tau)$) it is $\phi_1(\tau) = 0$. In these new co-ordinates, the equations (5.2) are rewritten as

$$\begin{cases} \phi_1'' + \beta\phi_1' + \frac{1}{2}F(\tau)(\sin\theta_1 + \sin\theta_2) = 0 \\ \phi_2'' + \beta\phi_2' + \frac{1}{2}F(\tau)(\sin\theta_1 - \sin\theta_2) + 2k\phi_2 = 0. \end{cases} \tag{5.4}$$

We can simplify the sums of the sines in equations (5.4) using the identities

$$\begin{aligned} \sin(\phi_1 + \phi_2) + \sin(\phi_1 - \phi_2) &= 2\sin\phi_1\cos\phi_2 \\ \sin(\phi_1 + \phi_2) - \sin(\phi_1 - \phi_2) &= -2\cos\phi_1\sin\phi_2. \end{aligned} \tag{5.5}$$

Using these identities equations (5.4) transform to

$$\begin{cases} \phi_1'' + \beta\phi_1' + F(\tau)\sin\phi_1\cos\phi_2 = 0 \\ \phi_2'' + \beta\phi_2' + F(\tau)\cos\phi_1\sin\phi_2 + 2k\phi_2 = 0. \end{cases} \tag{5.6}$$

From these equations of motion we can now investigate the in-phase motion $(\phi_2, \phi_2') = (0, 0)$, as well as the out-of-phase motion $(\phi_1, \phi_1') = (0, 0)$. All we have to do is to linearise the respective equations about these two states, and then finding a way

of evaluating the eigenvalues in these states.

The equation for in-phase oscillations is obtained by using the condition $\phi_2 = 0$,and so from equation (5.6) this equation can be shown to be

$$\phi_1'' + \beta\phi_1' + F(\tau)\sin\phi_1 = 0. \tag{5.7}$$

This equation has two periodic terms. The forcing $F(\tau)$, that has period $2\pi/\omega$, and the second one is $\phi_1(\tau)$, because it is assumed we used parameter values for which a single parametrically excited pendulum displays a periodic behaviour. Several different periodic solutions can coexist for a fixed setting of parameters. For small values of p, we can approximate the equation of the pendulum by the linearised equation

$$\phi_1'' + \beta\phi_1' + (1 + p\cos(\omega\tau))\phi_1 = 0. \tag{5.8}$$

Following the work of [Hayashi, 1964], we can approximate the zones in which the hanging solution is unstable by the method of harmonic balance. Using the harmonic balance method we look for a solution to (5.8) in the form

$$\phi_1 = a(\tau)\cos(\Omega\tau) + b(\tau)\sin(\Omega\tau). \tag{5.9}$$

Now, assume that $a''(\tau) \approx 0$ and $b''(\tau) \approx 0$, $\omega = 2/n\Omega$, $n = 1, 2, \ldots$. We will consider the case when $n = 1$ which corresponds to the main resonance zone of in-phase periodic synchronisation. Using the identities from equation (5.10)

$$\begin{cases} \cos(2\Omega\tau)\cos(\Omega\tau) = 1/2\cos(3\Omega\tau) + 1/2\cos(\Omega\tau) \\ \cos(2\Omega\tau)\sin(\Omega\tau) = 1/2\sin(3\Omega\tau) - 1/2\sin(\Omega\tau), \end{cases} \tag{5.10}$$

equation (5.8) becomes

$$\begin{cases} [2b'\Omega - a\Omega^2 + \beta a' + \beta b\Omega + a + \frac{pa}{2}]\cos(\Omega\tau) \\ +[-2a'\Omega - b\Omega^2 + \beta b' - \beta a\Omega + b - \frac{pb}{2}]\sin(\Omega\tau) = 0. \end{cases} \tag{5.11}$$

We demand that coefficients of $\cos(\Omega\tau)$ and $\sin(\Omega\tau)$ be identically zero, from which we get

$$\begin{bmatrix} \beta & 2\Omega \\ -2\Omega & \beta \end{bmatrix} \begin{bmatrix} a' \\ b' \end{bmatrix} = \begin{bmatrix} (\Omega^2 - 1 - \frac{p}{2}) & -\beta\Omega \\ \beta\Omega & (\Omega^2 - 1 + \frac{p}{2}) \end{bmatrix} \cdot \begin{bmatrix} a \\ b \end{bmatrix}. \tag{5.12}$$

We look for solutions of the form

$$\begin{cases} a(\tau) = ae^{\lambda\tau} \\ b(\tau) = be^{\lambda\tau} \end{cases} \longrightarrow \begin{cases} a'(\tau) = a\lambda e^{\lambda\tau} \\ b'(\tau) = b\lambda e^{\lambda\tau}. \end{cases} \tag{5.13}$$

Put equation (5.13) into equation (5.12) then we get

$$\begin{bmatrix} \beta & 2\Omega \\ -2\Omega & \beta \end{bmatrix}^{-1} \begin{bmatrix} (\Omega^2 - 1 - \frac{p}{2}) & -\beta\Omega \\ \beta\Omega & (\Omega^2 - 1 + \frac{p}{2}) \end{bmatrix} \begin{bmatrix} a \\ b \end{bmatrix} = \lambda \begin{bmatrix} a' \\ b' \end{bmatrix}. \tag{5.14}$$

The proposed solution will explode (be unstable) when the eigenvalue λ has a positive real part, and die out (be stable) when its real part is negative. Thus, the hanging solution is unstable when $Re(\lambda) > 0$.

At the boundary of stability of the hanging solution we get from equation (5.14)

$$p = 2\sqrt{(\Omega^2 - 1)^2 + \beta\Omega^2}. \tag{5.15}$$

But $\Omega = \omega/2$ for the main zone of instability of the hanging solution, so the boundary of stability becomes

$$p = 2\sqrt{(\frac{\omega^2}{4} - 1)^2 + \beta\frac{\omega^2}{4}}. \tag{5.16}$$

Similarly for the Out-of-phase motion periodic synchronisation the equation of motion is

$$\phi_2'' + \beta\phi_2' + F(\tau)\sin\phi_2 + 2k\phi_2 = 0. \tag{5.17}$$

which we obtained by setting $\phi_1 = 0$ in (5.6). This equation of motion is no more the one of a single parametrically excited pendulum and displays periodic solutions for certain values of k. Using similar arguments as those we used for the in-phase periodic synchronisation we can obtain a condition for stability of the out-of-phase oscillations by requiring that at the boundary of stability the eigenvalues must satisfy $Re(\lambda) = 0$. This condition gives the result:

$$p = 2\sqrt{[\frac{\omega^2}{4} - (1+2k)]^2 + \frac{\beta^2\omega^2}{4}}. \tag{5.18}$$

For increasing coupling strength, the zone of in-phase motion remains fixed while the zone of out-of-phase motion shifts to the right. Figure 5.2 illustrates the shifting of the zone of out-phase motion as the coupling increases. The zones of in-phase and out-of-phase motion shown in Figure 5.2 where numerically determined by evaluating the expressions (5.16) and (5.18).

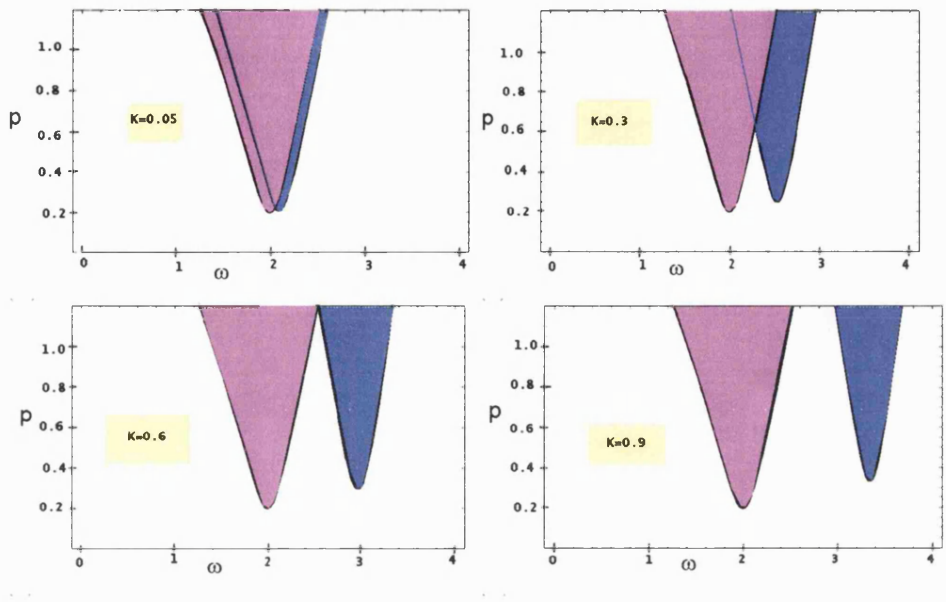

Figure 5.2: Zones of in-phase (located around $\omega = 2$) and out-of-phase (which shifts to the right as k increases) periodic synchronisation determined analytically with $\beta = 0.1$ for increasing k: (a) $k = 0.05$, (b) $k = 0.3$, (c) $k = 0.6$, (d) $k = 0.9$. Note that the zone of in-phase oscillations remains fixed at $(\omega, p) = (2, 0)$ as coupling increases while the zone of out-of-phase motion shifts to the right.

It is clear from Figure 5.2 that as coupling increases, the zone of out-of-phase periodic synchronisation drifts away from the zone of in-phase periodic synchronisation. This means that as coupling increases, out-of-phase periodic synchronisation can only be realised for higher values of the frequency of parametric forcing.

In this work we will confine our investigation to periodic synchronisation in the two resonance zones which are located around $\omega = 2$ and $\omega = 2\sqrt{1+2k}$ in the (ω, p) space. One of our main tasks is to investigate the effect of increasing the coupling when the parameters of the system are fixed either in the in-phase zone or out-of-phase zone.

In order to give examples of the effect of increasing the coupling, we approximate the basin of attraction for variation of initial position of in-phase and out-of-phase oscillations at $k = 0$ as shown in Figure 5.3. We assume that the initial angular velocities are zero.

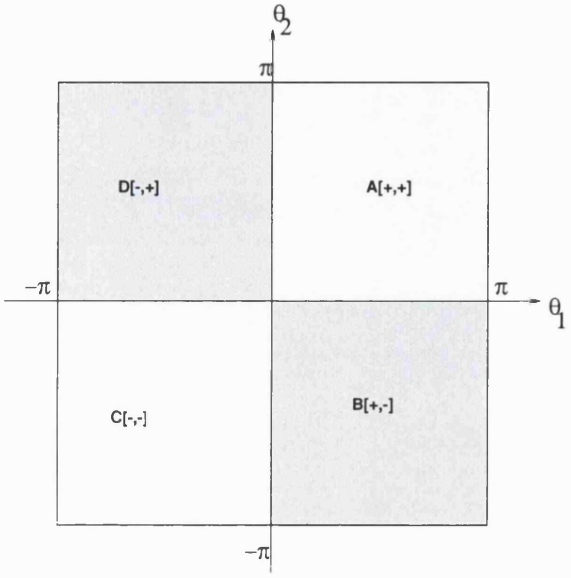

Figure 5.3: Approximate basins for initial condition for in-phase and out-of-phase periodic synchronisation when parameters are fixed in the zone around $(\omega, p) = (2, 0)$. For small values of the coupling, motions started in $A[+,+]$ and $C[-,-]$ will synchronise in-phase while motions started in $B[+,-]$ and $D[-,+]$ will synchronise out-of-phase. This is only true if we assume that there are no initial angular velocity perturbations. For sufficiently large values of k all periodic motions are in-phase regardless of initial conditions when parameters are fixed in the first resonance zone.

This corresponds to experimental situation where initial perturbations to angular velocities are assumed zero particularly if the experiments are initiated when the motor is not running. However, if the motor is running it might be easier to disturb the velocity from the fixed position $\theta_1 = \theta_2 = 0$. We will not report on experimental results here but broad comparison with previous experimental results are useful to provide insight into the dynamical response of the system [Oliveira et al., 2001]. Throughout this work we will fix the values of β, the damping at a representative value of $\beta = 0.1$. This is the value generally used in this thesis and will facilitate comparison of results in the

different chapters.

For now we want to briefly discuss the effect of initial conditions as illustrated in Figure 5.3 when the motion is confined to the main zone of in-phase motion around $\omega = 2$ in the (ω, p) space. Although the motion is predominantly in-phase around this zone, we can also realise out-of-phase motion for low coupling k depending on initial conditions. In our case where we assumed no initial perturbations to the velocities, Figure 5.3 shows the initial conditions which result in in-phase and out-of-phase periodic synchronised motions for low values of the coupling strength.

In Figure 5.3 motions started from $A[+,+]$ and $C[-,-]$ will be in-phase periodic synchronised for low values of the coupling strength while those started from $B[+,-]$ and $D[-,+]$ will be out-of-phase periodic synchronised for low values of the coupling strength. For high values of the coupling strength, all motions with parameters fixed in the resonance zone around $(\omega, p) = (2, 0)$ will be in-phase regardless of the spatial initial conditions.

5.3 Periodic Synchronisation in the In-phase Zone

Now we want to study the bifurcation structure of the periodic synchronised motions when the parameters ω and p are fixed in the first resonance zone. We already know that in the (ω, p)-space periodic motions occur after the loss of stability of the trivial downward hanging solutions ($\theta_i = \theta_i' = 0$) (see Figure 5.2). However, our main interest here is to understand the bifurcation structure in the (k, p)-space. The aim is to explore periodic synchronisation in the major zone of in-phase periodic synchronisation around $\omega = 2$ in the (k, p) space. We assume static coupling, that is, where the coupling does not change with time. Among other things, we want to understand the mechanism leading to transitions from out-of-phase periodic synchronisation to in-phase periodic synchronisation. We use initial conditions as represented by Figure 5.3 where initial

perturbations to angular velocities are set to zero. With these assumptions for initial conditions we know that for very small coupling values, the in-phase and out-of-phase periodic synchronisation motions coexist.

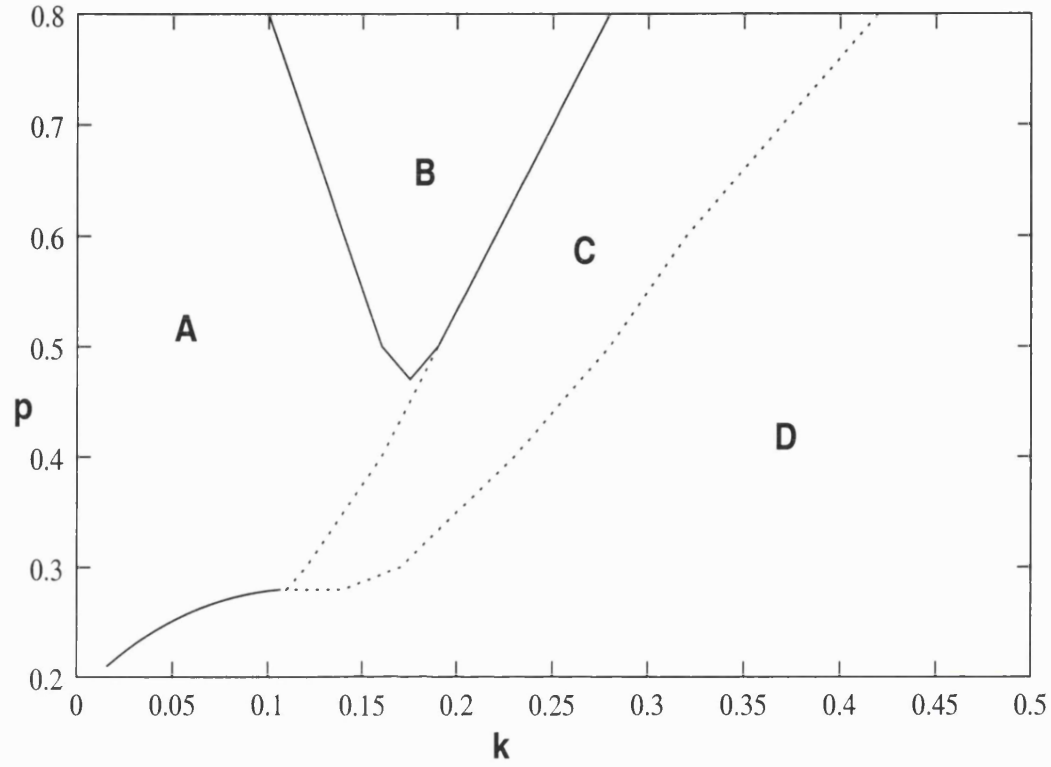

Figure 5.4: Zones of different periodic synchronisation regimes for $\omega = 1.9$ in the (k, p)-space: zone **A**: Out-of-phase synchronisation, zone **B**: In-phase synchronisation with transient rotation, zone **C**: Phase synchronisation with intermittency in amplitude of oscillation, zone **D**: In-phase synchronisation without transient rotation.

If the initial conditions are such that the system results in out-of-phase motion as represented in Figure 5.3, the system remains out-of-phase for very small coupling values and as coupling increases the out-of-phase periodic synchronisation destabilises giving birth to in-phase periodic synchronisation. Figure 5.4 shows the different zones in which the various types of periodic synchronisation occur as the coupling is gradually increased in the (k, p) space when ω is fixed around the main resonance zone for in-phase motion around $(\omega, p) = (2, 0)$ (more specifically $\omega = 1.9$). Here the value $\omega = 1.9$ was chosen to avoid any particular symmetries which may occur for $\omega = 2.0$.

The zones marked **A**, **B**, **C** and **D** in Figure 5.4 in the (k, p)-space exhibit different forms of periodic synchronisation.

The zones were calculated for initial conditions which would result in out-of-phase periodic synchronisation as represented in Figure 5.3 with the coupling strength being gradually increased. But the results shown in Figure 5.4 do not change significantly if initial conditions which would give rise to in-phase periodic synchronisation for low values of the coupling strength were used. The only significant change would be in zone **B**; preliminary numerical results indicate that it would be significantly reduced in size and shifted upwards if in-phase initial conditions are used. Typical trajectories for motions started in zones **A**, **B**, **C** and **D** are shown in Figure 5.5.

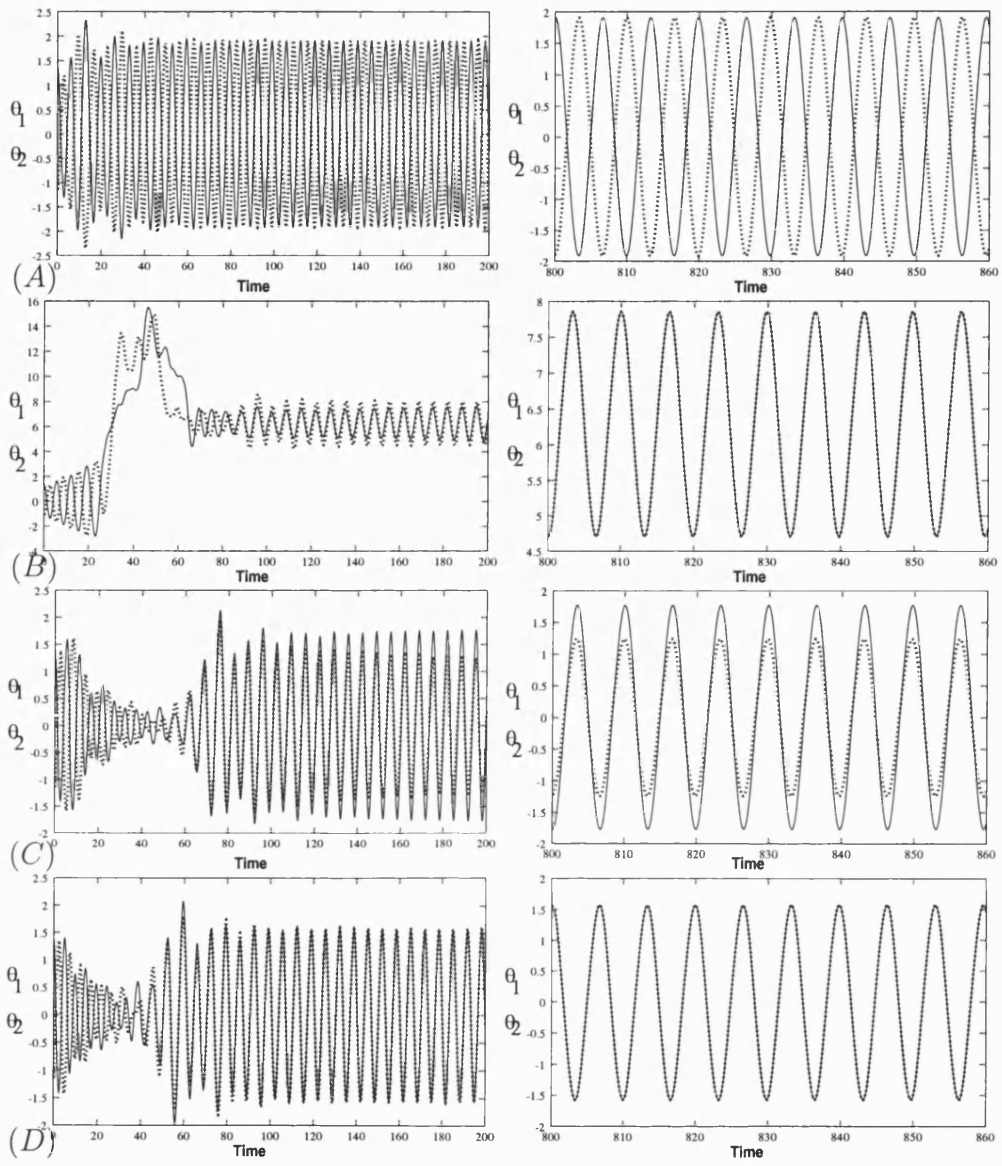

Figure 5.5: Typical trajectories for motions of the two pendula in zones **A**, **B**, **C**, and **D** for $p = 0.6$, $\omega = 1.9$. All the motions had initial conditions $(\theta_1, \theta_1', \theta_2, \theta_2') = (1.37, 0.0, -1.17, 0.0)$: (a) in zone **A** for $k = 0.08$: out-of-phase synchronisation, (b) in zone **B** for $k = 0.21$: in-phase synchronisation attained after rotating motion, (c) in zone **C** for $k = 0.28$: phase synchronised oscillations with different amplitudes and (d) in zone **D** for $k = 0.42$: in-phase synchronisation attained with no rotating motions. **Left**: Transient motion, **Right**: Steady state motion.

Let us consider in detail the various synchronisation regimes that occur in the different zones shown in Figure 5.3 as the coupling increases. The example given here is for system when the initial conditions are out-of-phase. But we confirmed that the results

would be similar if we had started with in-phase initial conditions.

(1) **Synchronisation in zone A**: In zone **A**, the pendula are in out-of-phase synchronisation. This is mainly because we chose initial conditions which would give out-of-phase synchronisation for small coupling as shown in Figure 5.3. Therefore in the first resonance zone initial conditions play a crucial role in determining the final synchronised state. Since the coupling is very small here it does not influence the final synchronised state in a significant way.

(2) **Synchronisation in zone B**: In zone **B** the system of coupled pendula exhibits in-phase synchronised oscillations. Thus the boundary between zone **A** and zone **B** is marked by a desynchronisation bifurcation which destabilises the out-of-phase periodic synchronisation giving birth to in-phase periodic synchronisation. An important feature of the in-phase periodic synchronisation which occurs in zone **B** is that it almost always occurs after the coupled pendula have undergone rotating motion. This rotation before the system converges onto the synchronised state (or indeed any other attractor), corresponds to the well documented phenomenon of escape from a local energy well [Clifford and Bishop, 1993, 1994; Stewart and Faulkner, 2000]. Therefore zone **B** represents the parameter space in which trajectories of a system of two coupled parametrically excited pendula initially contained within an energy well escape the confines of the local potential well and transverse through one or several adjacent energy wells before converging onto stable synchronised oscillatory behaviour.

The property of escape from a local potential energy is a common problem in science and engineering. Examples of this phenomena occur in capsize of ships [Gottwald et al., 1995; Thompson et al., 1990a; Thompson and Soliman, 1990b], the toppling of rigid blocks [Hogan, 1989a,b, 1990; Virgin et al., 1996], in the response of Josephson junctions and in electrical power engineering and also in phase-locked loops [Booker et al., 2000]. In most of these

systems, it is the disruptive nature of this escape phenomena which can cause failure in the smooth functioning of the technological systems. The motions which may be disruptive by leaving the local energy may correspond to periodic rotations [Garira and Bishop, 2002; Janicki and Szemplińska-Stupnicka, 1995], chaotic tumbling [Bishop and Clifford, 1996a; Thompson, 1989] or indeed long transients induced by a fractal basin boundary [Thompson et al., 1987; Lansbury and Thompson, 1990]. So in short, we can say that for the system of two coupled pendula and for a given set of initial conditions zone **B** represents combinations of amplitude of forcing p and coupling strength k for fixed frequency of forcing ω which cause the system to escape the confines of a local energy well as a transient process towards stable synchronous behaviour. The zone was determined numerically by simulating a series of start-ups involving different combinations of (k, p) for fixed ω for a number of initial conditions. Each simulation which resulted in transient escape from a local energy well before the system became synchronised was recorded.

(3) **Synchronisation in zone C**: In zone **C** another type of periodic synchronisation is realised. This periodic synchronisation is different from the out-of-phase synchronisation in zone **A** and in-phase synchronisation in zone **B**. Here the two coupled parametrically excited pendula are only phase synchronised and continue to perform oscillatory motion but with different amplitude of oscillations. Therefore the boundary between zone **B** and zone **C** is marked by another desychronisation bifurcation which destabilises the in-phase periodic synchronisation, giving birth to yet another form of periodic synchronisation (phase synchronisation) in which the pendula oscillate with different amplitudes.

(4) **Synchronisation in zone D**: Another desynchronisation bifurcation occurs at the boundary of zone **C** and **D** where the phase synchronisation is destroyed and the pendula become in-phase synchronised again with equal amplitudes of oscillation. However, the distinction between in-phase synchronisation in zone **B** and **D** is that in zone **B** in-phase motion is only realised after the pendula have

undergone transient rotating motion (transient escape), while within zone **D** the two pendula synchronise without any transient rotating motion.

Because of the existence of the different synchronisation regimes in the parameter space there can be no sharp synchronisation coupling threshold. Instead there are multiple thresholds. We recall that in zone **A** of Figure 5.4 and for given initial conditions, the pendula are out-of-phase synchronised even for $k = 0$. Thus the periodic synchronisation manifold **M**, that is, the plane $(\theta_1, \theta_1') = (-\theta_2, -\theta_2')$ is invariant and attracting even for $k = 0$ for a given set of spatial initial conditions. As k increases and sweeps across zone **A**, it reaches a value when the orbits in **M** lose transverse stability through a desynchronisation bifurcation. This takes us to another synchronisation regime in zone **B**. This again is subsequently destabilised as the coupling increases and so on until zone **D** where any further increase of k does not destabilise the periodic synchronisation.

The different synchronisation regimes occur because as coupling increases, the symmetries of the coupled pendula change. These changes in the symmetry of the system account for the different periodic synchronisation regimes. The study of symmetry of two coupled parametrically excited pendula is beyond the scope of this thesis. But we note that the occurrence of desynchronisation bifurcations as coupling increases is a fundamental property of this system and is caused by the different symmetry properties introduced into the system as the coupling increases. So we have a situation where different forms of periodic synchronisation are realised as coupling increases.

5.4 Periodic Synchronisation in the Out-of-phase Zone

In this section we consider periodic synchronisation in the second resonance zone which is located around $(\omega, p) = (2\sqrt{1+2k}, p)$ in the parameter space. What is surprising about the synchronous behaviour when parameters are fixed in this zone is that for whatever spatial initial conditions, we only realise out-of-phase periodic synchronisation.

This out-of-phase periodic synchronisation is different from the one that we discussed in the previous section which is due to initial conditions. The out-of-phase periodic synchronisation here is due to parameters of the system and does not depend on initial conditions. Whether the initial conditions are out-of-phase or in-phase as shown in Figure 5.3, the system will always asymptotically synchronise to the out-of-phase motion. The dominant factor here is the high frequency and high coupling. Another important point to note about the out-of-phase periodic synchronisation here is that the out-of-phase periodic synchronisation only exists for a finite interval of coupling strength. Figure 5.6 shows typical coupling values for out-of-phase synchronisation in the (k, p) when ω is fixed in the out-of-phase zone.

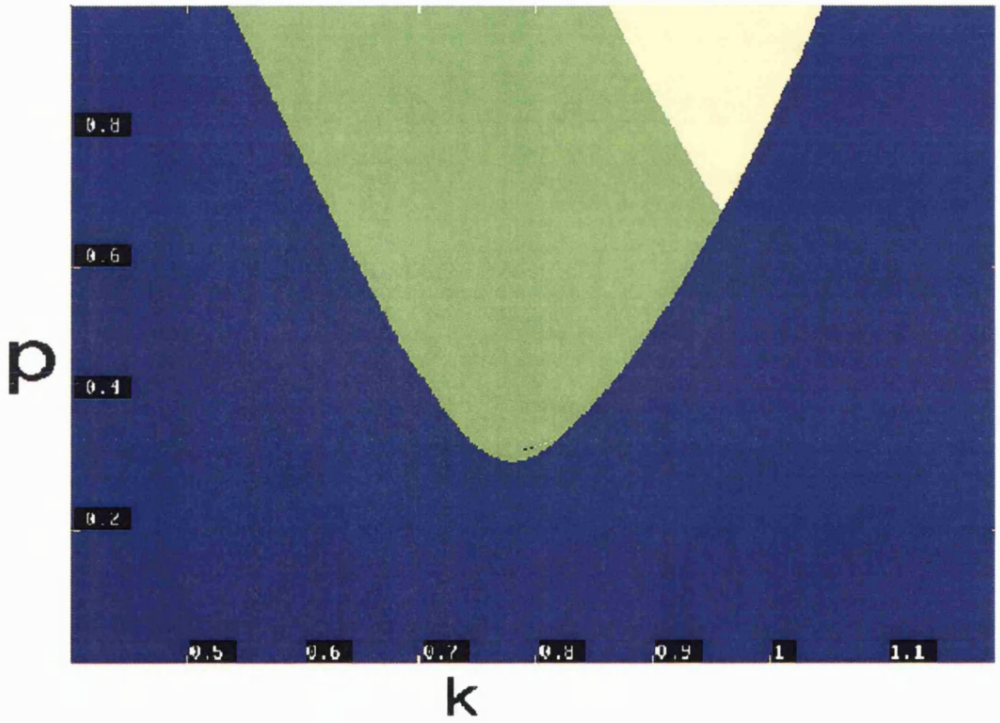

Figure 5.6: Zone of out-of-phase periodic synchronisation in the (k, p)-space for ω fixed at $2\sqrt{1+2k} = 3.2$. This zone is shifted further to the left for higher values of ω. Green colour represents regions of out-of-phase synchronisation, yellow represents regions of chaos while blue represents regions of parameter space where the downward equilibrium is realised for both pendula.

However, it has to be noted that for each ω value the out-of-phase motion is only stable for a finite interval of the coupling strength. This is clearly illustrated in Figure 5.6 in the (k, p) space. In order to give a rough idea of the interval of coupling values for which the out-of-phase periodic synchronisation is stable when the parameters are fixed in the second resonance, we illustrate this by some bifurcation diagrams shown in Figure 5.7.

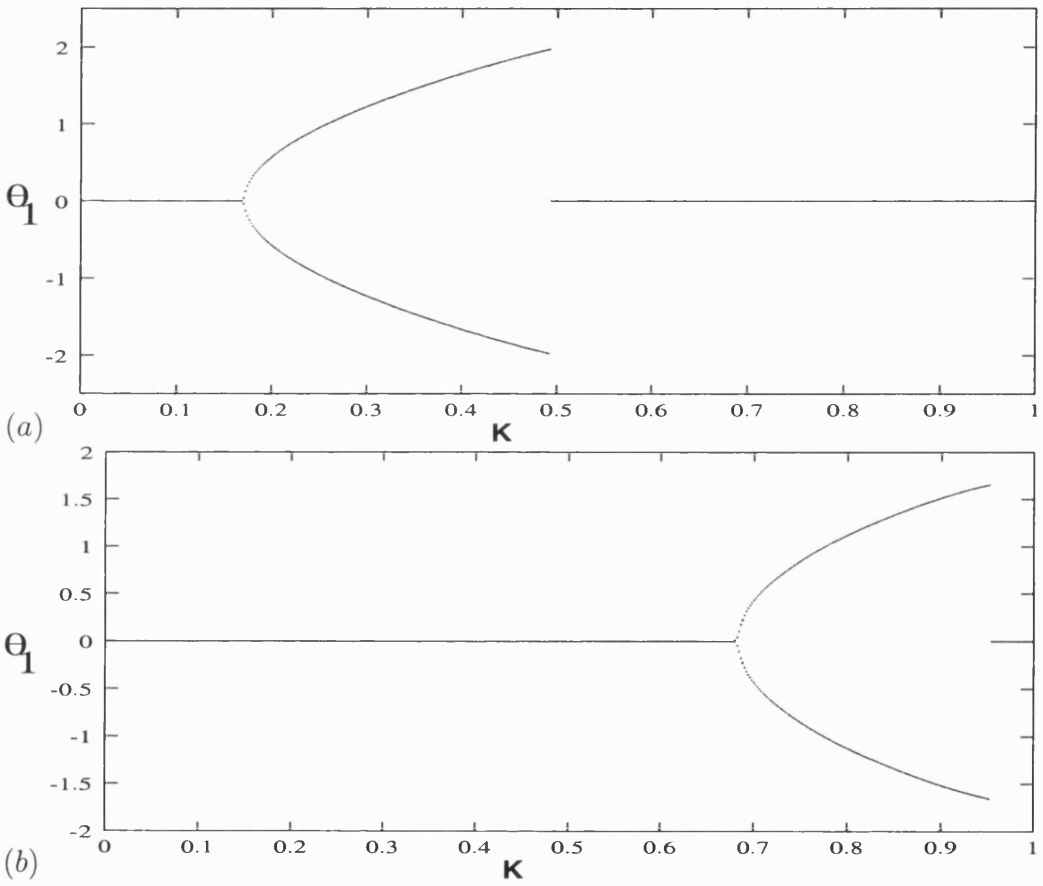

Figure 5.7: Bifurcation diagrams with coupling strength k as bifurcation parameter for different values of the amplitude of forcing and frequency. (a) $\omega = 2.5$, $p = 0.5$: we have out-of-phase periodic synchronisation for $0.17 < k < 0.492$. For k outside this interval the system synchronises into the downward equilibrium point. (b) $\omega = 3.2$, $p = 0.5$: we have out-of-phase periodic synchronisation for $0.68 < k < 0.953$. For k outside this interval the system synchronises into the downward equilibrium point.

It is clear that the out-of-phase motion in the (k, p) space occurs after the loss of stability of the trivial solutions ($\theta_i = \theta_i' = 0$). The implication of this is that at the stability boundary, the pendula undergo periodic doubling bifurcation as illustrated in Figure 5.7.

5.5 Final Remarks

To conclude we would like to recall some of the most important, or should we say, the most intriguing results of this chapter. It is perhaps not surprising that coupling introduces a new zone of periodic motion in the parameter space, when compared with the single parametrically excited pendulum. However, what we find most interesting is that in-phase and out-of-phase synchroninization cease to co-exist, and for high values of the coupling parameter k are only observed in two separate regions of the parameter space. The main issues studied in this chapter are:

- Use of normal coordinates to study in-phase and out-of-phase periodic oscillations.
- In-phase and out-of-phase periodic synchronisation of two coupled parametric pendula which occurs in the resonance zones located around $(\omega, p) = (2, 0)$ and $(\omega, p) = (2\sqrt{1+2k}, 0)$ respectively.
- The different periodic synchronisation regimes which occur in the resonance zone located around $(\omega, p) = (2, 0)$ as coupling varies.

Chapter 6

Chaos Synchronisation of Two Parametrically Excited Pendula

6.1 Introduction

This chapter builds on the earlier work of chapter 4 of this thesis in which we discussed the different chaotic regimes of the single parametrically excited pendulum. Here we consider chaos synchronisation of two parametrically excited pendula. This is part of our continuing study of the synchronous behaviour of two parametrically excited pendula which we initiated in chapter 5 by looking at synchronisation when the dynamics is both periodic and oscillatory. Previous studies of chaos synchronisation in a system of two coupled parametrically excited pendula include the paper by [Zhang et al., 1999]. In this paper the authors studied the synchronisation of tumbling chaos of two parametrically excited pendula which were coupled through a variable feedback, where the feedback was designed to periodically impose on one pendulum. In some time intervals the feedback was active while in other time intervals the chaotic pendula were uncoupled. There is also a paper by [Weele and Banning, 2001] which discusses mode interaction in a system of two coupled parametrically excited pendula and gives further insight into the dynamics of the system.

Here the fundamental question to be addressed is: If we coupled two pendula both of which are in chaotic state, be it oscillatory chaos, rotating chaos or tumbling chaos,

what are the different chaotic synchronisation regimes that can be realised as we vary parameters of the system? In part answer to this question we show in this chapter that the in-phase and out-of-phase dynamics of the two parametrically excited pendula which we considered in chapter 5 in the context of periodic synchronisation can also be realised when the dynamics is chaotic.

We also want to explore if symmetry can be used to give insight into the type of synchronisation that can be realised. In chapter 4 we established in the case of a single parametrically excited pendulum that symmetry and chaos can coexist. This sounds weird because any particular chaotic solution that we look at for only a short period of time cannot have symmetry. Infact, a chaotic particle moves along a seemingly disordered trajectory, with no implicit local symmetry in its motion. However, we realised from chapter 4 that by looking at the global properties of the trajectory (e.g. the ω-limit set associated with the trajectory), we can build some insight into the symmetry of the chaos, in particular, on what is called symmetry on the average [Ashwin, 1999].

Thus in this chapter where we consider synchronisation of two parametrically excited pendula when their dynamics is chaotic we are still interested in pursuing the same question: can symmetry and chaos coexist? The answer is yes, leading to what is still called **symmetric chaos** as in chapter 4, but this time the symmetric chaos turns out to be synchronised chaos.

6.2 Symmetry of the Equations of Motion

An idealised model of the two parametrically excited pendula which are assumed to be linearly coupled by a torsion spring was shown in Figure 1.8. If the common suspension point of the two pendula is given by $z(t) = -a\cos(\Omega t)$ and configurations of the

pendula are defined by angles θ_1 and θ_2, then the equations of motion can be shown to be (after scalings as detailed in chapter 1):

$$\begin{cases} \theta_1'' + \beta\theta_1' + (1 + p\cos(\omega\tau))\sin(\theta_1) + k(\theta_1 - \theta_2) = 0 \\ \theta_2'' + \beta\theta_2' + (1 + p\cos(\omega\tau))\sin(\theta_2) - k(\theta_1 - \theta_2) = 0 \end{cases} \tag{6.1}$$

where k is a coupling parameter and β, p, ω are the damping, amplitude of parametric forcing and the frequency of parametric forcing of the pendula respectively.

A striking feature which makes the study of chaos synchronisation of the system described by equations (6.1) interesting is that apart from the usual properties of chaotic systems such as sensitive dependence on initial conditions as illustrated in Figure 6.1 and the apparent randomness of the trajectories, the chaotic dynamics here if "fragile" with

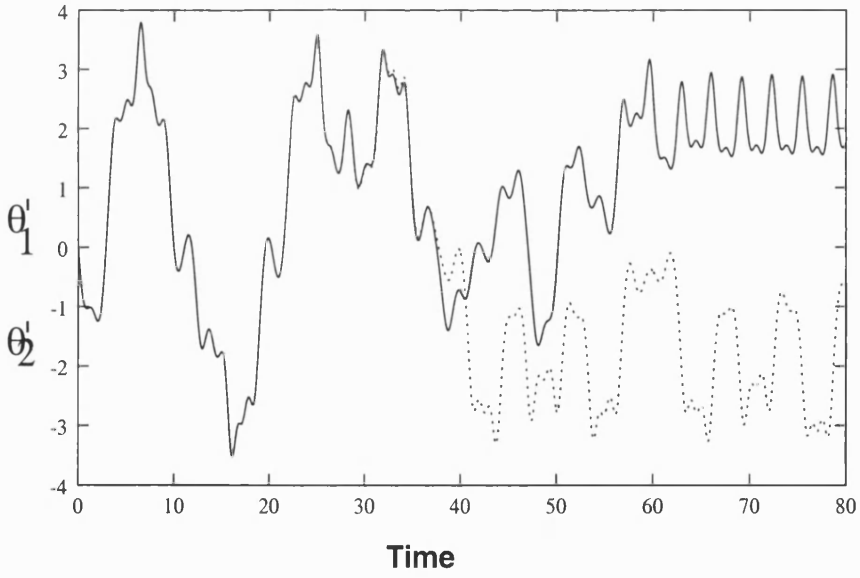

Figure 6.1: Trajectories started close together showing sensitive dependence on initial conditions for $\omega = 2$ and $p = 2$ with $(\theta_1, \theta_1') = (0.8001, 0)$, $(\theta_2, \theta_2') = (0.8005, 0.0)$.

respect to the parameters of the system, that is, a slight alteration of one of the parameters may destroy the chaos leading to either periodic or indeed any other types of stable response. This is particularly true at low values of the amplitude of forcing

while at large values of the amplitude of forcing the chaotic attractor persists.

Take for example Figure 6.2 which shows the different dynamical responses of the two coupled parametrically excited pendula in the (ω, p)-space when the coupling k and damping β are fixed at $k = 0.6$, $\beta = 0.1$.

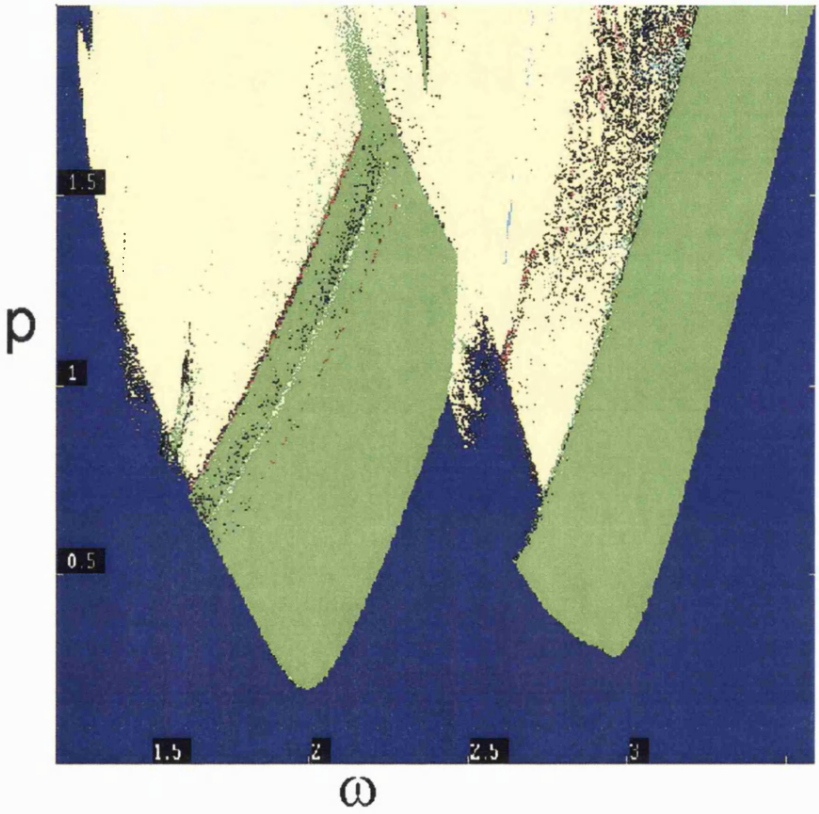

Figure 6.2: Zones of chaotic and periodic behaviour in the (ω, p)-space: The green regions are for period two oscillations while the yellow regions are the chaotic zones and blue regions are zones of stability of the downward equilibrium for both pendula.

Figure 6.2 shows the resonance zones located around $(\omega, p) = (2, 0)$ and $(\omega, p) = (2\sqrt{1+2k}, 0)$, where yellow regions represent parameter values for which chaotic behaviour is realised while the green regions represent parameter values for which periodic motion is realised (mainly in-phase and out-of-phase oscillations). Blue regions represent parameter values for which the downward equilibrium point

is stable for both pendula. It is evident from Figure 6.2 that for lower values of p the coupled pendula exhibit a wide variety of dynamical responses while for higher values of p the motion is predominantly chaotic.

In equations (6.1), the natural frequency is scaled to 1. For the work that follows, we fix the damping at $\beta = 0.1$. Now the accessible parameters are p, ω and k. Our primary goal is to describe the nature of the behaviour with respect to the parameters p, ω and k and indicate the different types of chaotic synchronisation that may be realised. We will systematically analyse the effect of varying the coupling strength both in terms of new dynamical features it introduces to the system and also in terms of influencing the dynamics of the system to converge onto (stable) synchronised state. But first let us briefly discuss the symmetry of equations (6.1) which govern the dynamics of the two coupled parametrically excited pendula.

It is now well-known that Synchrony is one of the most symmetrical states of coupled systems. The following are some of the **symmetries of the equations of motion** of the two coupled parametrically excited pendula:

(1) **Temporal translation T**: The corresponding transformation for this symmetry property is

$$[\theta_1, \theta_1', \theta_2, \theta_2', \tau] \rightarrow [\theta_1, \theta_1', \theta_2, \theta_2', \tau + T]. \tag{6.2}$$

This symmetry is induced into the system by the driving which is periodic. The implications of the periodic driving force are that the equations of motion are unaltered by a time translation over one driving period $T = 2\pi/\omega$.

(2) **Spatial translation S**: The transformation corresponding to this symmetry is

$$[\theta_1, \theta_1', \theta_2, \theta_2', \tau] \rightarrow [\theta_1 + 2\pi, \theta_1', \theta_2 + 2\pi, \theta_2', \tau]. \tag{6.3}$$

In the case of the two identical pendula considered here, the implications of this symmetry property is that the system possess an infinite number of invariant subspaces defined by $\theta_1 - \theta_2 = 2n\pi$ where n is an integer.

(3) **Reflection R**: The transformation that represents this symmetry is

$$[\theta_1, \theta_1', \theta_2, \theta_2', \tau] \rightarrow [-\theta_1, -\theta_1', -\theta_2, -\theta_2', \tau]. \tag{6.4}$$

Its implications on the dynamics of the two coupled pendula is that it does not make any difference for a single pendulum whether it swings toward the right or to the left.

(4) **Exchange E**: The corresponding mathematical representation of this symmetry is simply an exchange of indices:

$$[\theta_1, \theta_1', \theta_2, \theta_2', \tau] \rightarrow [\theta_2, \theta_2', \theta_1, \theta_1', \tau]. \tag{6.5}$$

This symmetry is present in the system because the coupled pendula are identical. Therefore it does not matter which one of the pendula is called 1 and which is called 2.

In the case of periodic oscillations of the two coupled parametrically excited pendula which we considered in chapter 5, we noted that as coupling is varied, the symmetries of the periodic oscillations of the two coupled parametrically excited pendula are changed. We indicated that this caused the system to exhibit different periodic synchronisation regimes including in-phase periodic synchronisation and out-of-phase periodic synchronisation. In this chapter where the dynamics of the pendula is chaotic the system of two parametrically excited pendula also experiences different types of chaos synchronisation as parameters are varied. For given initial conditions and parameters the following two types of chaotic synchronisation are realised:

(a) **Out-of-phase chaotic synchronisation**: Also widely known as antiphase chaotic synchronisation [Cao and Lai, 1998; Blazejczyk-Okolewska et al., 2001;

Astakhov et al., 2000; Uchida et al., 2001]. Typical examples of this type of chaotic synchronisation are shown in Figure 6.3 and Figure 6.4.

(b) **In-phase chaos synchronisation**: Widely known as complete synchronisation or identical synchronisation [Boccoletti et al., 2001; Bown and Kocarev, 2000]. In this case we have $\theta_1 = \theta_2$ after transients. Typical examples of this type of chaotic synchronisation are shown in Figure 6.5 and Figure 6.6.

Let us now consider each of these two types of chaos synchronisation and indicate their relationship with the different symmetry properties of the governing equations that we have just discussed.

6.3 Out-of-phase chaos synchronisation

In this section we describe a chaotic synchronisation regime of two parametrically excited pendula which occurs when the chaotic oscillations of the system possess the symmetry described by the transformations (6.4) and (6.5), that is they are invariant with respect to the reflection symmetry **R** and exchange symmetry **E**. For notational convenience we shall simply say the chaotic oscillations possess the symmetry **RE**. A chaotic motion of the two coupled parametrically excited pendula possess the **RE** symmetry if and only if the following relation holds

$$\begin{bmatrix} \theta_1(\tau) \\ \theta_1'(\tau) \\ \theta_2(\tau) \\ \theta_2'(\tau) \end{bmatrix} = \mathbf{RE} \begin{bmatrix} \theta_1(\tau) \\ \theta_1'(\tau) \\ \theta_2(\tau) \\ \theta_2'(\tau) \end{bmatrix} = \begin{bmatrix} -\theta_2(\tau) \\ -\theta_2'(\tau) \\ -\theta_1(\tau) \\ -\theta_1'(\tau) \end{bmatrix} \tag{6.6}$$

after the transients have died away. Equation 6.6 guarantees the existence of the out-of-synchronisation manifold (invariant manifold) defined by

$$\theta_1(\tau) = -\theta_2(\tau) \quad and \quad \theta_1'(\tau) = -\theta_2'(\tau). \tag{6.7}$$

This implies the existence of out-of-phase chaotic synchronisation which is characterised by the dynamics of the two pendula collapsing onto the synchronisation manifold defined by equation (6.7). Figure 6.3 and Figure 6.4 show some typical examples for some parameter values and initial conditions for which the out-of-phase chaotic synchronisation is realised. In Figure 6.3 we have out-of-phase chaos synchronisation for $p = 2.0$ and $\omega = 2.0$, $k = 0.2$ for different initial conditions while in Figure 6.4

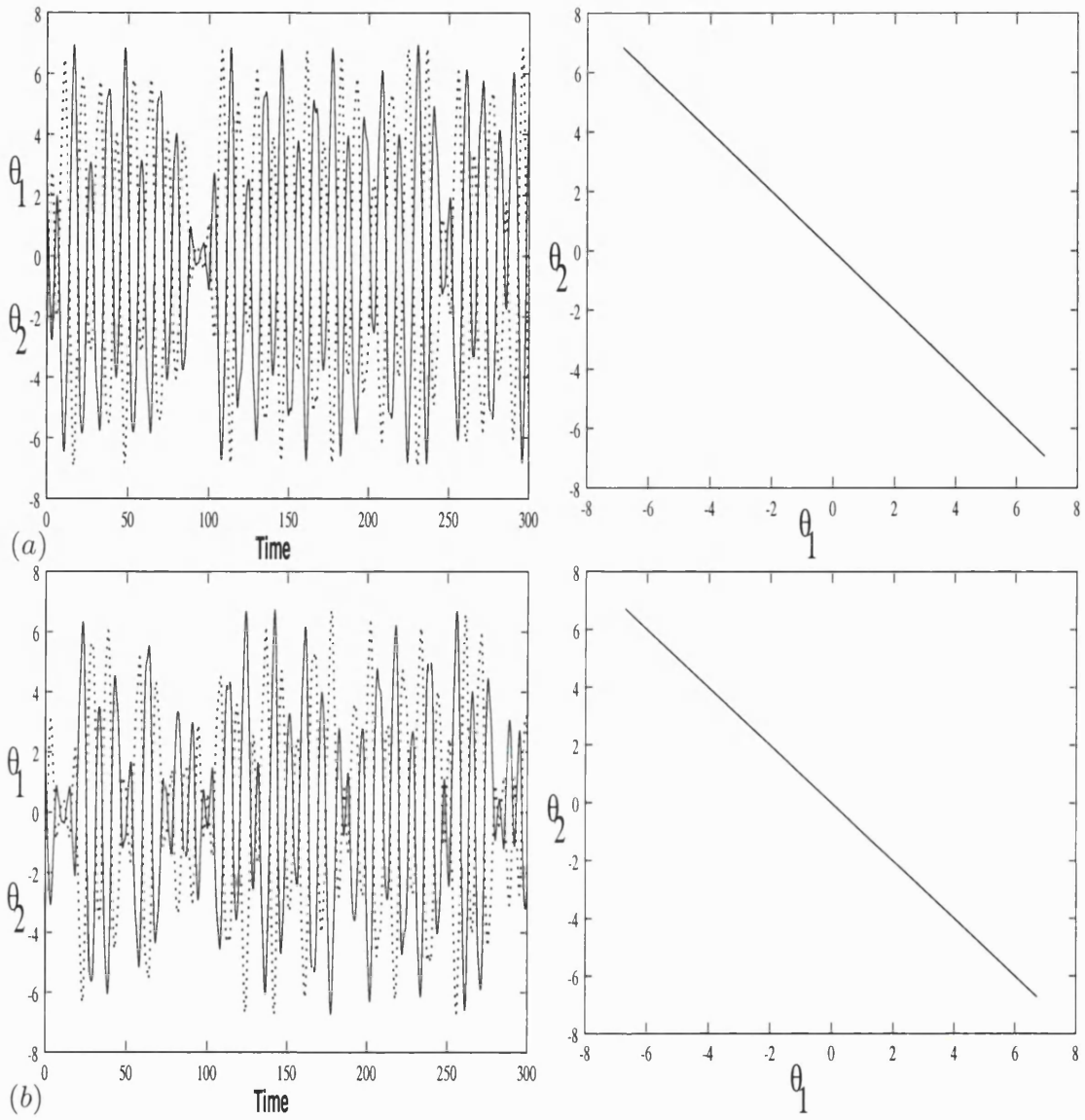

Figure 6.3: Out-of-phase chaos synchronisation of two parametrically excited pendula for $\omega = 2.0$, $p = 2.0$, $k = 0.2$ (a) with initial conditions $(\theta_1, \theta_1') = (1.37, 0)$, $(\theta_2, \theta_2') = (-1.37, 0)$. (b) with initial conditions $(\theta_1, \theta_1') = (1.57, 0)$, $(\theta_2, \theta_2') = (-1.57, 0)$. Left: the synchronised trajectories, Right: the synchronisation manifold.

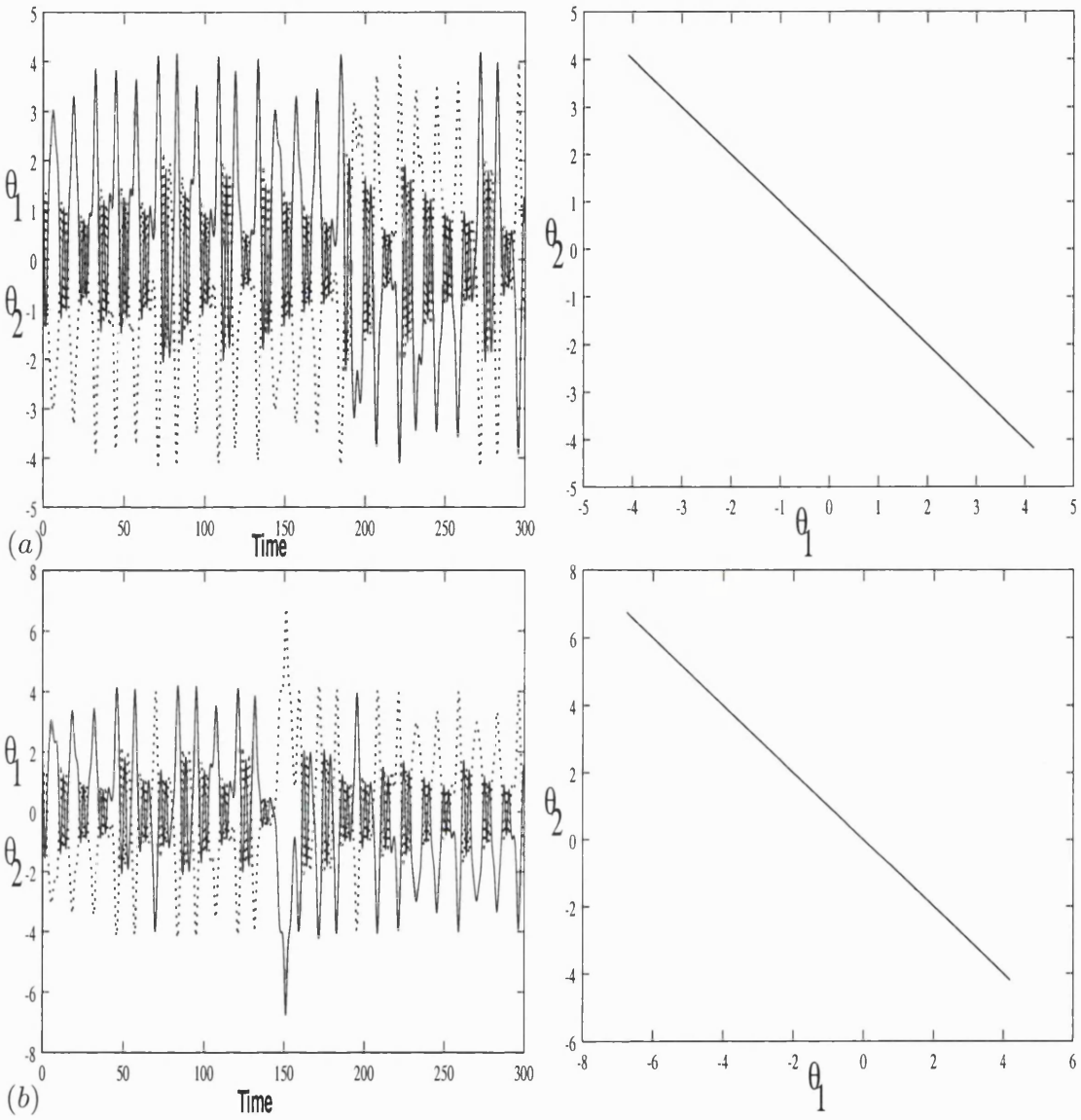

Figure 6.4: Out-of-phase chaos synchronisation of two parametrically excited pendula for $\omega = 0.5$, $p = 3.6$, $k = 0.2$ (a) with initial conditions $(\theta_1, \theta_1') = (1.37, 0)$, $(\theta_2, \theta_2') = (-1.37, 0.0)$. (b) with initial conditions $(\theta_1, \theta_1') = (1.57, 0)$, $(\theta_2, \theta_2') = (-1.57, 0.0)$. Left: the synchronised trajectories, Right: the synchronisation manifold.

we have out-of-phase chaos synchronisation for $p = 3.6$ and $\omega = 0.5$, $k = 0.2$ for different initial conditions as well. For these two particular examples, it was found that the out-of-phase chaotic synchronisation will be destroyed for higher values of the coupling strength. In the out-of-phase chaos synchronisation, initial conditions play a crucial role. Thus even if we have out-of-phase chaos synchronisation for the parameters

values given in these two examples, other initial conditions would not give out-of-phase chaos synchronisation. In general, it would appear that if have parameters p, ω and k for which the system is chaotic, then we can only realise out-of-phase chaos synchronisation for motions started on the out-of-phase synchronisation manifold for a certain range of coupling strengths.

6.4 In-phase Chaos Synchronisation

Now we describe a chaotic synchronisation regime of two parametrically excited pendula which occurs when the chaotic oscillations of the system possess the symmetry described by the transformations (6.5), that is they are invariant with respect to the exchange symmetry **E**. For notational convenience we shall simply say the chaotic oscillations possess the symmetry **E**. A chaotic motion of the two coupled parametrically excited pendula possess the **E** symmetry if and only if the following relation holds

$$\begin{bmatrix} \theta_1(\tau) \\ \theta_1'(\tau) \\ \theta_2(\tau) \\ \theta_2'(\tau) \end{bmatrix} = \mathbf{E} \begin{bmatrix} \theta_1(\tau) \\ \theta_1'(\tau) \\ \theta_2(\tau) \\ \theta_2'(\tau) \end{bmatrix} = \begin{bmatrix} \theta_2(\tau) \\ \theta_2'(\tau) \\ \theta_1(\tau) \\ \theta_1'(\tau) \end{bmatrix} \tag{6.8}$$

after the transients have died away. Equation 6.8 guarantees the existence of the in-phase synchronisation manifold defined by

$$\theta_1(\tau) = \theta_2(\tau) \quad and \quad \theta_1'(\tau) = \theta_2'(\tau). \tag{6.9}$$

This implies the existence of in-phase chaotic synchronisation which is widely known as complete or identical synchronisation and in our case is characterised by the dynamics of the two pendula collapsing onto the synchronisation manifold defined by equation (6.9).

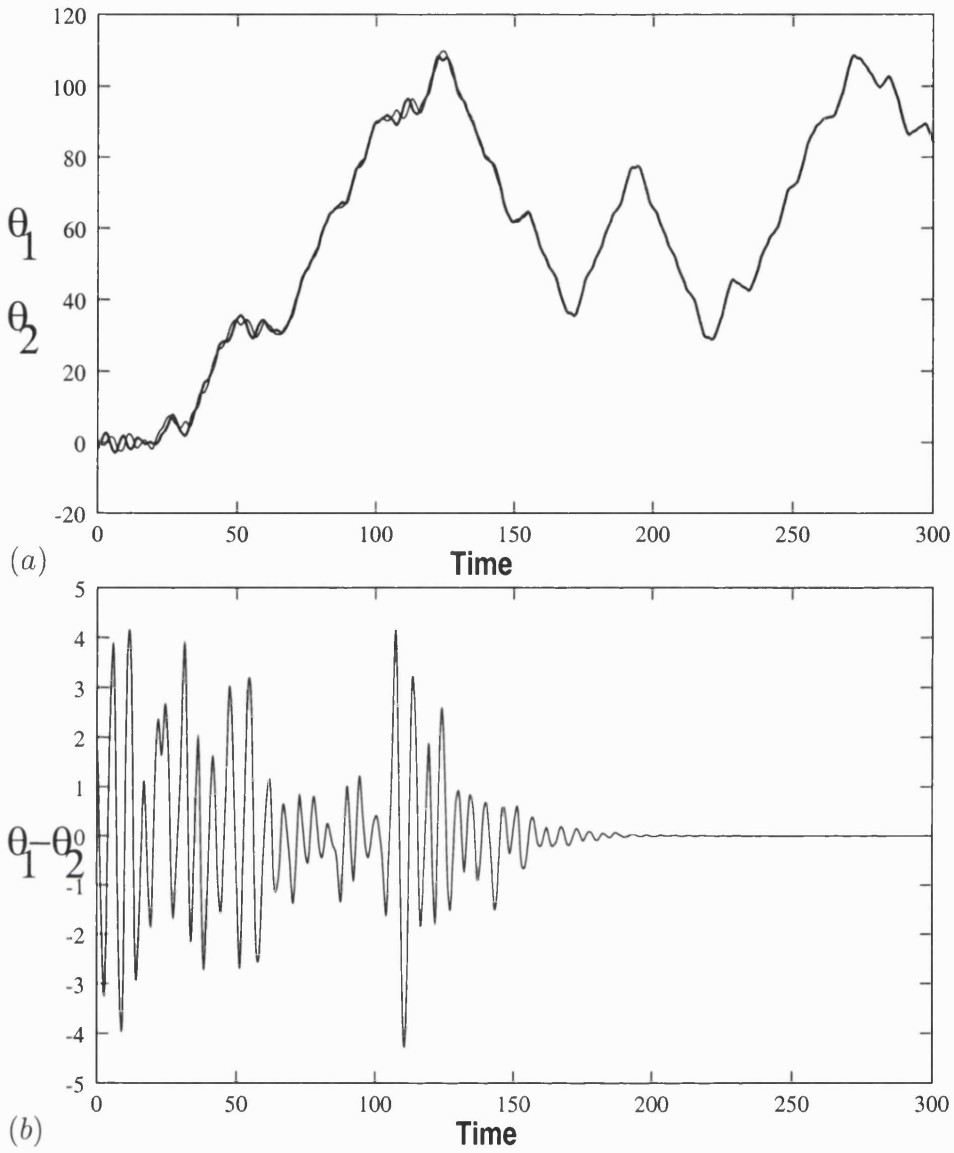

Figure 6.5: Synchronised chaotic orbits for two parametrically excited pendula with parameters $p = 2, \omega = 1.9$ and $k = 0.5$ (a) Time series of the chaotic orbits (b) Time series of the difference between the chaotic orbits.

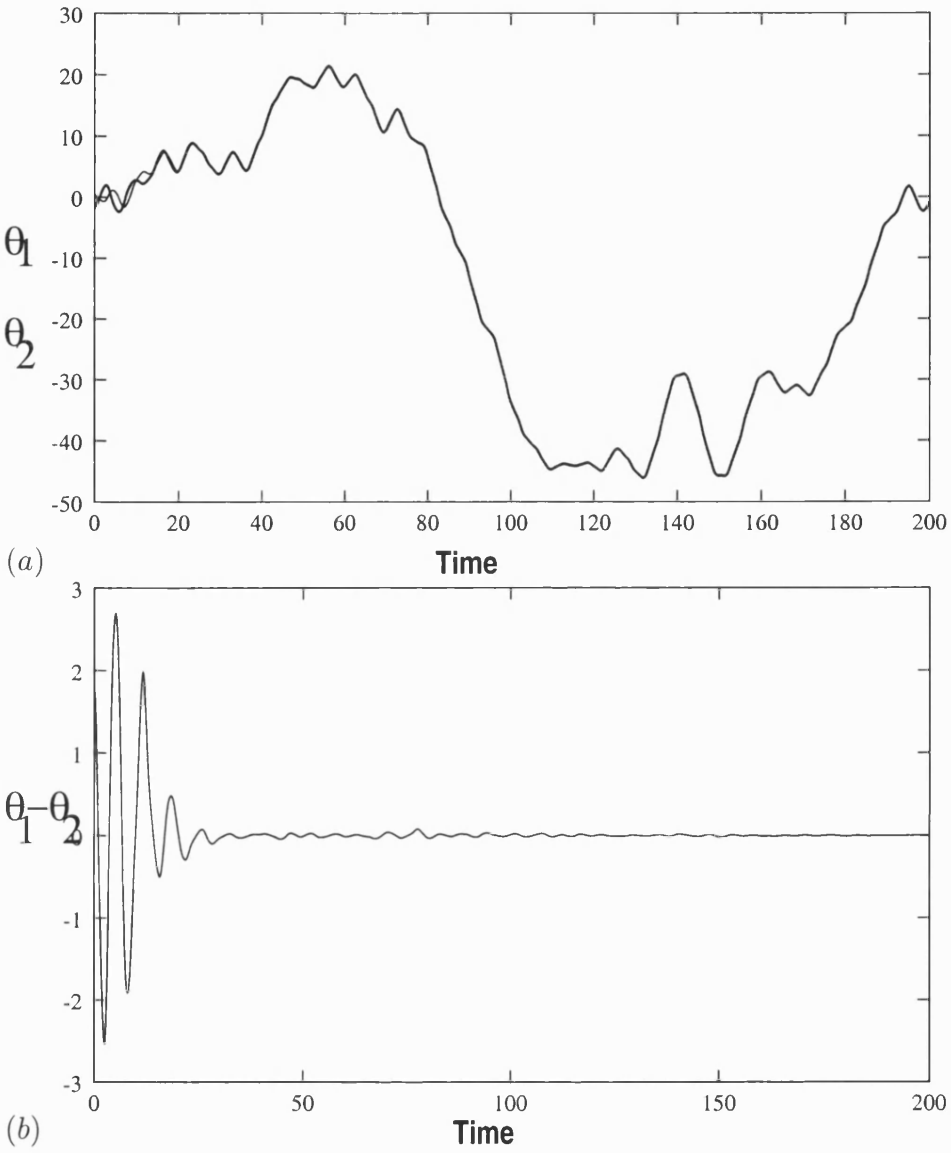

Figure 6.6: Synchronised chaotic orbits for two parametrically excited pendula with parameters $p = 1.4$, $\omega = 1.9$ and $k = 0.5$ (a) Time series of the chaotic orbits (b) Time series of the difference between the chaotic orbits.

Figure 6.5 and Figure 6.6 show some typical examples of in-phase chaos synchronisation for some parameter values when the initial conditions are set at $(\theta_1, \theta_1') = (0.2, 0)$, $(\theta_2, \theta_2') = (-1.57, 0.0)$. In Figure 6.5 we have in-phase chaos synchronisation for $p = 2.0$ and $\omega = 1.9$, $k = 0.5$ while in Figure 6.6 we have in-phase chaos synchronisation for $p = 1.4$ and $\omega = 1.9$, $k = 0.5$ for the same initial conditions. Further numerical computations indicated that when ω is fixed at $\omega = 1.9$ we have in-phase chaos

synchronisation for the given initial conditions for values of p in the range $1.4 < p < 2$ when $k = 0.5$. We also confirmed using numerical simulations that a further increase of the coupling may destroy the chaos leading to other forms of synchronisation and further increase of k again may result in-phase chaos synchronisation.

An intuitive measure of the quality of synchronisation is given by

$$\Delta = \sqrt{(\theta_1 - \theta_2)^2 + (\theta_1' - \theta_2')^2} \tag{6.10}$$

which is the distance between the point on the attractor of one of the pendula and the attractor of the other pendulum. The two pendula are in-phase chaos synchronised if

$$\Delta = 0. \tag{6.11}$$

When the pendula are synchronised out-of-phase this measure of the quality of chaos synchronisation is irrelevant because in that case $\Delta \neq 0$.

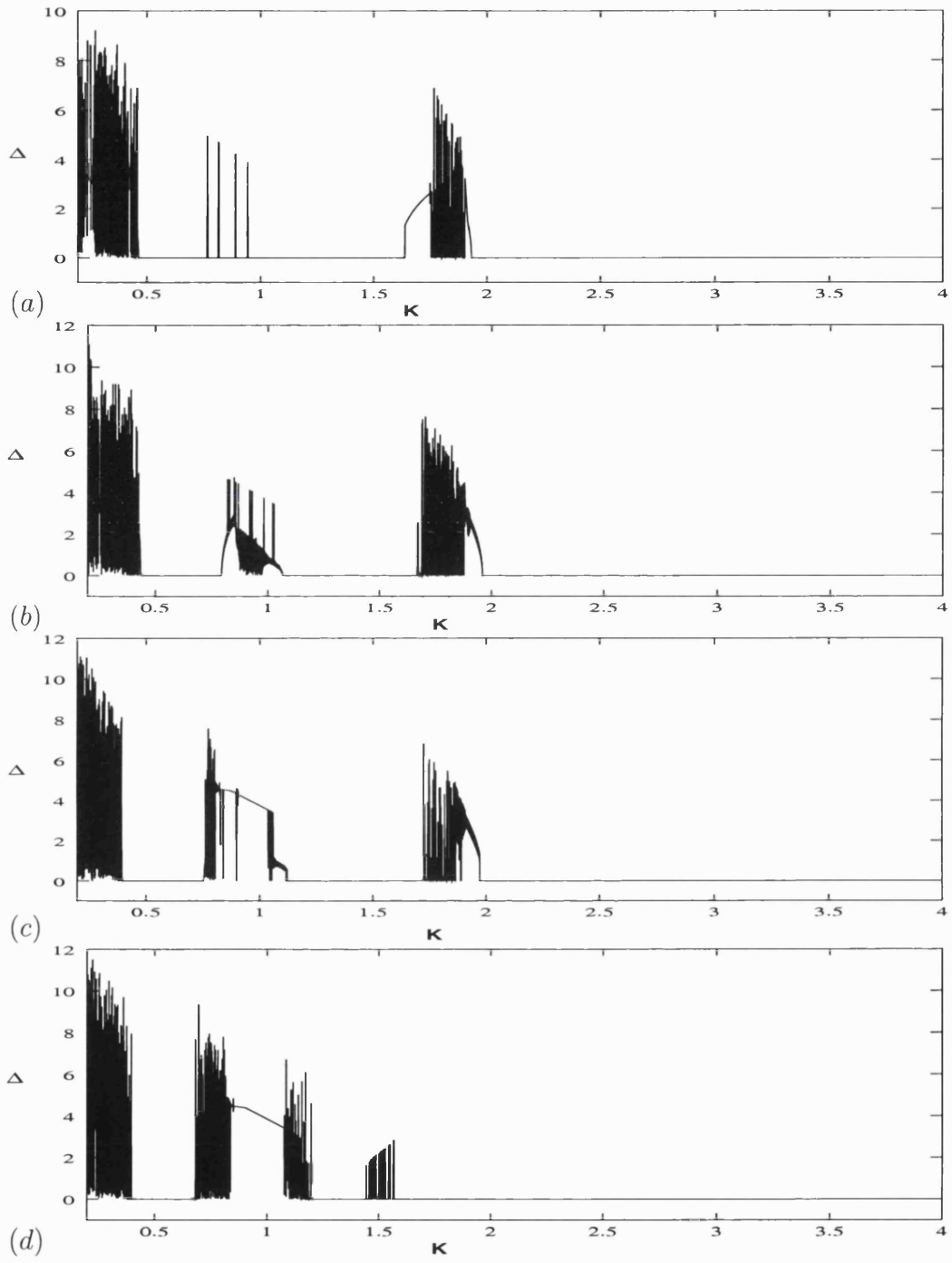

Figure 6.7: Effect of variation of linear coupling on in-phase chaos synchronisation: (a) $p = 1.4$, (b) $p = 1.6$, (c) $p = 1.8$,(d) $p = 2.0$, with $\omega = 1.9$, with varying coupling strength.

Figure 6.7 shows a plot of the measure of in-phase chaos synchronisation as defined by 6.10 when $\omega = 1.9$ for $p = 1.4, 1.6, 1.8, 2.0$ for increasing k. For all these values of the amplitude of parametric forcing the two pendula are in-phase chaos synchronised

for k around $k = 0.5$ as shown in Figure 6.7. But it is evident from the same Figure that there are intermediate values of k below $k = 2$ for which the in-phase chaos synchronisation is destroyed leading to periodic synchronisation. For values of k around $k = 1.4$ we have in-phase chaos synchronisation for $p = 1.4, 1.6, 1.8, 2.0$. The chaos synchronisation is destroyed again for k around $k = 1.8$. However, for $k \geq 2$ we have persistent in-phase chaos synchronisation for $p = 1.4, 1.6, 1.8, 2.0$. The results shown in Figure 6.7 indicate that for values of $k \leq 2$ we have multiple coupling thresholds for chaos synchronisation. The existence of multiple coupling thresholds for synchronisation implies that the calculation of transient time to synchronisation in this case is a tedious exercise.

6.5 Concluding Remarks

We have studied two types of chaos synchronisation: out-of-phase and in-phase chaotic synchronisation. An important observation we have made from these studies is that different symmetries of the chaotic oscillations are responsible for the existence of different chaotic synchronisation regimes. We note that the arguments used in this chapter to confirm the existence of in-phase and out-of-phase chaos synchronisation due to different symmetry properties of the chaotic oscillations can be used to justify the occurrence of in-phase and out-of-phase periodic synchronisation which we considered in chapter 5. The main issues studied in this chapter are:

- The symmetry of the governing equations of two coupled parametrically excited pendula and their relation to chaos synchronisation.
- In-phase and out-of-phase chaos synchronisation of two coupled parametric pendula which occurs in the resonance zone located around $(\omega, p) = (2, 0)$.
- The relationship between in-phase and out-of-phase chaos synchronisation and symmetry.

Chapter 7

Conclusions: Old Challenges and New Hopes

7.1 Introduction

Let us now take stock of what we have achieved in this thesis. The aim of this thesis was to study using numerical simulations as well as analytical methods the different synchronisation regimes of two parametrically excited pendula. The initial motivation was an experimental set-up of a system of two coupled parametrically excited pendula. The experiment lacked resources and only allowed a qualitative assessment of the dynamics of the system. This motivated me to reconsider the whole problem using numerical and analytical methods.

7.2 The Results Obtained

The results contained in this thesis are about both the dynamics of the single parametrically excited pendulum and the synchronisation regimes of two coupled parametrically excited pendula. The first part of this thesis is devoted to understanding of the dynamical response of the single parametrically excited pendulum. We paid particular attention to the dynamics in the lower resonance zones and uncovered some little-known modes of

the parametrically excited pendulum. Previous researchers have overlooked the dynamics of the parametrically excited pendulum when parameters are set in the lower resonance zones. In the second part of this thesis we discussed the different synchronisation regimes of two coupled parametrically excited pendula. The main results found in this thesis can be summarised as follows:

(1) We considered oscillatory, non-rotating solutions of the parametrically excited pendulum. We determined the zones in the parameter space in which different types of oscillatory solutions are realised. In particular we determined the zones in which the T-periodic and 2T-periodic harmonic and subharmonic oscillatory solutions are the dominant type of stable solutions. The symmetry properties of these solutions and the associated scenarios of transition to tumbling chaos were also discussed.

(2) We considered rotating periodic solutions of the parametrically excited pendulum. Four basic types of rotating periodic solutions were shown to exist and the zones in which they occur in the parameter space were determined. We investigated the properties of these rotating solutions and their symmetries.

(3) The transitions of periodic solutions of the parametrically excited pendulum to three different types of chaos, namely, oscillating chaos, rotating chaos and tumbling chaos were investigated. We showed that the transition to oscillating chaos and rotating chaos is through a cascade of period doublings of periodic solutions. We further investigated a mechanism of explosion of the attractors of these two types of chaos. Numerical results were presented which show that the explosion of these chaotic attractors of oscillating type and rotating type is the main mechanism by which structurally stable tumbling chaos is induced in the parametrically excited pendulum.

(4) Different periodic synchronisation regimes in a system of two coupled parametrically excited pendula were studied. Two kinds of periodic synchronisation were of particular interest: one in which the pendula are moving in-phase with

equal amplitudes and another in which the two pendula are always moving in counter-phase, that is, out-of-phase by π radians, but still with equal amplitudes of oscillation. We determined the zones in the parameter space in which these two types of periodic synchronisation are realised and considered the effect of coupling when the parameters are fixed within these zones. We showed that in-phase and out-of-phase periodic synchronisation of two coupled parametric pendula predominantly occurs in the resonance zones located around $(\omega, p) = (2, 0)$ and $(\omega, p) = (2\sqrt{1+2k}, 0)$ respectively.

(5) Special features of tumbling chaos synchronisation in a system of two coupled parametrically excited pendula were explored. In particular we investigated the occurrence and persistence of chaos synchronisation when system parameters are varied. We also give conditions under which tumbling chaos synchronisation fails.

7.3 Future Research Directions

The results of this thesis leave room for possible future work. The following future research directions are proposed:

(a) **Further Experimental Work**: In chapter 1 we discussed a physical experiment in which we got a qualitative assessment of the dynamics of two coupled parametrically excited. In the light of the work in this thesis this experiment can now be redesigned. The knowledge gained so far using numerical simulations can be used to successfully implement an experimental study of both the single parametrically excited pendulum and the coupled parametrically excited pendula.

(b) **Large amplitude Oscillations**: In chapter 2 of this thesis, we discussed oscillatory orbits of the parametrically excited whose amplitude of oscillation does not exceed π, that is $\mid \theta \mid < \pi$.

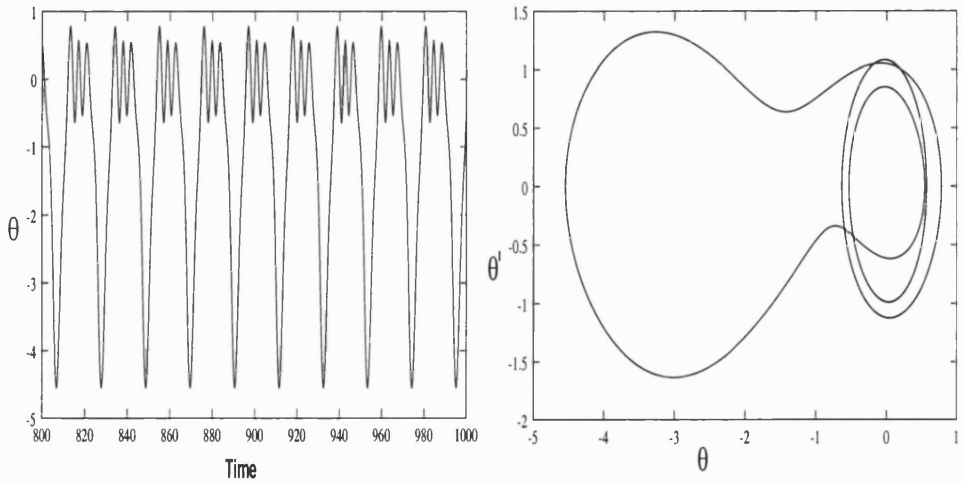

Figure 7.1: Large amplitude periodic oscillations of the parametrically excited pendulum: **Left**: time series, **Right**: Phase space plot.

Numerically simulations show that there is another type oscillation which whose behaviour is poorly understood. An example of this new type of oscillation is shown in Figure 7.1. For this oscillation the amplitude is greater than π with no rotation of the pendulum. It is essential if we are to have a better understanding of the dynamics of the parametrically excited pendulum to inaugurate a study specially targeted at understanding these types of oscillations and their relations with other dynamical responses of the parametrically excited pendulum.

(c) **Oscillations About the Vertical Equilibrium**: Of all the pendulum systems with external forcing, the parametrically excited pendulum is one of those with the same number of stationary points as the undriven pendulum namely, $\theta = 0$ and $\theta = \pi$. In the undriven case these points are always stable and unstable respectively. In chapter 2, we only considered oscillations about the downward equilibrium $(\theta, \theta) = (0, 0)$. A possible way of extending the work of chapter 2 is to consider oscillations about the vertical equilibrium $(\theta, \theta') = (\pi, 0)$.

(d) **Rotations of Two Coupled parametrically Excited pendula**: In chapter three of this thesis we considered rotating solutions of the single parametrically excited

pendulum. We know very little about rotating motions of the two coupled parametrically excited pendula. A possible extension of the work in this thesis would be to consider the rotating motions of two coupled parametrically excited. Such a study would be to see if there are any differences between the rotating motion of the single pendulum and the coupled pendula.

(e) **Transition to Tumbling Chaos in Two coupled pendula**: We have seen the transition of the single parametrically excited pendulum to tumbling chaos in chapter 4 of this thesis. Although we discussed about synchronisation of chaos of two coupled parametrically pendula, very little is known about the actual transition to tumbling chaos when we coupled two parametrically excited pendula. A possible line of research would be to consider the transition of two coupled parametrically excited pendula to tumbling chaos and compare that with the transition of the single parametrically excited pendula discussed in chapter 4 of this thesis.

(f) **Synchronisation in terms of symmetry**: It is well-known that synchrony is the most symmetrical single state of coupled oscillators and that as coupling increases, the symmetry of coupled oscillators may be broken leading to other states. An important extension of the work of this thesis would to reconsider the whole problem of synchronisation of two coupled parametrically excited pendula in terms of symmetry of the system.

(g) **Where will all this lead to**: Once we understand the dynamics of a single pendulum and two coupled pendula, especially their synchronous behaviour then the ultimate question to be addressed now is: If we now couple many such pendula together, and not just two, what can be said about their collective dynamics? Here the aim should be to consider the dynamics of large array of coupled parametrically excited pendula modelled by the following system of equations:

$$\dot{\mathbf{u}}_j = \mathbf{F}(\mathbf{u}_j, \mathbf{a}) + C\Gamma(\mathbf{u}_{j+1} - 2\mathbf{u}_j + \mathbf{u}_{j-1}), \quad j = 0, 1, 2, ..., N-1 \qquad (7.1)$$

where $\mathbf{u}_j \in \mathbb{R}^2$ and $\mathbf{F} : \mathbb{R}^n \rightarrow \mathbb{R}^n$ defines the nonlinear vector field of a single parametrically excited pendulum. In this case, we have $\mathbf{u}_j = \{x_j, y_j\}^T$ and $\mathbf{F}(\mathbf{u}_j) = \{y_j, -\beta y_j - [1 + p\cos(\omega t)\sin(x_j)]\}^T$. Here x_j is the angular displacement, and y_j is the angular velocity. The system parameters can be written as $\mathbf{a} = (\beta, p, \omega)$.

Using as reference point the synchronised state of two coupled parametrically excited pendula, we can aim to show that the system of ensembles of coupled parametrically excited pendula exhibits a pattern forming instability in which discrete waves arise. Depending on the parameters, these structures can have a periodic or chaotic waveform. We can study the routes connecting these behaviours. In particular, such a study would seek to establish if the dynamics of the two coupled pendula is the same as for a large system of coupled pendula. It is essential to find out if the size of the system has any effect on the stability of the synchronised states. Another issue that warrants investigation is to find out if the coupling strength required to bring about synchronisation in the two coupled parametrically excited pendula remains the same when we have a large ensemble of linearly coupled parametrically excited pendula.

Bibliography

D. J. Acheson. Multiple-nodding oscillations of a driven inverted pendulum. *Proceedings Royal Society London A*, 448:89–95, 1995.

J. A. Alexander, J. A. Yorke, Z. You, and I. Kan. Riddled basins. *International Journal of Bifurcation and Chaos*, 2:795, 1992.

K. T. Alligood, T. D. Sauer, and J. A. Yorke. *Chaos an introduction to dynamical systems*. Springer–Verlag, 1996.

F. T. Arecchi, R. Meucci, G. Puccioi, and J. Tredicce. Experimental evidence of subharmonic bifurcations, multistability, and turbulence in q-switched gas laser. *Physical Review Letters*, 49:1217–1220, 1982.

V. I. Arnold. *Ordinary differential equations*. MIT Press, Cambride, Massachusetts, 1973.

P. Ashwin. Chaotic intermittency of patterns in symmetric systems. In M. Golubitsky, D. Luss, and S. H. Strogatz, editors, *Pattern formation in continuous and coupled systems*, pages 11–24. Volume 115 of IMA volumes in Applied Mathematics and its Applications, 1999.

P. Ashwin, J. Buescu, and I. Stewart. From attractor to chaotic saddle: A tale of transverse instability. *Nonlinearity*, 9:703–737, 1996.

V. Astakhov, A. Shabunin, and V. Anishchenko. Antiphase synchronization in symmetrically coupled self-oscillators. *International Journal of Bifurcation and Chaos*, 10: 849–857, 2000.

E. J. Banning. *On the dynamics of two coupled parametrically driven pendulums: Mode competition and transition to chaos*. ISBN: 90-3650933-5, 1998.

E. J. Banning and J. P. Weele. Mode competition in a system of two parametrically driven pendulum: the hamiltonian case. *Physica A*, 220:485–533, 1995.

E. J. Banning, J. P. Weele, J. C. Ross, M. M. Kettenis, and E. Kleine. Mode competition in a system ot two parametrically driven pendulums; the dissipative case. *Physica A*, 245:11–48, 1997.

M. V. Bartuccelli, G. Gentile, and K. V. Georgiou. On the dynamics of a vertically driven damped planar pendulum. *Proceedings Royal Society London A*, 457:3007–3022, 2001.

V. N. Belovodsky, A. L. Tdyfansky, and V. I. Beresnevich. The dynamics of vibromachine with parametric excitation. *Journal of Sound and Vibration*, 254:897–910, 2002.

V. N. Belykh, I. V. Belykh, and E. Mosekilde. Cluster synchronization modes in an ensemmble of coupled chaotic oscillators. *Physical Review E*, 63:036216:1–4, 2001.

M. Bennett, M. F. Schatz, H. R. Rockwood, and K. Wiesenfeld. Huygens's pendulum clocks. *Proceedings Royal Society London A*, 458:563–579, 2002.

M. D. Berkemeier. Coupled oscillators in a platform with four springy legs and feedback. *Proc. 34^{th} IEEE conf. Decision and Control*, 3:2847–2852, 1995.

S. Bielawski, M. Bouazaoui, D. Derozier, and P. Glorieux. Stabilization and characterization of unstable steady states in a laser. *Physical Review A*, 47:3276–3279, 1993.

S R. Bishop and M. J. Clifford. Non-rotating orbits in the parametrically excited pendulum. *European Journal of Mechanics*, 13:581–587, 1994.

S. R. Bishop and M. J. Clifford. Zones of chaotic behaviour in the parametrically excited pendulum. *Journal of Sound and Vibration*, 189:142–147, 1996a.

B. Blazejczyk-Okolewska, J. Brindley, K. Czolczynski, and T. Kapitaniak. Antiphase synchronization of chaos by noncontinuous coupling: two impacting oscillators. *Chaos*, 12:1823–1826, 2001.

I. I. Blekhman. *Synchronisation in Science and technology*. ASME, New York, 1988.

S. Boccaletti and D. L. VallaDares. Characterization of intermittent lag synchronization. *Physical Review E*, 62:7497–7500, 2000.

S. Boccoletti, L. M. Pecora, and A. Pelaez. A unifying framework for synchronization of coupled dynamical systems. *Physical Review E*, 63:066219:1–066219:4, 2001.

S. M. Booker, P. D. Smith, P. Brennan, and R. Bullock. The effect of the forcing function on the disruption of a phase-locked loop (pll). *International Journal of Bifurcation and Chaos*, 10:2099–2117, 2000.

S. A. Bowling. *Animal Gaits*. http://bowlingsite.mcf.com/Movement/locoindex.html, 1999.

R. Bown and L. Kocarev. A unifying definition of synchronization for dynamical systems. *Chaos*, 10:344–349, 2000.

T. P. Bucklaew and C. S. Liu. Pitchfork-type bifurcations in parametrically excited pd-controlled pendulum or manipulator. *Journal of Sound and Vibration*, 247:655–672, 2001.

E. I. Butikov. The rigid pendulum- an antique but evergreen physical model. *European Journal of Physics*, 20:429–441, 1999.

L. Y. Cao and Y. C. Lai. Antiphase synchronism in chaotic systems. *Physical Review E*, 58:382–386, 1998.

D. Capecchi and S. R. Bishop. Periodic oscillations and attracting basins for a parametrically excited pendulum. *Dynamics and Stability of Systems*, 9:123–143, 1994.

T. L. Carroll and L. M. Pecora. Synchronizing chaotic circuits. *IEEE Transactions: Circuits and Systems*, 384:453–456, 1991.

M. J. Clifford and S. R. Bishop. Generic features of escape from a potential well under parametric excitation. *Physics Letters A*, 184:57–63, 1993.

M. J. Clifford and S. R. Bishop. Approximating the escape zone for the parametrically excited pendulum. *Journal of Sound and Vibration*, 174:572–576, 1994.

M. J. Clifford and S. R. Bishop. Rotating periodic orbits of the parametrically excited pendulum. *Physics Letters A*, 201:191–196, 1995.

M. J. Clifford and S. R. Bishop. Locating oscillatory orbits of the parametrically excited pendulum. *Journal of Australian Mathematical Society. Series B*, 37:309–319, 1996.

M. J. Clifford and S. R. Bishop. Inverted oscillations of a driven pendulum. *Proceedings Royal Society London A*, 454:2811–2817, 1998.

J. J. Collins and I. N. Sterwart 1993. Hexapodal gaits and coupled nonlinear oscillator models. *Biological Cybernetics*, 68:287–298, 1993.

M. Dellnitz and C. Heinrich. Admissible symmetry increasing bifurcations. *Nonlinearity*, 8:1039–1066, 1995.

R. L. Devaney. *An Introduction to Chaotic Dynamics*. Addison-Wisley, 1992.

R. Van Doreen. Zones of chaotic behaviour in the parametrically excited pendulum. *Journal of Sound and Vibration*, 200:105–109, 1997.

T. Endo, W. Ohno, and Y. Ueda. Explosion of strange attractors and crisis-induced intermittency from a forced phase-locked loop circuit: Theory and experiments. *International Journal of Bifurcation and Chaos*, 10(4):891–912, 2000.

M. Feigenbaum. Quantitative universality for a class of nonlinear transformations. *Journal of Statistical Physics*, 19:25–52, 1978.

H. Fujisaka and T. Yamada. Stability theory of synchronized motion in coupled-oscillator systems. *Progress in Theoretical Physics*, 69:32–47, 1983.

H. Fujisaka and T. Yamada. A new intermittency in coupled dynamical systems. *Progress in Theoretical Physics*, 74:918–921, 1985.

W. Garira and S. R. Bishop. Rotating solutions of the parametrically excited pendulum. *Preprint*, 2002.

M. Golubitsky, I Stewart, P. L. Buono, and J. J. Collins. A modular network for legged locomotion. *Physica D*, 115:56–72, 1998.

M. Golubitsky, I Stewart, P. L. Buono, and J. J. Collins. Symmetry in locomotor central pattern generators and animal gaits. *Nature*, 401:693–695, 1999.

J. A. Gottwald, L. N. Virgin, and E. H. Dowell. Routes to escape from an energy well. *Journal of Sound and Vibration*, 187:133–144, 1995.

C. Grebogi, E. Otto, and J. Jorke. Critical exponents of chaotic transients in nonlinear dynamical systems. *Physical Review Letters*, 57:1284–1287, 1986.

C. Grebogi, E. Otto, F. Romeiras, and J. A. Yorke. Critical exponents for crisis-induced intermittency. *Physical Review E*, 36(11):5365–5380, 1987.

C. Grebogi, E. Otto, and J. A. Yorke. Are three-frequency quasiperiodic orbits to be expected in typical nonlinear dynamical systems. *Physical Review Letters*, 51:339–342, 1983a.

C. Grebogi, E. Otto, and J. A Yorke. Sudden changes in chaotic attractors and transient chaos. *Physica D*, 7:181–200, 1983b.

J. K. Hale. *Ordinary differential equations*. Wiley, New York, 1969.

M. Hasler, Yu. Maistrenko, and O. Popovych. Simple example of partial synchronization of chaotic systems. *Physical Review E*, 58:6843–6846, 1998.

J. F. Heagy, T. L. Carroll, and L. M. Pecora. Desynchronization by periodic orbits. *Physical Review E*, 2:R1253–R1256, 1995a.

J. F. Heagy, T. L. Carroll, and T. L. Pecora. Short wavelength bifurcations and size instabilities in coupled oscillator systems. *Physical Review Letters*, 74:4185, 1995b.

J. F. Heagy, T. L. Carroll, and T. L. Pecora. Synchronization conditions and desynchronization patterns in coupled limit-cycle chaotic oscillators. *Physical Review E*, 58: 347–360, 1998.

J. S. Hogan. On the dynamics of rigid block motion under harmonic forcing. *Proceedings Royal Society London A*, 425:441–476, 1989a.

J. S. Hogan. On the dynamics of rigid block motion under harmonic forcing. *Proceedings Royal Society London A*, 425:441–476, 1989b.

J. S. Hogan. The many steady state responses of a rigid block under harmonic forcing. *Earthquake Engineering and Structural Dynamics*, 19:1057–1071, 1990.

C. Hugenii. Horoloquim oscilatorium, [1673] (apud f. muguet, parisiis, france); english translation [1986] the pendulum clock. *Iowa State University Press, Ames*, 1673.

E. A. Jackson. *Perspectives of Nonlinear Dynamics, Volume 1*. Cambridge University Press, Cambridge, 1991.

K. L. Janicki and W. Szemplińska-Stupnicka. Subharmonic resonances and criteria for escape and chaos in a driven oscillator. *Journal of Sound and Vibration*, 180:253–269, 1995.

K. Josić. Invariant manifolds and synchronization of coupled dynamical systems. *Physical Review E*, 80(14):3053–3056, 1998.

C.-M. Kim, G.-S. Yim, and Y. S. Kim. Experimental evidence of characteristic relations of type-i intermittency in an electronic circuit. *Physical Review E*, 563:2573–2577, 1997.

S. Y. Kim. Symmetry and dynamics of a magnetic oscillator. *Journal of Korean Physical Society*, 32:735–738, 1998.

L. Kocarev, K. Halle, K. Eckert, and L. O. Chua. Experimental observation of antimonotocity in chua's circuit. *International Journal of Bifurcation and Chaos*, 3:1051–1053, 1993.

B. P. Koch and R. W. Leven. Subharmonic and homoclinic bifurcations in a parametrically excited pendulum. *Physica D*, 16:1–13, 1985.

D. J. Kortewerg. Les horoges sympathiques de huygens. *Archives Neerlandasises, sér. II: The Hague: Martinus Nijhoff*, tome IX:273–295, 1906.

Y. Kuramoto. *Chemical oscillations, waves and turbulence*. Springer-Verlag, Berlin, 1984.

A. N. Lansbury and J. M. T. Thompson. Incursive fractals: a robust mechanism of basin erosion preceding the optimal escape from a potential well. *Physics Letters A*, 150: 355–361, 1990.

C. Lepers, J. Legrand, and P. Glorieux. Experimental investigation of the collision of feigenbaum cascades in lasers. *Physical Review A*, 43:2573–2575, 1991.

E. N. Lorenz. Deterministic non-periodic flow. *Journal of Atmospheric Science*, 20: 130–141, 1963.

R. Mainieri and J. Rehacek. Projective synchronization in three-dimensional chaotic systems. *Physical Review Letters*, 82:3042–3045, 1999.

N. W. McLachlan. *Theory an Applications of Mathieu Functions*. Dover, New York, 1964.

I. Melbourne, M. Dellnitz, and M. Golubitsky. The structure of symmetric attractors. *Archive for Rational Mechanics and Analysis*, 123:75–98, 1993.

A. H. Nayfeh and B. Balachandran. *Applied Nonlinear Dynamics*. ASME, New York, 1995.

R. C. Newell, P. M. Alsing, A. Gavrielides, and V. Kovanis. Synchronization of chaos using proportional feedback. *Physical Review E*, 49(1):313–318, 1994.

H. E. Nusse and J. A. Yorke. *Dynamics: Numerical Explorations*. Springer-Verlag, New York, 1998.

J. R. Ockendon and A. B. Taylor. The dynamics of current collection systems for an electric locomotive. *Proceedings Royal Society London A*, 322:447–468, 1971.

A. G. Oliveira, W. Garira, and S. R. Bishop. Out-of-phase vs in-phase synchronisation of two parametrically excited pendula. In S. Boccaletti, J. Burguete, W. González-Viñas, H. L. Mancini, and D. L. Valladares, editors, *Space-Time Chaos: Characterization, control and synchronization*, pages 233–250. Word Scientific, 2001.

D. Pazó, E. Sánchez, and M. A. Maías. Transition to high-dimensional chaos through quasiperiodic motion. *International Journal of Bifurcation and Chaos*, 11:2683–2688, 2001.

L. M. Pecora and T. L. Carroll. Synchronization in chaotic systems. *Physical Review Letters*, 64:821–824, 1990.

L. M. Pecora and T. L. Carroll. Master stability function for synchronized coupled systems. *Physical Review Letters*, 80:2109–2112, 1998.

K. Pyragas. Generalized synchronization, predictability, and equivalence of unidirectionally coupled dynamical systems. *Physical Review Letters*, 76:1816–1819, 1996a.

K. Pyragas. Weak and strong synchronization of chaos. *Physical Review E*, 54:R4508–R4511, 1996b.

C. Robert, K. T. T. Alligood, E. Otto, and J. A. Yorke. Explosion of chaotic sets. *Physica D*, 144:44–61, 2000.

M. G. Rosenblum, A. S. Pikovysky, and J. Kurths. From phase to lag synchronization in coupled chaotic oscillators. *Physical Review Letters*, 78:4193–4196, 1997.

R. Roy and K. S. Thornburg Jr. Experimental synchronization of chaotic lasers. *Physical Review Letters*, 72**13**:2009–2012, 1994.

N. F. Rulkov, M. M. Sushchik, L. S. Tsimring, and H. D. I. Abarbanel. Generalized synchronization in directionally coupled chaotic systems. *Physical Review E*, 51: 980–994, 1995.

M. A. F. Sanjuań. Symmetry restoring crises, period adding and chaotic transitions in the cubic van der pol oscillator. *Journal of Sound and Vibration*, 193(4):863–875, 1996.

S. Sano, M. Sano, and Y. Sawanda. Practical methods of measuring the generalized dimension and the largest lyapunov exponent in high dimensional chaotic systems. *Physical Review Letters*, 55**10**:1082–1085, 1985.

M. F. Schatz. Huygens's pendulum clocks. *Adapted from: http://www.physics.gatech.edu/schatz/clocks.html*, 2001.

A. K. Sen. An experimental study of nonlinear dynamics and chaos in a nonautonomous electronic circuit. *International Journal of Bifurcation and Chaos*, 11:583–589, 2001.

D. L. Stein. *Lectures in the sciences of complexity*, volume (Ed.). Addison-Wiley, Reading, MA, 1989.

A. Stephenson. On a new type of dynamical stability. *Manchester Memoirs*, *lii*(8):1–10, 1908.

I. W. Stewart and T. R. Faulkner. Estimating the escape zone for a parametrically excited pendulum-type. *Physical Review E*, 62:4856–4861, 2000.

T. Sugawara, M. Tachikawa, T. Tsukamoto, and T. Shimizu. Synchronization of mutually coupled chaotic systems. *Physical Review Letters*, 7222:p.3502, 1994.

J. W. Swift and K. Wiesenfeld. Suppression of period doublings in symmetric systems. *Physical Review Letters*, 52(9):705–708, 1984.

W. Szemplińska-Stupnicka, E. Tyrkiel, and A. Zubrzycki. The global bifurcations that lead to transient tumbling chaos in a parametrically driven pendulum. *International Journal of Bifurcation and Chaos*, 10(9):2161–2175, 2000.

D. Y. Tang and N. R. Heckenburg. Synchronization of mutually coupled chaotic systems. *Physical Review E*, 556:6618–6623, 1997.

J. M. T. Thompson. Chaotic phenomena triggering the escape from a potential well. *Proceedings Royal Society London A*, 421(1861):195–255, 1989.

J. M. T. Thompson, S. R. Bishop, and L. M. Leung. Fractal basins and chaotic bifurcations prior to escape from a potential well. *Physics Letters A*, 121:116–120, 1987.

J. M. T. Thompson, C. T. Rainey, and M. S. Soliman. Ship stability criteria based on chaotic transients from incursive fractals. *Proceedings Royal Society London A*, 332: 149–167, 1990a.

J. M. T. Thompson and M. S. Soliman. Fractal control boundaries of driven oscillators and their relevance to safe engineering design. *Proceedings Royal Society London A*, 428:1–13, 1990b.

J. M. T. Thompson and H. B. Stewart. *Nonlinear Dynamics and Chaos, 2nd Edition.* Wiley, 2002.

A. Uchida, Y. Liu, I. Fischer, P. Davis, and T. Aida. Chaotic antiphasing dynamics and synchronization in multimode semiconductor lasers. *Physical Review A*, 64: 023801:1–6, 2001.

A. Varone, G. Santoboni, and F. Meloni. Chaotic desynchronization with negative conditional exponents. *Open Systems & Information Dynamics*, 5, 1998.

L. N. Virgin, W. T. Fielder, and R. H. Plaut. Fractal control boundaries of driven oscillators and their relevance to safe engineering design. *Journal of Sound and Vibration*, 191(1):177–187, 1996.

J. Warmiński, G. Litak, and K. Szabelski. Synchronisation and chaos in a parametrically and self-excited system with two degrees of freedom. *Nonlinear Dynamics*, 22:135–153, 2000.

J. P. Weele and E. J. Banning. Mode interaction in horses, tea, and other nonlinear oscillators: The universal role of symmetry. *American Journal of Physics*, 69:953–965, 2001.

S. W. Wiggins. On the detection and dynamical consequences of orbits homoclinic to hyperbolic periodic orbits and normally hyperbolic invariant tori in a class of ordinary differential equations. *SIAM Journal of Applied Mathematics*, 482:262–285, 1988.

S. W. Wiggins. *Introduction to Applied Nonlinear Dynamics*. Springer-Verlag, New York, 1990.

A. T. Winfree. *The geometry of biological time*. Springer-Verlag, New York, 1980.

C. W. Wu and L. O. Chua. Application of graph theory to the synchronization in an array of coupled nonlinear oscillators. *IEEE Transactions: Circuits and Systems*, 42: 494–497, 1995.

T. X. Wu and M. J. Brennan. Dynamic stiffness of a railway overhead wire system and its effect on pantograph-catenary dynamics. *Journal of Sound and Vibration*, 219: 483–502, 1999.

T. Yalcinkaya and Y. C. Lai. Phase characterization of chaos. *Physical Review Letters*, 79:3885–3888, 1997.

T. Yamada and H. Fujisaka. Stability theory of synchronized motion in coupled-oscillator systems. ii - a mapping approach. *Progress in Theoretical Physics*, 70: 11240–1248, 1983.

T. Yamada and H. Fujisaka. Stability theory of synchronized motion in coupled-oscillator systems. iii - mapping model for continuous systems. *Progress in Theoretical Physics*, 72:885–894, 1984.

J. Yang. Quasiperiodicity and transition to chaos. *Physical Review E*, 61:6521–6526, 2000.

Y. H. Yu, K. Kwak, and T. K. Lim. On-off intermittency in experimental synchronization process. *Physics Letters A*, 198(1):34–38, 1995.

Y. Zhang, S. Q. Hu, and G. H. Du. Chaos synchronisation of two parametrically excited pendulums. *Journal of Sound and Vibration*, 223:247–254, 1999.